

**RADON AND THORON CONCENTRATIONS AS A
PRECURSOR TO EARTHQUAKES ALONG CHITE
FAULT IN AIZAWL DISTRICT**

**Thesis submitted in fulfillment of the
requirements for the degree of
Doctor of Philosophy
in Physics**

By

Sanjay Singh

To



**School of Physical Sciences
Department of Physics
Mizoram University, Aizawl
Mizoram, India
June 2016**

**RADON AND THORON CONCENTRATIONS AS A
PRECURSOR TO EARTHQUAKES ALONG CHITE
FAULT IN AIZAWL DISTRICT**

**Thesis submitted in fulfillment of the
requirements for the degree of
Doctor of Philosophy
in Physics**

By

Sanjay Singh

Registration No. MZU/Ph.D/503 of 15.05.2012

To



**School of Physical Sciences
Department of Physics
Mizoram University, Aizawl
Mizoram, India
June 2016**



Prof. R. C. Tiwari
Supervisor

MIZORAM UNIVERSITY

DEPARTMENT OF PHYSICS

Aizawl - 796004, MIZORAM, India

(A Central University Established by an Act of Parliament of India)

Ph:+91-389-2330522(O) +91-9862300514 (M) & Fax: +91-389-2330435

Email: ramesh_mzu@rediffmail.com

Date: 23. 6. 2016

Certificate

This is to certify that the thesis entitled “*Radon and thoron concentrations as a precursor to earthquakes along Chite fault in Aizawl district*” submitted by Sanjay Singh (Registration No. MZU/Ph.D/503 of 15.05.2012), for the degree of Doctor of Philosophy in Physics, of the Mizoram University: Aizawl, India, embodies the record of original investigations carried out by him under my supervision. He has been duly registered and the thesis presented is worthy of being considered for the award of Ph.D. degree. This research work has not been submitted for any degree of any other university.

(Prof. Ramesh Chandra Tiwari)
Supervisor

(Prof. Raghvendra Prasad Tiwari)
Joint Supervisor

Department of Geology

DECLARATION

MIZORAM UNIVERSITY

JUNE 2016

I, **Sanjay Singh** hereby declare that the subject matter of this thesis is the record of work done by me, that the contents of this thesis did not form basis of the award of any previous degree to me or to do the best of my knowledge to anybody else, and that the thesis has not been submitted by me for any research degree in any other University/institute.

This is being submitted to the Mizoram University for the degree of *Doctor of Philosophy* in Physics

Dated:

(SANJAY SINGH)

Candidate

Acknowledgement

First and foremost I would like to express my gratitude to my supervisor, Prof. R. C. Tiwari, Department of Physics and Dean, School of Physical Sciences, for his support and deep insights. His colossal support, endless ideas and high spirits encouraged me during the entire period of the study. I am also very grateful to my co-supervisor, Prof. R. P. Tiwari for introducing me to the basics of geology and steering me towards the right direction until this thesis was completed.

I would like to express my gratitude to the peoples, especially Dr. Victor Z. Ralte (Late) and Dr. Paul Lalnuntluanga, Dept. of Geology, for their kind co-operation in site selection and installation of the device in the study area. The field survey was carried out on a private land. I would like to thank the owners of the land, Horticulture Department, Govt. of Mizoram and Park Eden, whose kind permission made our field based experiments possible.

In a very special way I would like to thank my friend, Dr. Hari Prasad Jaishi, a research scholar for always helping me in the field survey, laboratory works, literature works and giving me assistance whenever I needed. I am happy that I met Dr. Amit Shankar, from Theoretical Condensed Matter research group. I learned a lot of important life matters from him. Thank you for all the good time we spent together.

My special thank also go to Prof. R. K. Thapa, Ex-Dean, School of Physical Sciences whose very helping nature, encouragement and nice behavior motivate me to improve the knowledge. It would have been difficult for me to solve the administrative problem on my own. I would like to thank Prof. Zaithanzauva Pachuau, Head, Department of Physics and all the faculty members as well as non-teaching for helping me whenever required. Also, I want to thank all the research scholars in the department

for the friendship and the productive intellectual atmosphere that I have enjoyed all these years.

I gratefully acknowledge the Ministry of Earth Science, Govt. of India, New Delhi for financial grants to carry out the research work.

Beside Science, friendship is an important aspect of life that one should never forget. I would like to thank all my friends from my home town Kolasib for their encouragement, support and warm friendship. Over the past few years I have enjoyed a lot staying in the hostel. My special thanks go to all the boarders of Lengteng PG Boys' Hostel for creating a study environment and always making me feel at home. Thanks to all of you.

I would also like to thank the family members of my Supervisor Prof. R.C. Tiwari, especially to his wife Mrs. Bandana Devi, for her good wishes and continuous support because of which I could work with my Supervisor during holidays as well.

As a final thought, I am really lucky to have such a wonderful family. I can never give enough thanks to my parents, sister and brother. It is their love, affection, endless support of all kind that makes this work possible. They always encourage me to learn from others.

Date:

(SANJAY SINGH)

Contents

Title of the Thesis	i
Certificate	ii
Declaration	iii
Acknowledgement	iv
List of Figures	x
List of Tables	xv
Dedication	xvi
Chapter 1 : Introduction	1
1.1 : Mechanism governing the behavior of Radon and earthquake	2
1.2 : Dynamics of earthquake	7
1.2.1 : Description of Fault	8
1.2.2 : Formulation of energy produced during fault formation	9
1.3 : Models of earthquake precursors	12
1.3.1 : The IPE Model	13
1.3.2 : The Dilatancy-Diffusion Model	16

1.3.3	: Slider-Block Model	19
1.4	: Migration mechanism of radon and thoron in soil	23
1.4.1	: Recoil effect	24
1.4.2	: Migration by diffusion	26
1.4.3	: Migration by advection	27
1.5	: Description of the statistical method applied in the study	27
1.5.1	: Artificial Neural Networking's (ANNs)	27
1.5.2	: Multiple Linear Regressions (MLRs)	30
1.6	: Geological setting of the study area and its seismicity	32
1.7	: Possible empirical relation of radon and earthquake	36
1.8	: Background and the main scope of the study	37
Chapter 2	: Review of Literature	39
Chapter 3	: Materials and Methods	57
3.1	: Solid State Nuclear Track Detectors (SSNTDs)	57
3.1.1	: General description of LR-115 films	59
3.2	: Principle and salient feature of the technique	61
3.2.1	: Track registration and formation process	61
3.2.2	: Ion explosion spike model	63

3.2.3	: Restricted energy loss model	65
3.3	: Track etching	66
3.4	: Track counting	68
3.5	: Monitoring technique of radon and thoron in soil gas	69
3.5.1	: Description of twin cup dosimeter	71
3.5.2	: Constant temperature bath	73
3.5.2.1	: General recommendations	74
3.5.3	: Spark counter	75
Chapter 4	: Results and Discussion	80
4.1	: External influence of meteorological parameters on radon emanation	82
4.2	: Meteorological parameters influence on thoron emanation	85
4.3	: Radon concentration associated with seismic events (using standard deviation from related mean value)	87
4.4	: Correlation of Thoron anomalies with relevant earthquakes (using standard deviation method)	90
4.5	: Statistical analysis of soil radon and thoron data at Chite fault, Aizawl using Artificial Neural Networking	

(ANN) and Multiple Linear Regressions (MLRs)	92
4.5.1 : Artificial Neural Networking	92
4.5.2 : Multiple Linear Regressions	97
4.6 : Comparisons of the results with different statistical approaches	102
Chapter 5 : Summary and Conclusion	108
References :	112
List of Research publications	134
Brief Bio-Data of the author	138
Appendix: Formulae	139
Reprints of research papers	146

List of Figures

Fig. Nos.	Figure Captions	Page No.
1.1	Radioactive decay chains. (a) uranium 238 to lead 210, (b) thorium 232 to lead 208, and (c) uranium 235 to lead 207. Half-life and primary mode of decay are shown for each isotope. For each decay chain, inhalation of the shaded isotopes constitutes the primary health concern (after Nazaroff, 1992).	3
1.2	Dilatancy: increasing stress causes cracks in the rock, which enlarges the material perpendicular to the main axis of stress. This causes an effective increase in volume (after Friedmann, 2012).	5
1.3	Schematic of the orientation of the principal stresses and the corresponding type of faulting.	9
1.4	A slab of crustal rock with two equal and opposite forces acting tangentially (after Kanamori and Brodsky, 2001).	10
1.5	Illustration of simple stress release pattern during faulting. (a) Simple case. (b) Slip-weakening model. Hatched and cross-hatched areas indicate the fracture energy and frictional energy loss.	11
1.6	Change of average deformation velocity during the seismic cycle (from Mjachkin <i>et al.</i> 1975).	14
1.7	An ideal scheme of formation of the zones of unstable deformation. A – zone of unstable deformation, B – zone of unloading (from Mjachkin <i>et al.</i> , 1975).	14
1.8	Predicted Changes in various physical parameters as a function in time during the earthquake cycle for the dilatancy model (from Scholz <i>et al.</i> , 1973)	17
1.9	Compression velocity (V_P), shear velocity (V_S) and V_P/V_S as a function of pore fluid bulk modulus and porosity. The lower panel gives the pore fluid bulk modulus as a function of pore	18

	pressure (P_p) and temperature. Circled numbers refer to successive stages from onset of dilatancy 1 to fracture 5 with initial porosity of 0.2% (after Anderson and Whitcomb, 1973)	
1.10	Illustration of the two-dimensional slider block model (after Rundle <i>et al.</i> , 2003)	20
1.11	Schematic of a simple one-dimensional slider block model	21
1.12	Schematic sketch of the possible emanation scenarios in a solid-water-air system. Radium atom, indicated by solid circles, decay, producing an alpha particle and a recoiling radon atom which may end its recoil at the point indicated by the open circle; R = recoil range; case A-A') ^{222}Rn remains inside the grain; case B-B') ^{222}Rn reaches the adjacent grain; case C-C') ^{222}Rn atom reaches the water filled pore space, possibly reaching the air filled pore space by diffusion; case D-D') recoil energy is large, ^{222}Rn crosses the air filled pore space and penetrates into the adjacent grain (after Tanner, 1980).	25
1.13	Schematic representation of radon generation and migration in the soil and its entry into the atmosphere or buildings (after Nazaroff <i>et al.</i> , 1992)	26
1.14	The block diagram of a neuron (Haykin, 1994)	28
1.15	Seismic zone map of India (GIS, 1988).	33
1.16	Map of Northeast-India showing major lineaments/faults in Tripura-Mizoram fold belt.	34
1.17	Location map of study area showing the geology of the region	35
3.1	Closed Track-etch monitor.	59
3.2	Schematic diagram representing the different stages of penetration of a particle into a detector. Not all the stages are necessarily apparent for a given set of conditions. Stages: 1) Electrons are stripped from particle. 2) Particle moving too fast to leave etchable damage. 3) Main region of damage. 4) Particle regaining electrons and damage no longer etchable. 5) Some elastic collisions as particle come to rest which may cause	62

	damage if particle is heavy (after Hepburn and Windle, 1980).	
3.3	Model of track etching in which the normal surface is removed at a velocity V_G and the damaged track at a velocity V_T , leading to a cone-shaped pit. (b) Tracks formed at an angle ϕ less than the critical angle θ_c are not revealed because the normal surface advances faster than the etch rate along the track. (c) The case in which the particle enters at the critical angle θ_c . Tracks entering the surface at an angle greater than the critical angle will be visible after etching (after Fleischer <i>et al.</i> , 1975)	67
3.4	Schematic representation of Radon and Thoron detection in soil.	70
3.5	Methods of measurement in soil. (a) Bore hole at a depth of 80 cm below soil surface. (b) LR-115 loaded in the dosimeter. (c) Loaded dosimeter inserted in a metallic cylinder. (d) The metallic cylinder sealed by a plastic cover	71
3.6	Schematic representation of a twin-cup dosimeter: 1) Radon cup mode SSNTD film. 2) Radon + thoron cup mode SSNTD film. 3) Bare mode SSNTD film	72
3.7	Picture of radon thoron discriminating dosimeter. Oval shaped circles represent the pin holes	72
3.8	(a) Picture of a constant temperature bath. (b) LR-115 films loaded in cartridges before etching. (c) Loaded films in NaOH solution inside the etching vessels.	74
3.9	(a) Spark counter model PSI-SC 1. (b) Etched LR-115 film placed on top of a thick conductive electrode. (c) Film covered by aluminum foil. (d) Track counting.	76
3.10	Schematic diagram of a spark counter. The SSNTD placed between the electrode forms a capacitor. When high voltage is applied across the capacitor C, an electric spark takes place through a track hole. The voltage pulse produced across the resistor R can easily be counted electronically (after Azimi-	77

	Garakani, 1990).	
3.11	Applied voltage vs. counts, showing the plateau region. The plateau region depicts the operating voltage.	78
4.1	Spatial distribution of the earthquakes that occurred around the study areas during the observation period.	81
4.2	Linear fitting of radon data with meteorological parameters at Chite fault: (a) rainfall, (b) temperature, (c) relative humidity and (d) pressure.	83
4.3	Linear fitting of Thoron data with meteorological parameters at Chite fault: (a) rainfall, (b) temperature, (c) relative humidity and (d) pressure	85
4.4	(a) Radon concentration variation in the soil along with the; (b) pressure, (c) relative humidity, (d) temperature and (e) rainfall. The vertical bands passing through all the diagrams represent the earthquakes along with their magnitude that occurred during the observation period. The solid horizontal lines in (a) represents the average value of radon and the dotted lines indicate the standard deviations (+1 STD, +2 STD and -1STD) from the average values.	88
4.5	(a) Thoron concentration variation in the soil along with the; (b) pressure, (c) relative humidity, (d) temperature and (e) rainfall. The vertical bands passing through all the diagrams represent the earthquakes along with their magnitude that occurred during the observation period. The solid horizontal lines in (a) represents the average value of radon and the dotted lines indicate the standard deviations (+1 STD, +2 STD and -1STD) from the average values.	91
4.6	The ANN topology for learning radon concentration dependency on environmental parameters.	93
4.7	Variation of (a) Predicted radon concentration (ANN) and (b)	95

	Measured radon concentration during the Investigation period at Chite fault. The solid vertical lines represent the earthquakes along with their magnitudes (M).	
4.8	Variation of (a) Predicted thoron concentration (ANN) and (b) Measured thoron concentration during the Investigation period at Chite fault. The solid vertical lines represent the earthquakes along with their magnitudes (M).	96
4.9	Variation of (a) Predicted radon concentration (MLR) and (b) Measured radon concentration during the Investigation period at Chite fault. The solid vertical lines represent the earthquakes along with their magnitudes (M).	100
4.10	Variation of (a) Predicted thoron concentration (MLR) and (b) Measured thoron concentration during the Investigation period at Chite fault. The solid vertical lines represent the earthquakes along with their magnitudes (M).	103
4.11	Variation of (a) Predicted radon concentration (ANN), (b) Predicted radon concentration (MLR) and (c) Measured radon concentration during the Investigation period at Chite fault. The solid vertical lines represent the earthquakes along with their magnitudes (M).	104
4.12	Variation of (a) Predicted thoron concentration (ANN), (b) Predicted thoron concentration (MLR) and (c) Measured thoron concentration during the Investigation period at Chite fault. The solid vertical lines represent the earthquakes along with their magnitudes (M).	106

List of Tables

Table Nos.	Captions	Page No.
3.1	Commonly used Track-etch Materials.	58
4.1	Details of earthquakes occurred around the measuring site during the investigation period	81
4.2	Descriptive Statistics of Radon concentration and the Meteorological parameters during the observation Period	84
4.3	Descriptive Statistics of Thoron concentration and the Meteorological parameters during the observation Period	86
4.4	Coefficients of the Backward Regression output of Radon	98
4.5	Coefficients of the Backward regression output of Thoron	101
4.6	Descriptive statistics of Measured Radon concentration, predicted Radon (ANN) and Predicted Radon (MLR)	105

Dedication

To my parents, brother and my nephew

1

Introduction

Understanding complex phenomena such as the physics of earthquakes is a formidable challenge. The reason is that we are constrained by our inability to do experiments on earthquake faults and our present knowledge about the dynamics of earthquake rupture process is still poor. The earth's relatively rigid upper layer called lithosphere which is approximately 100 km thick, consists of the crust and a portion of the upper mantle. According to the theory of plate tectonics, it says that the lithosphere is broken into a dozen major rigid plates and several minor ones. These plates slowly glide against each other, building up stress and creating faults. The first modern theory of earthquakes (i.e. the elastic rebound theory) emphasizes about the importance of elastic strain energy during the earthquake generation process. It states that the elastic strain increases monotonically along the weakened region (i.e. fault) resulting in an increase of stress. When the stress accumulates to the breaking strength, this region becomes unstable and rapidly rebounds to a lower stable stress state. Therefore the released elastic strain energy manifests itself as seismic radiation and violent ground motion and rearrangement (Ferguson *et al.*, 1998).

During the several decades, the studies of earthquakes precursory phenomena have revealed that significant geophysical and geochemical changes can occur prior to intermediate and large earthquakes. The term earthquake precursor is used to describe a wide variety of physical phenomena that convey information prior to some earthquakes. These physical phenomena include induced electric and magnetic fields, groundwater level changes, gas emissions, temperature changes, surface deformation and anomalous seismicity patterns. More recently, a large number of geophysical and geochemical

measurements have been made in many seismic active countries such as USSR, China, Japan and United States, including India for the purpose of earthquake prediction, both in groundwater and soil air (Thomas, 1988; King, 1986; Cicerone *et al.*, 2009). From a geochemical perspective, most of the rocks in the earth crust contain a small amount of gases that can be distinguished from the atmospheric gases. Among these gases, one is Radon whose distribution in various geological environments depends on the abundance of its parent. The mean abundance of Uranium in the earth's crust is estimated at 2.7 ppm (Dongarra and Martinelli, 1993). Therefore, radon has been indicated as possible precursor of earthquakes and numerous scientific literature reports many example of radon anomalies observed before and after seismic events. However, the variation of radon in soil is not only controlled by earthquake activities but also gets influenced by environmental parameters (Ghosh *et al.*, 2009; Kraner *et al.*, 1964; Tanner, 1980). Perhaps, it is necessary that the non-tectonically induced variations must be carefully identified or eliminated in the search of true earthquake-related anomalies.

1.1 Mechanism governing the behavior of Radon and Earthquake

Frederick Dorn a German scientist was the first who found that radium-226 was giving off a gas which he named it "radium emanation" in 1900. In 1901, Rutherford and Brooks demonstrated that radon is a noble radioactive gas and the same year he discovered the active deposits of thorium. Later in 1918, Schmidt introduced the name "Radon" which becomes the universal name of this element (George, 2008). ^{222}Rn is entirely governed by its immediate parent, ^{226}Ra (Radium) which is one of the members of alkaline earth family. Radon is a mono-atomic noble gas, the only natural occurring radioactive gas with atomic weight of 222.0175 and atomic number 86. It has thirty known isotopes (Neri *et al.*, 2011). Out of these only three are naturally occurring radio-

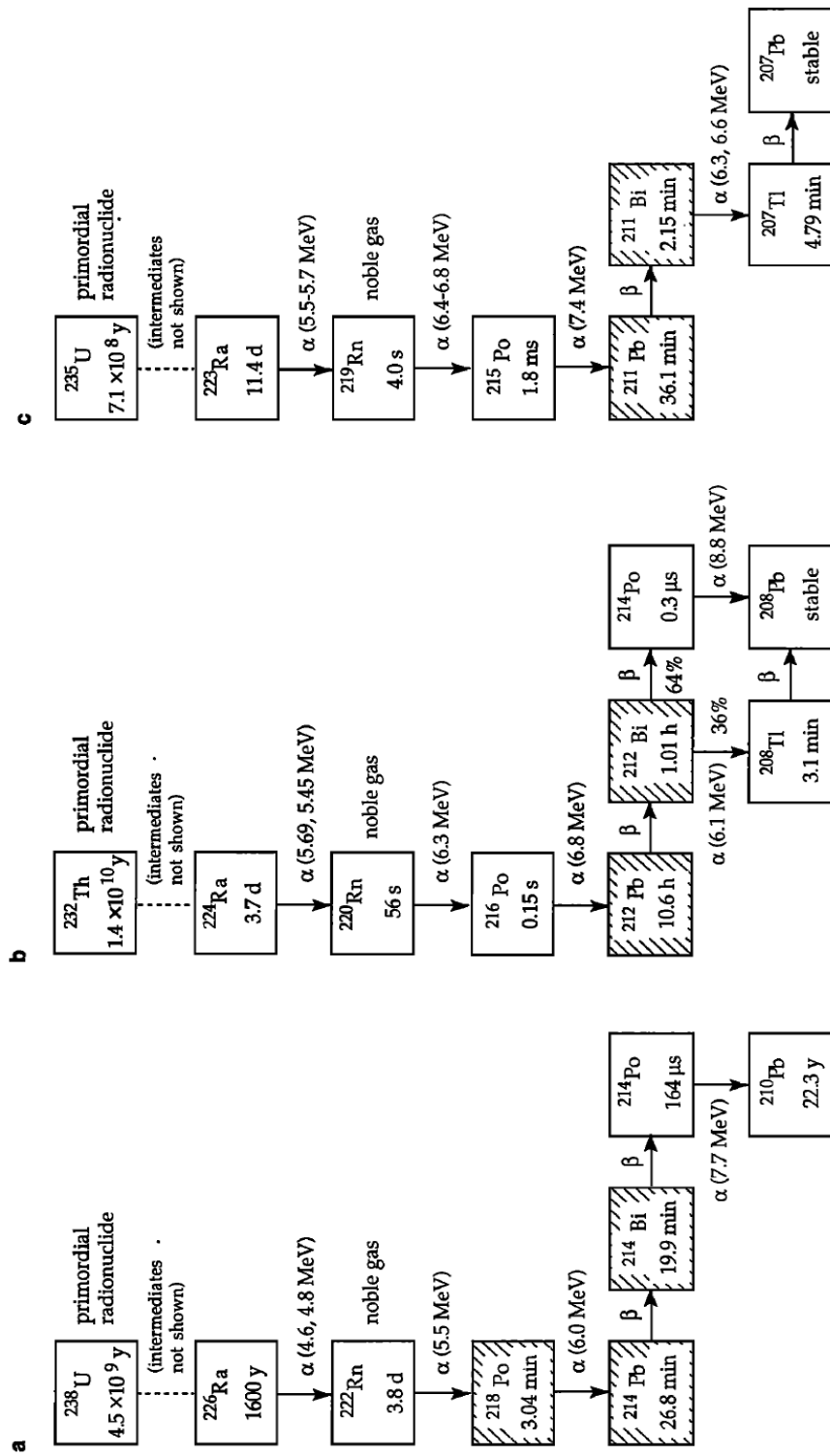


Fig. 1.1: Radioactive decay chains. (a) uranium 238 to lead 210, (b) thorium 232 to lead 208, and (c) uranium 235 to lead 207. Half-life and primary mode of decay are shown for each isotope. For each decay chain, inhalation of the shaded isotopes constitutes the primary health concern (after Nazaroff, 1992).

active and unstable isotopes namely; ^{219}Rn (Actinon), ^{220}Rn (Thoron) and ^{222}Rn (Radon) respectively (see Fig. 1.1). Rn-222 belongs to the U-238 decay chain generated by α -decay from its mother nuclide Ra-226 and it has a mean half-life of 3.823 days. Rn-220 is generated by α -decay of Ra-224 which belongs to the decay chain of Th-232 with a mean half-life of 56 sec. (Nazaroff, 1992). Rn-219 obtains from the decay series of U-235 and has a very short mean half-life of 3.96 sec. Because of its short half-life (3.96 sec.), ^{219}Rn is generally ignored in geochemical exploration. Rn-222 due to its longer half-life as compared to other isotopes, it undergoes a diffusive transport through thick soil layers or other materials. So it is considered to be most useful in geochemical surveys. In case of Rn-220, because of its relatively short half-life it is only useful in those areas where advective transport of soil-gas is particularly high or in areas containing significant amount of thorium-rich minerals phases in rocks. Moreover, being a gas ^{222}Rn near the ground surface has a great tendency to escape into the atmosphere. It has been indicated as possible precursor of earthquakes and volcanic eruptions (Giammanco *et al.*, 2007; Neri *et al.*, 2011). Besides, radon concentration in ground surface increases with depth which depends on the soils properties and moisture content (Jonsson, 1995; Kristianson and Malmqvist, 1984). Radon acts as an indicator for changes in the gas streams and such changes is most sensitive at the depth between 0.5 and 1m (Friedmann, 2012).

A meaningful earthquake prediction must give the information about the time, location and the size of a future earthquake. Many of the observation regarding earthquake prediction could give information about the location and the size of a future earthquake, but in most cases the time of the seismic event cannot be predicted. Therefore, an additional assumption is a must which are combined in the dilatancy theory and this theory was developed between 1970 and 1985 on the basis of dilatancy

and fluid flow (Scholz *et al.*, 1973). Dilatancy means an inelastic increase in volume under stress (Fig. 1.2).

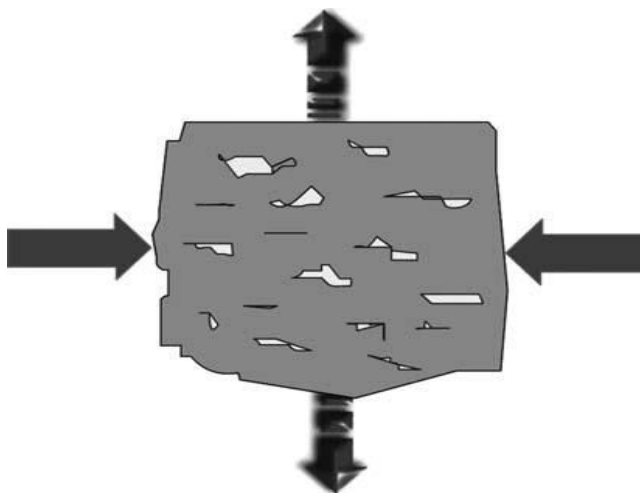


Fig. 1.2: Dilatancy: increasing stress causes cracks in the rock, which enlarges the material perpendicular to the main axis of stress. This causes an effective increase in volume (after Friedmann, 2012).

Under stress, cracks will be formed in rock material which enlarges the materials perpendicular to the main axis of stress and further causing an effective increase in volume (Friedmann, 2012). According to dilatancy theory, a considerable change in the rock properties will shortly occur before an earthquake assisting either water penetrates the cracks and/or the number of cracks increases exponentially. As a result, significant masses are moved which further causes the movement of sub- surface gases towards the earth's surface (Friedmann, 2012). In dry rocks opening or closing of cracks will lead to significant changes of the diffusion co- efficient of radon. Volumetric changes in the rock will also lead to a subsurface gas flow and therefore to an additional radon transport. If the new open cracks are filled with water the increased water-rock interface leads to an increase in the transfer of radon from the rock matrix to the water. If water filled cracks close, the water will be compressed to another subsurface volume where the emanation from the rock to the water may be different. All these effects result in

pressure and water level variations of the relevant aquifer. This also can lead to changes in the mixing ratios for the water which can be observed at the earth's surface. Finally gas flows can also move some groundwater and again all previously discussed mechanisms which are consequences of the redistribution of water in the earth's crust can take effects (Imme and Morelli, 2012). One of the main drawbacks of this theory is that it is confined to a small volume surrounding the impending earthquake and is not applicable to far field areas where many geochemical anomalies occur.

More realistic explanation of rock fracturing was proposed by Anderson and Grew (1977) in the study of stress corrosion cracking and Atkinson (1984) in subcritical crack growth. These studies have shown that the crack propagation is dependent on moisture content and crack growth can take place at very low strain rates under moderate to high level of humidity. Thomas (1988) suggests that the same phenomena could be useful for many of the ground gas anomalies observed at substantial distances from the impending earthquake. The observed radon anomalies are due to slow crack growth controlled by stress corrosion in a rock matrix saturated by ground waters. King (1978) proposed a compression mechanism to radon release. According to this mechanism, anomalous high radon release may be due to the crustal compression before an impending earthquake that squeezes out soil gas into the atmosphere at an increasing rate. Although several models have been proposed regarding geochemical precursors and its relation with earthquakes, most are associated with one of the following mechanism (Thomas, 1988).

- Physico-Chemical release by ultrasonic vibration (UV model).
- Chemical release due to pressure sensitive solubility (PSS model).
- Physical release by pore collapse (PC model).

- Chemical release by increased loss from, or reaction with, freshly created rock surfaces (IRSA model).
- Physical mixing due to aquifer breaching/fluid mixing (AB/FM model).

1.2 Dynamics of Earthquake

Most of the earthquakes are the result of movement of earth's crust produced by plate tectonics. As a whole, tectonic plates tend to move gradually. Due to the earth's relatively rigid upper layer called the lithosphere, these shallow- focus quakes would occur. The lithosphere, an approximately 100 km thick layer, which is made of the crust and a portion of the upper mantle, consists of two principal parts that are coupled. Although the upper part can sustain tremendous shear stresses and undergoes brittle fracture and seismic slip, the lower part behaves ductility and experiences aseismic slip. Particularly, earthquake occurs in the upper ten kilometers or so of the earth's crust. They arise as a consequence of frictional instabilities that cause stress, accumulated by large- scale plate motions over periods of hundreds of years, to be relieved in sudden stick-slip events. In other cases, deep in the crust frictional properties may allow stable sliding, so that strain is relieved smoothly and aseismically. The known deep earthquakes occurs along subducting plates, at depth of hundreds of kilometers and the basic physical processes that are responsible for these type of earthquakes are not well understood. But these types of events are suspected to be caused by the plates undergoing phase changes at the high temperature and pressures associated with large depths.

The motions of tectonic plates are driven by large- scale convective flows in the mantle. These flows take place on length scales of thousands of kilometers with turnover times of hundreds of millions of years; thus characteristic speeds are of the

order of centimeter per year. Thus, understanding these motions of the earth is yet another important object of research. These inner motions may be intrinsically chaotic; i.e. materials from the earth's core may be brought to the surface by intermittent plumes that rise through the mantle (Carlson *et al.*, 1994). The most seismological interest is the manner in which the inner flows couple to the brittle outer layers, thereby driving relative motions of the plates and producing the intricate patterns of cracks that what we called as earthquake faults. The basic principles of fracture mechanisms are the way how stresses applied to the crust have produced the kinds of faults that are known exist (Scholz, 1990). The earth's crusts are often driven by external forces in such a way that they are always at or near a threshold of instability. Tectonic plates retain their integrity or remain locked to one another until the stresses that are imposed upon as soon as an event is over. The occurrence of earthquake is predominantly along such zone is higher which makes it useful in earthquake precursory (Vaupotic *et al.*, 2010).

1.2.1 Description of Fault

Geological faults have an impact on geochemical anomalies. Faults on their own provide least strength zones constituted by fractured materials, gouge and fluids. The instabilities in crustal fluids are associated with active tectonic regions and triggers fluids flow. These fluids in turn have an impact on faulting as they influence the strength of a fault (Bernard *et al.*, 1996). Especially active faults are suitable for gas leakage, as gas migration is facilitated by increased soil permeability. King *et al.* (1996) measured ^{222}Rn in soil gas across a creeping fault, suggesting the presence of fault gouge leads to a low permeability zone. Muir wood *et al.* (1994) put forward that soil gas anomalies are dependent on the fault type (i.e. reverse or normal faults). Sometimes variations in permeability or porosity characteristics of the faulted zone due to self

sealing of fractures or weathering processes influence the geochemical signal. There may be an amplification of anomalies in pre- existing faults, if former stresses were near the critical levels and pore fluids are abundant (King, 1986; King, 1993). Active faults are faults describe distinctively by active slip, usually determined by seismic signals. Sudden motion along a fault is expressed by earthquakes. Along pre- existing faults, “stick- slip” frictional instability is responsible for slip of these faults, thus initiating earthquakes (Brece and Byerlee, 1966). Moreover, faults can be classified into different types depending upon the direction of relative displacement or slip (Fig. 1.3). Reverse fault form as a result of horizontal and vertical compression that squeezes the rock and creates a shortening of the crust. Normal fault, its movement is partly horizontal and partly vertical. In case of strike- slip fault is mainly horizontal and in opposite direction (Fig. 1.3).

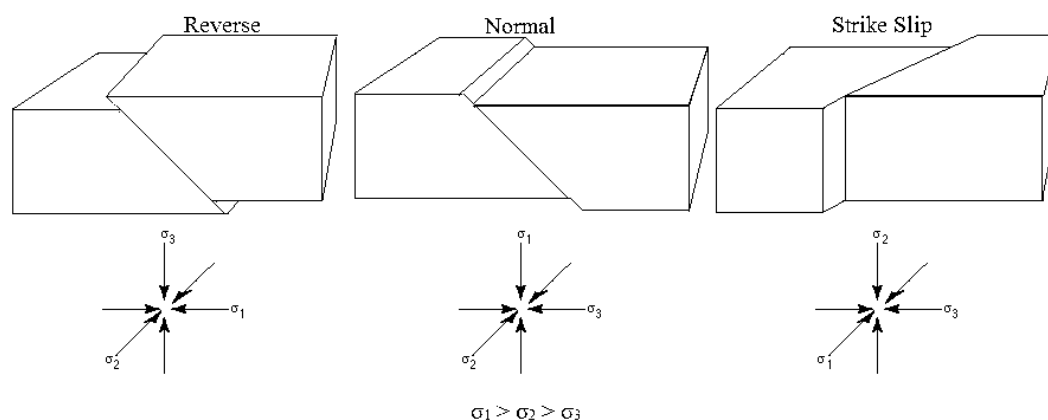


Fig. 1.3: Schematic of the orientation of the principal stresses and the corresponding type of faulting.

1.2.2 Formulation of Energy produced during fault formation

Let us take into account a simple stress-release model (Kanamori and Heaton, 2000). Fig.1.4 demonstrates the stress on the fault plane as a function of slip. An earthquake is caused when the stress on a fault plane exceeds the static frictional stress

(shear stress), σ_o . Plates on either side of the fault experience a relative displacement (slip), D over an area S as shown in Fig. 1.4.

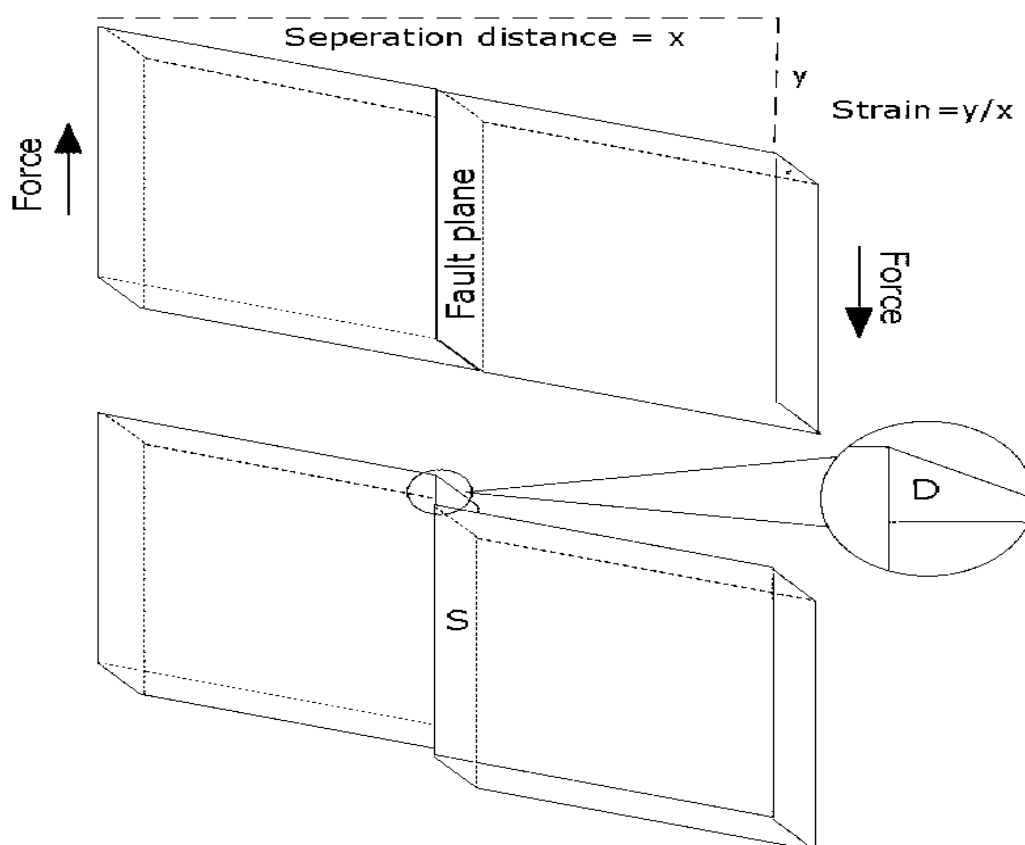


Fig. 1.4: A slab of crustal rock with two equal and opposite forces acting tangentially (after Kanamori and Brodsky, 2001).

At the initiation of an earthquake, the initial shear stress σ_o drops to a constant dynamic friction σ_f . At the end, the stress on the fault plane is σ_l (final stress) and the average slip offset is D . For the example which is shown in Fig. 1.5a, $\sigma_f = \sigma_l$. The dynamic stress drop, $\Delta\sigma_d = \sigma_o - \sigma_f$, initially drives the sliding. The sliding stops when the shear stress drops below a final frictional stress, σ_l . A variety of mechanism can stop sliding, such as geometric and compositional heterogeneity, dynamically changing velocity or history dependent friction and so σ_l is not necessarily equal to σ_f (Kanamori and Brodsky, 2001).

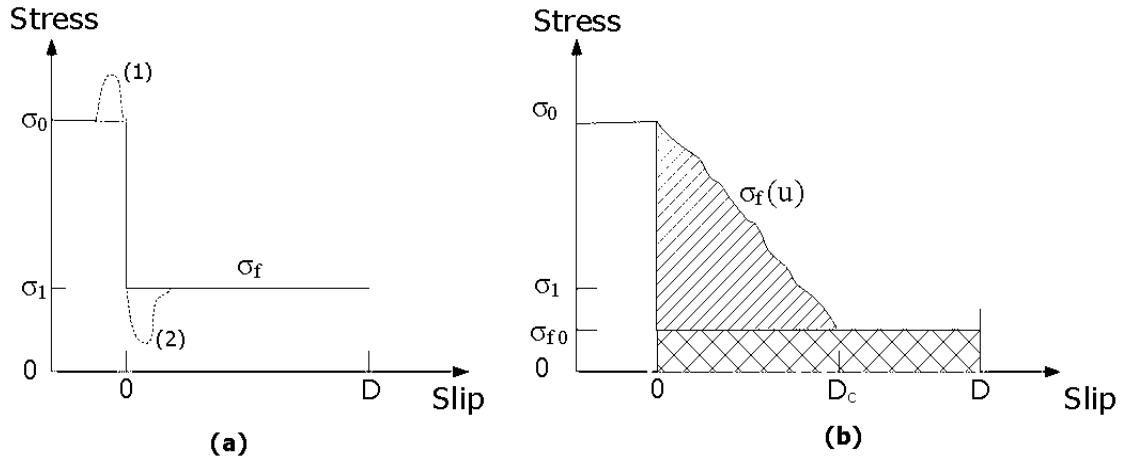


Fig. 1.5: Illustration of simple stress release pattern during faulting. (a) Simple case. (b) Slip-weakening model. Hatched and cross-hatched areas indicate the fracture energy and frictional energy loss.

The difference between the initial and the final frictional stresses is the static stress drop, $\Delta\sigma_s = \sigma_o - \sigma_1$. The overall size of the earthquake is the seismic moment defined by $M_o = \mu SD$. The seismic moment is measured in energy unit, but it does not directly represent the energy released by an earthquake. The magnitude M , of an earthquake is given in terms of seismic moment (Kanamori and Brodsky, 2001),

$$M = (\log M_o - 9.1)/1.5 \quad (M_o \text{ in Nm}) \quad (1.1)$$

During the process of earthquake, the potential energy (strain energy plus gravitational energy) of the system, W , drops to $W - \Delta W$ where ΔW is the strain energy drop and the seismic wave is radiated carrying energy E_R . Then the energy budget can be written as (Kanamori and Heaton, 2000),

$$\Delta W = E_R + E_F + E_G \quad (1.2)$$

where, $E_F = \sigma_f DS$ is the frictional energy loss, E_G is the fracture energy, and $\Delta W = (\sigma_o - \sigma_1)/2$ (Knopoff, 1958; Dahlen, 1977). Therefore, Eq. (1.2) becomes,

$$\begin{aligned}
E_R &= (\sigma_o + \sigma_1)DS/2 - \sigma_f DS - E_G = \frac{1}{2}(2\Delta\sigma_d - \Delta\sigma_s)DS - E_G \\
&= M_o(2\Delta\sigma_d - \Delta\sigma_s)/2\mu - E_G
\end{aligned} \tag{1.3}$$

For large and shallow earthquakes E_G can be ignored (Heaton, 1990), and Eq. (1.3) can be written as,

$$E_R = M_o(2\Delta\sigma_d - \Delta\sigma_s)/2\mu \tag{1.4}$$

Stress variation during faulting can be more complex than shown in Fig. 1.5a. It may increase in the beginning of the slip motion (curve (1) in Fig. 1.5a) because of loading caused by advancing rupture, or of the state-rate dependent friction law (Dieterich, 1979). Also, the friction may not be constant during faulting. It may drop drastically in the beginning and later resume a larger value (curve (2) in Fig. 1.5a) or, it may decrease gradually to a constant level (Fig. 1.5b). If the friction is not constant, σ_f drops to a constant value σ_{fo} until the slip becomes D_c . The final stress σ_l can be different from σ_{fo} . Then the average friction $\bar{\sigma}_f$ is given by (Kanamori and Heaton, 2000),

$$\bar{\sigma}_f = \frac{1}{D} \int_0^D \sigma_f(u) du \tag{1.5}$$

where, u is the slip (offset) of the fault plane. Then Eq. (1.5) can be written as,

$$E_R = M_o(2\Delta\bar{\sigma}_d - \Delta\sigma_s)/2\mu \tag{1.6}$$

where, $\Delta\bar{\sigma}_d = \sigma_o - \bar{\sigma}_f$.

1.3 Models of Earthquake precursors

There is various earthquake rupture process having some common features that is the earthquake precursory anomalies are thought to be driven by rapid and probably

non- linear strain and strain changes within the earth in the rock near or in the fault zone at the region of the eventual earthquake rupture. Some of the discrete models explaining the critical state in earthquake preparation process are discussed below

1.3.1 The IPE model

The concepts of fracture mechanics allows us to create a qualitative picture of the earthquake preparation process and to explain the characters of the precursors are summarized as follows (Mjachkin *et al.*, 1975)

- 1) Fracture of statistically heterogeneous materials is caused by the increase of number and size of crack-like defects.
- 2) The defects may develop in time under approximately constant stress and the rate of their formation increases with the increase of stress.
- 3) The total deformation consists of intrinsic elastic deformation and deformation caused by mutual displacement of crack edges.
- 4) Macro fracture (development of the main fault) is the result of the avalanche-like growth and resulting instability which occurs on reaching a certain density of cracks.
- 5) Formation of the main fault results in the decrease of stress level in the surrounding volume; as a result the growth of new defects stops and the number of active cracks is decreased.
- 6) The fracture process does not depend strongly on scale.

According to these concepts, the temporal-spatial course of the earthquake preparation process can be visualized as follows. In real rocks there always exist randomly distributed defects (microcracks). Under the influence of tectonic shear stress the number and size of favorably oriented defects slowly increases and new one are

formed. In statistically homogeneous media, such cracking takes place through- out the whole volume. One of the causes of uniformity of cracking is the formation of stable tension cracks at the end of shear cracks (Brace and Bombolakis, 1963). During this stage there should be changes in medium properties such as effective modulus of elasticity and anisotropy. Fig.1.6 depicts the deformation process in the earthquake preparation zone.

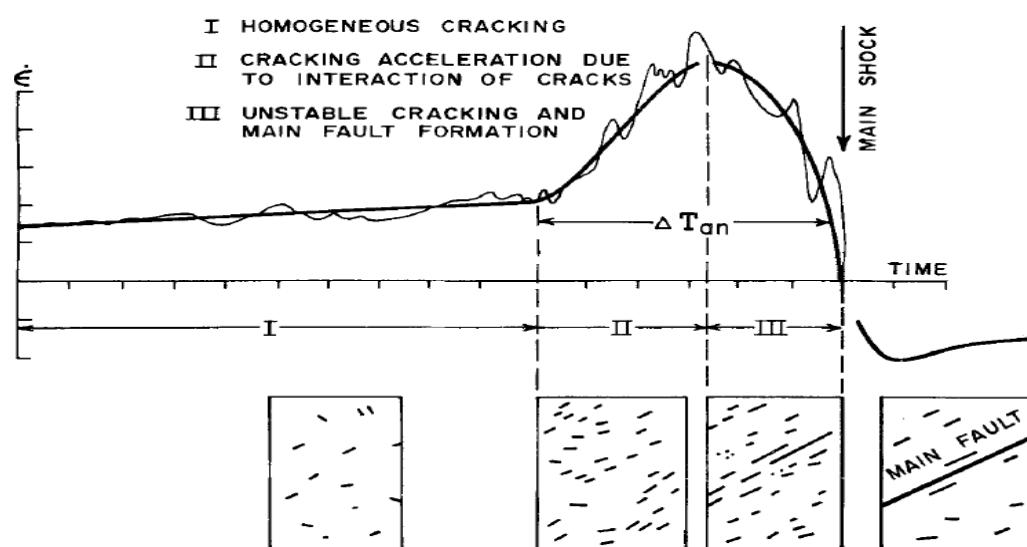


Fig. 1.6: Change of average deformation velocity during the seismic cycle (from Mjachkin *et al.* 1975).

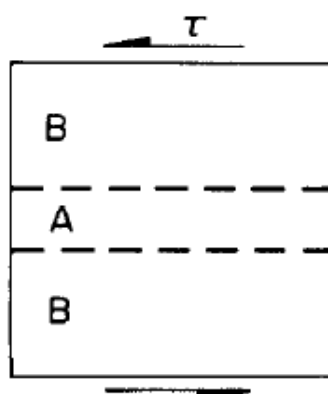


Fig. 1.7: An ideal scheme of formation of the zones of unstable deformation. A – zone of unstable deformation, B – zone of unloading (from Mjachkin *et al.*, 1975).

Stage I indicates the uniform cracking in which precursors do not yet develop. Then transition to stage II happens when a certain critical average density of cracks is reached in most of the volume. Because of the interaction of cracks in stage II, an accelerating or avalanche took place which result in a sharp increase in the rate of total deformation. Therefore cause sudden changes in physical characteristics of the medium. If this process leads to the earthquake then it is by definition, unstable. It means that the further increase of deformation is accompanied by decrease of stress. Due to heterogeneity of the medium, unstable deformation is restricted to a narrow zone where several relatively large cracks are formed. From Fig. 1.7, in narrow zone A the process of unstable deformation occurs, while in the surrounding zone B stop developing. Because of the general decrease of stresses in stage III the cracks in B stop developing. Rate of deformation of the whole zone is reduced during this of instability and restoration of many original characteristics of the rock takes place. The narrow zone of unstable deformation, A is characterized by increased concentration of small faults parallel to the future main fault. This main fault, assumed to form during the earthquake, which is formed by collapse of the solid material between the small faults. Qualitatively, formation of the main fault is similar to the growth or extension of small cracks in II and III. Therefore those small events should be preceded by a short- term, small-amplitude change of deformation velocity. There may be several such short-term changes of deformation velocity, these fluctuations might appear as foreshocks to the main event (Mjachkin *et al.*, 1975). Moreover, the increase of radon content and other products of radioactive decay is connected with the amount of cracking of rocks. Therefore, is sharply increased at stage II and flattens out at stage III. Decrease can be expected before the earthquake when many small cracks become closed. The behavior of precursors applies to the region where the processes of avalanche- like increase of

cracking and their further localization to the fault surface takes place. When crustal deformation and physical characteristics are measured outside this region the effects will be connected not only with cracking but also with relatively sharp change in the stress field.

1.3.2 The dilatancy- diffusion model

Much effort has been devoted to explaining the earthquake precursors on the basis of dilatancy and fluid flow in USA since 1971. Dilatancy is the non- elastic increase in volume caused by stress and it has been well known in the field of soil mechanics, first being noticed for rocks by Bridgman in 1949. In soils, the dilatant volume change is in the form of void space between the grains. In case of rocks, the dilatant expansion takes the form of new cracks which open up between and through the grains (Mjachkin *et al.*, 1975). In rock masses one might expect dilatant cracks in two forms- firstly as simply a large- scale version of the micro- crack having the same relation to the principal stresses as dilatant micro- cracks. Secondly, large- scale form of dilatant crack might be along those joints, faults which oriented in the appropriate direction relative to maximum compression. Nur and Simmons (1969) suggested that the dry cracks have large effects on seismic velocities. Opening of new cracks and/or the expansion of old cracks may be responsible for large decrease in velocity and V_p/V_s ratio prior to thrust type earthquakes (Nur, 1972; Whitcomb *et al.*, 1973). Nur (1972) put forward that the effect of dilatancy on velocity might depend strongly on whether the dilatant cracks contained water or mixture of water and/or air or vapour. And the changes in V_p/V_s ratio should be reverse in these two cases. The different steps of the complete dilatant model are as follows (see Fig. 1.8) (Scholz *et al.*, 1973). During stage

I stress is increasing but dilatant cracks have not yet begun to open or form. In stage II dilatant cracks form and become under saturated. The various properties like velocity and resistivity respond appropriately to this effect. In stage III it is assumed that water

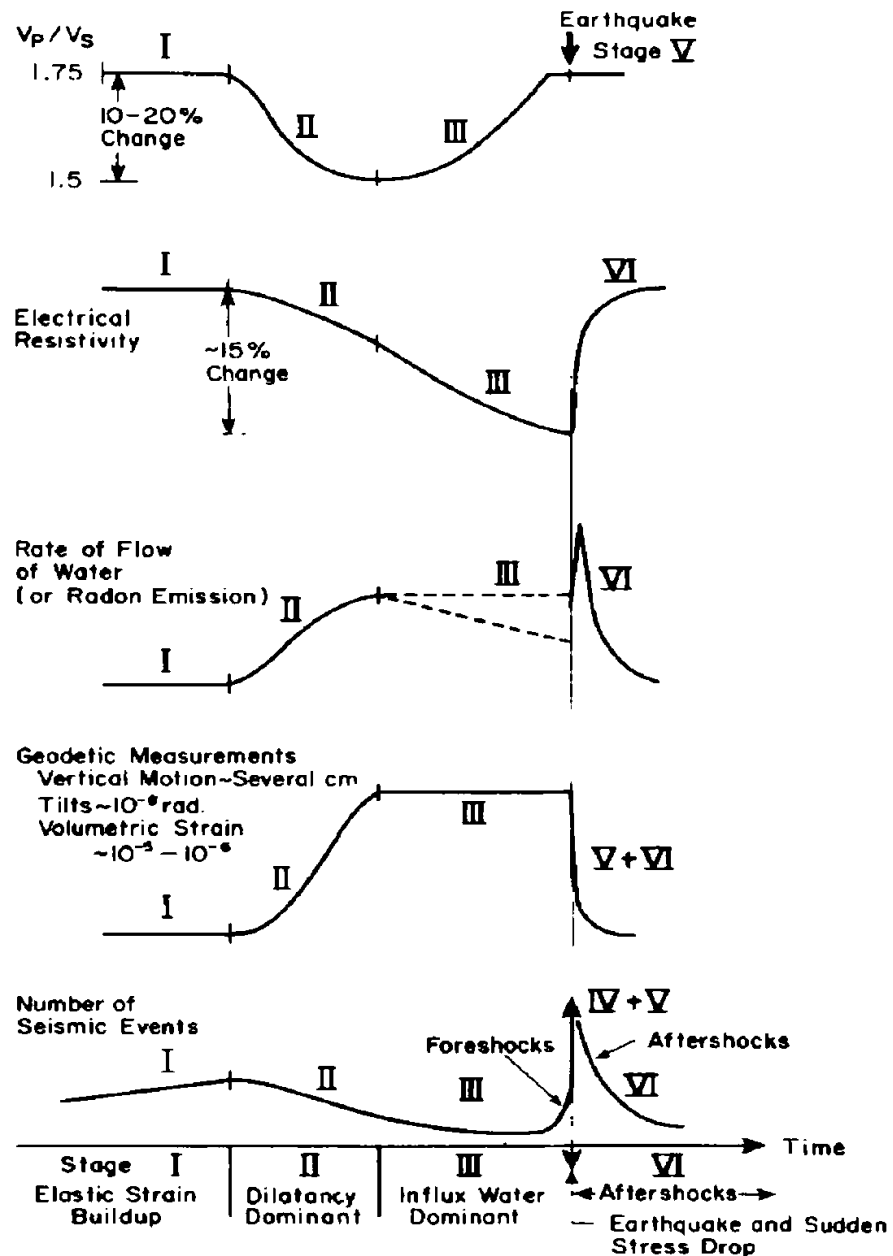


Fig. 1.8: Predicted Changes in various physical parameters as a function in time during the earthquake cycle for the dilatancy model (from Scholz *et al.*, 1973)

re-enters the dilatant rocks causing a recovery of the various physical properties back to their initial level. This re- entering of water and subsequent increase in the pore pressure

lowers the effective confining pressure and hastens the fracture or frictional sliding which causes the earthquake at the end of stage III. The influx of water in stage II comes about because permeability also increases extreme rapidly in dilatants rock. The effect of pore fluid on seismic velocities has been studied in detail by Anderson and Whitcomb (1973) which is shown in Fig.1.9.

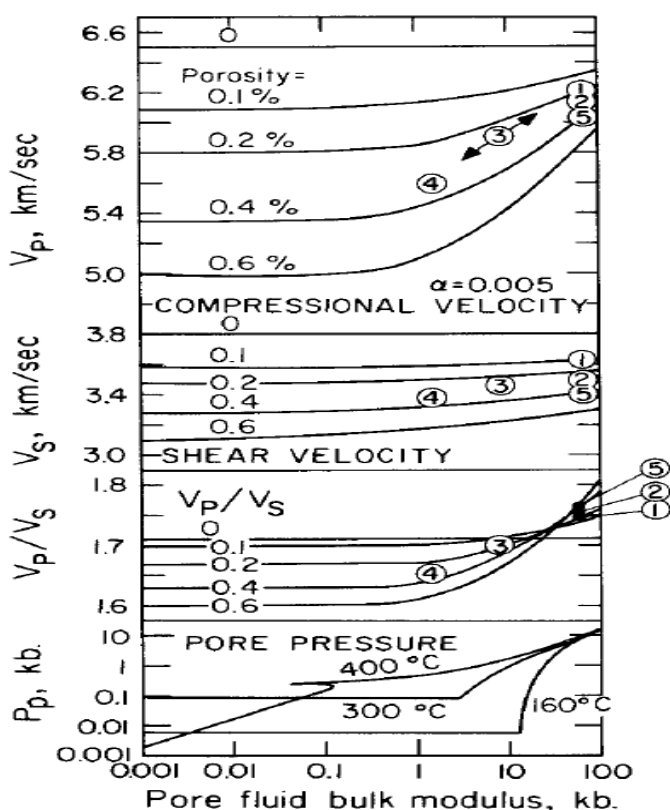


Fig. 1.9: Compression velocity (V_p), shear velocity (V_s) and V_p/V_s as a function of pore fluid bulk modulus and porosity. The lower panel gives the pore fluid bulk modulus as a function of pore pressure (P_p) and temperature. Circled numbers refer to successive stages from onset of dilatancy 1 to fracture 5 with initial porosity of 0.2% (after Anderson and Whitcomb, 1973).

A brief comparison of the IPE and the DD models was given by Mjachkin *et al.* (1975) which include the following points.

- According to the IPE model the earthquake occur as a fault is formed; it involves fracture of intact rock on a large scale comparable with the dimensions of the

main rapture. This might involve either new faulting, the extension of an old fault into new rock, or the re-fracture of a healed fault. According to the DD model an earthquake can result from motion on a pre existing fault; it does not require large-scale fracture.

- In the IPE model, the earthquake occurs after a stress drop having duration of approximately half the anomaly time. The main earthquake occurs at significantly less than the maximum stress prior to the earthquake. By contrast, the earthquake in DD model occurs near the peak stress.
- In both models cracks develop uniformly at first over some volume of rock adjacent to the future rapture surface. In the IPE model cracks of a different orientation form in a zone near the fracture fault (zone A in Fig. 1.7) just prior to the earthquake, even in the central part of a long fracture fault. No such zone is required according to the DD model; cracks may enlarge prior to the earthquake but orientation should remain same throughout the anomalous period.
- Pore fluids play a central role in the DD model whereas they are not required in the IPE model.

In the IPE model, the cracks which form in response to stress have an orientation parallel to the main fault prior to the earthquake. In the DD model cracks are parallel to the plane of the least compression and thus inclined to the main fault.

1.3.3 Slider- Block Model

The Burridge- Knopoff spring- block model is a two- dimensional dynamical system of blocks interconnected by springs. It was first introduced by Burridge and Knopoff in 1967 with a family of high-dimensional dynamical models with the most direct

relevance to the behavior and understanding of earthquake faults. Each block is connected to the four nearest neighbors. This model with massive blocks with the same size and mass connected to each other by springs with spring constant K_C . The whole mass- spring system is fixed to a rigid plate and connected to the slider plate (with constant velocity V) by springs with spring constant K_L as shown in Fig. 1.10. When the mass-spring system is dragged on the fixed rigid plate by the driving plate, some blocks slip at regular interval of time.

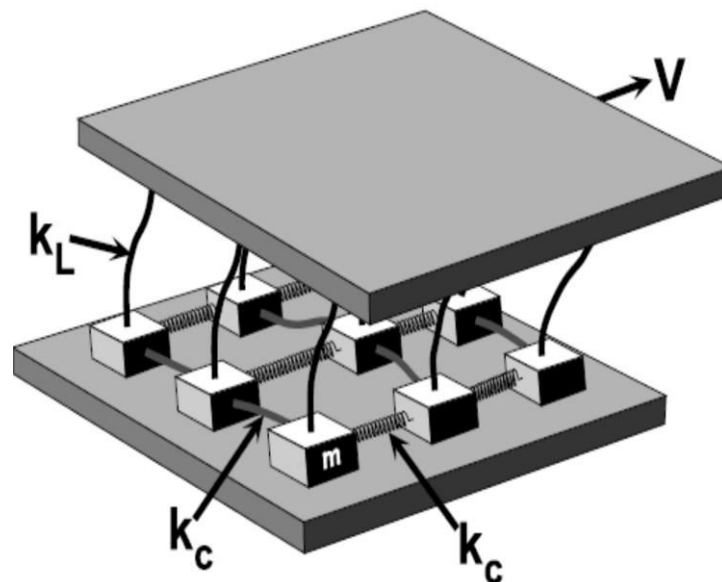


Fig. 1.10: Illustration of the two-dimensional slider block model (after Rundle *et al.*, 2003).

The slip of a single block is interpreted as small earthquakes with the release of some potential energy. Sometimes, the slip of a single block will redefine the forces on its nearest neighbors and triggers slip of adjacent blocks causing large earthquake with larger amount of potential energy released (Kanamori and Brodsky, 2004). The interaction between the blocks is described by a differential equation that involves the spring stiffness, mass and friction. In order to derive the differential equation let us consider a block of mass m pulled over a surface by a spring constant k_L attached to the

constant velocity V driver plate. For simplicity let us consider a one-dimensional chain of slider blocks (Fig. 1.11). The springs simplify the dynamics by restricting the blocks to move along or opposite to the plate's motion. To produce dynamic instability the velocity-dependent frictional force should decrease as the sliding block's velocity increases.

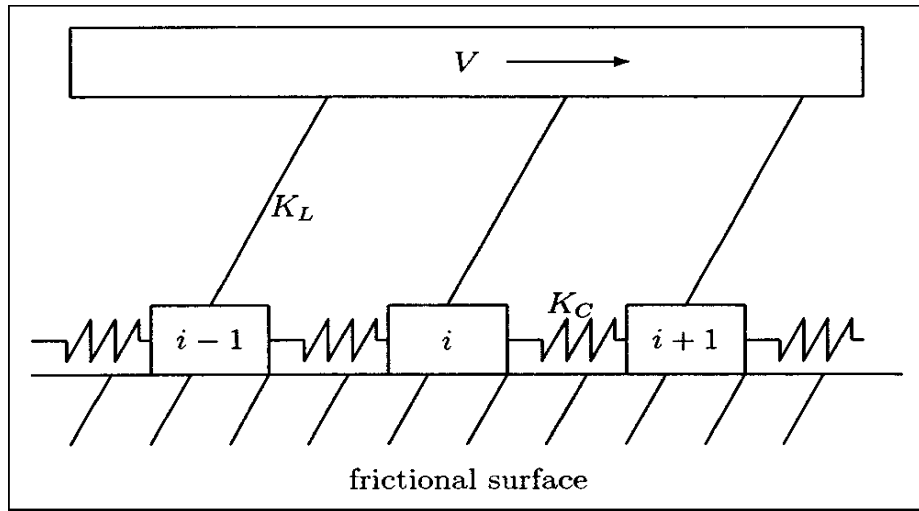


Fig. 1.11: Schematic of a simple one-dimensional slider block model.

The total force acting on the i^{th} block is given by,

$$F_i = F_C + F_L - \Phi \quad (1.7)$$

where, F_C is the force arising from the springs connected to the neighboring blocks, F_L is the force due to the spring which connect the block to the driver plate and Φ is the velocity dependent friction force acting on the block (Olami *et al.*, 1992). According to Newton's second law of motion, the equation of motion for block i is,

$$F_i = m\ddot{X} \quad (1.8)$$

Now,

$$F_C = F_{i-1} + F_{i+1}$$

$$\Rightarrow F_C = k_C(X_{i-1} - X_i) + k_C(X_{i+1} - X_i)$$

$$\Rightarrow F_C = k_C (X_{i+1} - 2X_i + X_{i-1}) \quad (1.9)$$

And,

$$F_L = k_L (Vt' - X_i) \quad (1.10)$$

where, X_i is the displacement of the block from the initial position and t' is the time. Substituting, Eq. (1.8), (1.9) and (1.10) in Eq. (1.7) we have the equation of motion as follows

$$m\ddot{X}_i = k_L (Vt' - X_i) + k_C (X_{i+1} - 2X_i + X_{i-1}) - \Phi(\dot{X}_i) \quad (1.11)$$

In order to make the equation dimensionless, the time t' is measured in units of characteristics frequency, $\omega = \sqrt{k_L/m}$ and the displacement X_i in units of length $L = \Phi(0)/k_L$, $\Phi(0)$ being reference value of the friction force. The dimensional quantities can be written as follows (Kawamura *et al.*, 2012),

- Dimensionless time: $t = t'\omega \Rightarrow t' = t/\omega$
- Dimensionless displacement: $x_i = X_i/L \Rightarrow X_i = Lx_i = \frac{\Phi(0)}{k_L} x_i$
- Dimensionless stiffness parameter: $l = \sqrt{k_C/k_L}$
- Dimensionless loading rate: $v = V/(L\omega)$
- Dimensionless friction force: $\phi(\dot{x}_i) = \Phi(\dot{X}_i)/\Phi(0)$

Substituting these new quantities in Eq. (1.11) we get the dimensional equation of motion as,

$$\ddot{x}_i = vt - x_i + l^2 (x_{i+1} - 2x_i + x_{i-1}) - \phi(\dot{x}_i) \quad (1.12)$$

The dimensionless friction force is given by (Carlson *et al.*, 1991),

$$\phi(\dot{x}) = \begin{cases} (-\infty, 1], & \text{for } \dot{x}_i \leq 0, \\ \frac{1 - \sigma}{1 + 2\alpha\dot{x}_i / (1 - \sigma)}, & \text{for } \dot{x}_i \geq 0 \end{cases} \quad (1.13)$$

The friction force is characterized by two parameters, σ and α . σ represents an instantaneous drop of the friction force and α represents the rate at which the friction force decreases as the sliding velocity increases. It is assumed that the loading rate v to be infinitesimally small ($v = 0$) during an earthquake event (Mori and Kawamura, 2005).

1.4 Migration mechanism of Radon and Thoron

The concentrations of radon and thoron vary essentially with time and space. Its activity level in air is much more significant contribution to radiation exposure than those in water. Radon and thoron levels in air or water depends on four factors i.e., the nature of the source, its emanating power, transport of radon and thoron from the source and their ultimate dispersal. The main sources of radon and thoron in soil are radium and thorium in the global atmosphere. In practice, ^{228}Th ($T_{1/2}$ 1.9 a) and ^{228}Ra ($T_{1/2}$ 5.8 a) control the thoron exhalation rate. The physical mechanism of radon and thoron release from the structure of the rocks is not yet fully understood. The fraction of the radon or thoron atoms obtained in a solid which enters into the pores of the medium and thereby becomes amenable to transport, is defined as the emanating power of the solid for radon or thoron (Andrews and Wood, 1972; Tanner, 1980).

The transport and emanation process of radon and thoron from a solid into air or water occurs through diffusion and flow of the air or water. High porosity in soil increases the diffusion rate (Megumi K. and Mamuro T., 1974). The short half- life of thoron (55s) limits its migration to less than one percent of that of radon (Jacobi and

Andre, 1963). Radon in rock or soil may be released by mechanism forces in the earth causing changes of pore space through compression stresses. Such type of mechanism might explain intermittent variation in radon exhalation from soil surfaces.

1.4.1 Recoil effect

Tanner (1980) proposed a physical mechanism describing radon emanation from soil by recoil effect (Fig 1.12). He expressed that radon atom which terminates their recoil path into the liquid or gas phase may escape from the crystalline matrix (solid grains). The atoms which are specified at a distance from the edge of grain which is greater than the recoil length or those which terminate their path inside the adjacent grain remain trapped within solid phase and therefore not available for convective transport. The recoil energy of radon and thoron atoms are 86 and 103 Kev respectively (Bossus, 1984). The newly developed atom travel from its site of generation until its energy is transferred to the host material and the distances travelled depend on the density and composition of the material (Nazaroff, 1992). The range of recoil of radon in air is 63 μ m and for thoron is 83 μ m (Tanner, 1980). The emanation coefficient can be strongly affected by the moisture content in the soil (Stranden *et al.*, 1984), its coefficient increases with soil moisture up to saturation in the normal range of soil moisture content.

In a very dry solid the release of radon or thoron is reduced by re- adsorption of radon and thoron atoms on surfaces in the pores and fractures in the solid. If the solid is slightly moist, the release is enhanced up to certain moisture content, at higher level it decreases again because of the lower diffusion rate in water- filled pores (Megumi and Mamuro, 1974). Apart from the soil moisture effect, grain size and temperature dependence has also been analyzed. Radon emanation increases with decreasing grain

size (Markkanen and Arvela, 1992; Moraoska and Jeffris, 1994). This can be clearly explained by the recoil theory, the fact that the smaller the grain size, the larger the surface area which is available for Ra-226 adsorption (Megumi and Mmuro, 1974).

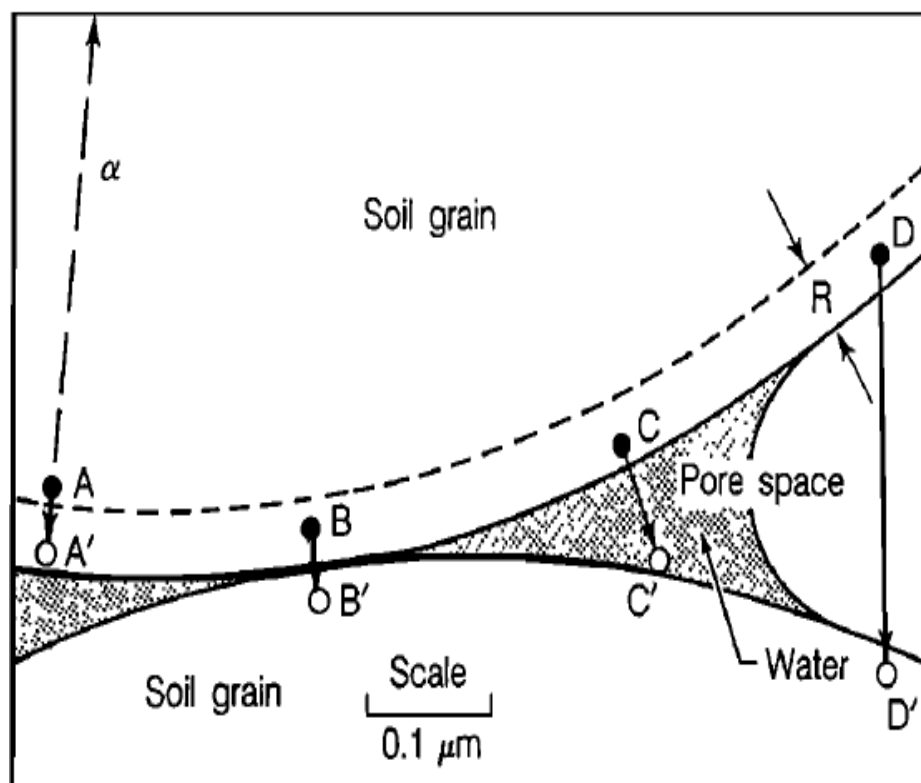


Fig. 1.12: Schematic sketch of the possible emanation scenarios in a solid-water-air system. Radium atom, indicated by solid circles, decay, producing an alpha particle and a recoiling radon atom which may end its recoil at the point indicated by the open circle; R = recoil range; case A-A') ^{222}Rn remains inside the grain; case B-B') ^{222}Rn reaches the adjacent grain; case C-C') ^{222}Rn atom reaches the water filled pore space, possibly reaching the air filled pore space by diffusion; case D-D') recoil energy is large, ^{222}Rn crosses the air filled pore space and penetrates into the adjacent grain (after Tanner, 1980).

Stranden *et al.* (1984) observed that radon exhalation rate for a soil sample increases by 55% with the increase in temperature from 5 to 50°C. Once radon and thoron atoms have reached the pore space (surrounding water or air phase), they are

further transported towards the earth's surface by the process of diffusion and advection, thus moving away from the source. A schematic diagram regarding the generation of radon in soil followed by the migration and entry in to the atmosphere or building is shown in Fig. 1.13.

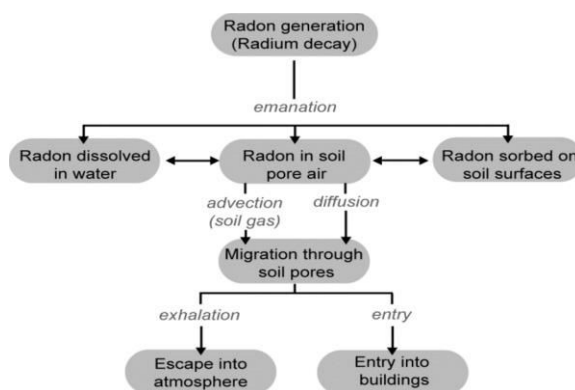


Fig. 1.13: Schematic representation of radon generation and migration in the soil and its entry into the atmosphere or buildings (after Nazaroff *et al.*, 1992).

1.4.2 Migration by Diffusion

Radon and thoron enter the air contained in soil by diffusion from soil particles or sometimes from radon- rich ground water at greater depths. The concentration of radon and thoron in this air decreases with decreasing distance from the surface because the gases escape to the open air above the ground. Diffusion is the process by which a substance is transported from one part of a system to another. This occurs predominantly in interstitial pores and micro fractures where the net migration to regions of low concentration (Nazaroff, 1992; Dongarra and Martinelli, 1993). This diffusion process can be expressed as follows

$$C_x = C_0 \exp[-x / L] \quad (1.14)$$

Where C_x is the radon or thoron concentration at a distance x in water or air from the surface, C_0 is the concentration at the surface, $L=D/\lambda$ where D is the diffusion co-

efficient and λ the decay constant (Tanner, 1964). The value of the length of diffusion (L) for dry to moist soils is 1m for radon and 1cm for thoron (Nazaroff, 1992).

1.4.3 Migration by advection

The term advection is due to migration by pressure gradient. Migration due to pressure gradient necessitates the presence of certain amount particular gas species. The transport velocity of radon in the earth is quite low ($\leq 10^{-3} \text{ cm s}^{-1}$). The concentration of radon is reduced by radioactive decay to the background level before even 10 m is traversed (Etiope and Martinelli, 2002; Fleischer, 1981) and the amount of radon in the sub-surface is too small to flow autonomously by advection. Therefore, it must be carried by macroscopic flow of gases such as CO_2 , CH_4 and N_2 which serve as the carrier gases for radon (Etiope and Martinelli, 2002; Kristiansson and Malmqvist, 1982). Taking into account the addition of a component v (velocity of transport), Grammakov (1936) computed the concentration of radon at a distance x from the surface with concentration C_o by the following equation,

$$C_x = C_o \exp \left[\left\{ \left(\frac{v}{2D} \right) - \left(\frac{v^2}{4D^2} + \frac{\lambda}{D} \right)^{1/2} \right\} x \right] \quad (1.15)$$

Diffusion or advection migration of radon may occur simultaneously whereas diffusion may take place alone (Monnin and Seidel, 1992).

1.5 Description of the statistical methods applied in the study

1.5.1 Artificial Neural Network

Artificial neural network (ANN), originally developed to mimic basic biological neural system – the human brain particularly, is composed of a number of

interconnected simple processing elements called neurons or nodes. Each node receives an input signal which is the total “information” from other nodes or external stimuli processes it locally through an activation or transfer function and produces a transformed output signal to other nodes or external outputs. Although each individual neuron implements its function rather slowly and imperfectly but however collectively a network can perform a surprising number of tasks quite efficiently (Reilly and cooper, 1990). This information processing characteristics makes ANN powerful computational tools that enable us to learn from examples and then generalized to examples never seen before (Zhang *et al.*, 1998).

There is no universally accepted definition of an artificial neural network. It is a massively parallel distributed information processing system that has certain performance characteristics resembling the biological neural networks of the human brain (Haykin, 1994). Fig. 1.14 shows the block diagram of a neuron (C.R. Arjun and Ashok, 2009).

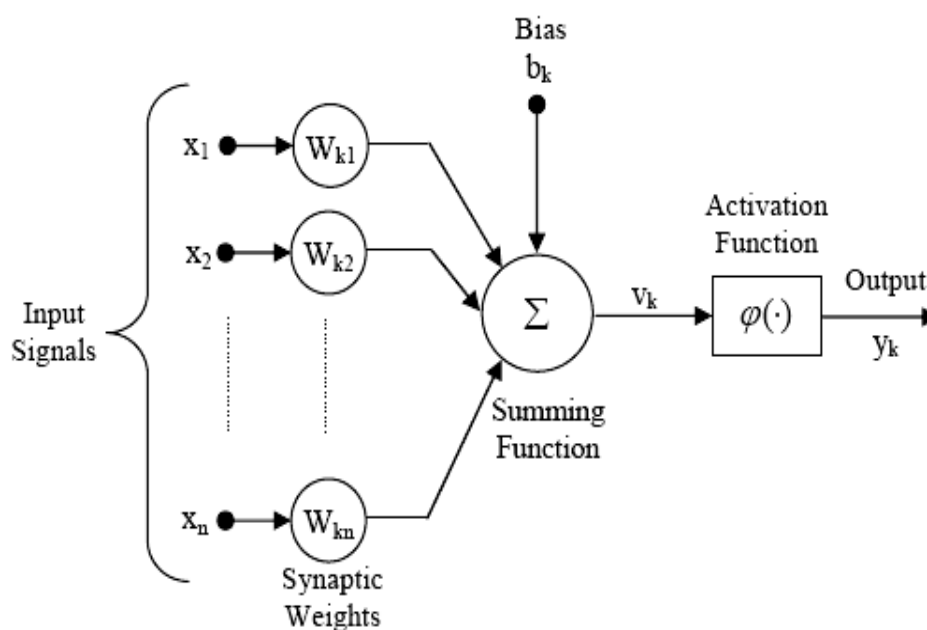


Fig. 1.14: The block diagram of a neuron (Haykin, 1994).

A neuron consists of three main parts: a set of synapses, which connect the input signal x_j to the neuron via. A set of weight W_{kj} ; an adder U_k which sums up the input signal, weighted by the respective synapses of the neuron; and an activation function $\phi(\bullet)$ for limiting the amplitude of the output of the neuron. At times, a bias b_k is added to the neuron to increase or decrease the net output of the neuron. Mathematically, a neuron k is describe as (Haykin, 1994)

$$U_k = \sum_{j=1}^n W_{kj} X_j \quad (1.16)$$

$$Y_k = \phi(U_k + b_k) \quad (1.17)$$

Where $x_1, x_2, x_3, \dots, x_n$ are the input signal; $w_{k1}, w_{k2}, \dots, w_{kn}$ are the weights for the neuron k ; b_k is the bias; U_k is the adder or the linear combiner; $\phi(\bullet)$ is the activation function; and Y_k is the output signal of the neuron.

The output range of the neuron depends on the type of activation function used. There are four types of activation function namely, the hard- limit activation function, the log-sigmoid activation function, the tan-sigmoid activation function and the linear activation function. Many different ANN models have been proposed since 1980s. Perhaps the most influential model are the multi-layer perceptrons (MLPs), Hopfield networks and Kohonens self organizing networks. The MLP networks are used in a variety of problems especially in prediction and forecasting because of their inherent capabilities of arbitrary input-output mapping. There are also other types of ANNs such as radial- basis functions networks (Park and Sandberg, 1993; Chng *et al.*, 1996), ridge polynomial networks (Shin and Ghosh, 1995) and wavelet network (Zhang and Benveniste, 1992) are also very useful in some application due to their function approximation ability.

1.5.2 Multiple Linear Regressions (MLRs)

The Multiple linear regressions model is an extension of a simple linear regression model incorporate two or more explanatory variable in a prediction equation for a response variable. Multiple regressions modeling are now a mainstay of statistical analysis in most of the fields because of its power and flexibility. It requires very little effort to estimate very complicated models with large numbers of variables. In a regression analysis we study the relationship, called the regression function between one variable Y , called the dependent variable and several others X_i , called the independent variables. Regression function also involves a set of unknown parameters b_i . If a regression function is linear in the parameters, it is termed as linear regression model. Otherwise, the model is called non-linear. Linear regression models with more than one independent variable are referred to as multiple linear models as just opposite to simple linear models with one independent variable. The following notations have been used in this work:

- Y^* - dependent variable (predicted by a regression model)
- Y - dependent variable (experimental value)
- p - number of independent variables (number of co-efficients)
- X_i ($i=1, 2, \dots, p$) - i^{th} independent variable from total set of p variables
- b_i ($i= 1, 2, \dots, p$) - i^{th} co-efficient corresponding to X_i
- b_0 - intercept (or constant)
- $i= 1, 2, \dots, p$ - independent variable index

A general MLR model can be formulated as the following equation

$$Y^* = b_0 + \sum_i^p b_i X_i, \quad i = 1, 2, \dots, p \quad (1.18)$$

I. Multiple r and r²

For simple linear regression it is important to look at the correlation between the outcome and explanatory variable (Pearson's r) and the r^2 (the co-efficient of determination) to ascertain how much of the variation in the outcome could be explained by the explanatory variable. Multiple r is the equivalent of Pearson's ' r ' rather than representing the magnitude and direction of a relationship between two variables. It shows the strength of the relationship between the outcome variable and the values predicted by the model as a whole. It tells us how well the model predicts the outcome (or how well the model fits with the data). A multiple r of 1 means a perfect fit while a multiple r of 0 means the model is very poor at predicting the outcome. The r^2 can be interpreted in the exact same way as for simple linear regression; it represents the amount of variation in the outcome that can be explained by the model, although now the model will include multiple explanatory variables rather than just one.

II. Methods of variable selection

When creating a model with more than one explanatory variable a couple of complications may arise. Firstly, we may be unsure about which variable to include in the model. We want to create a model which is detailed and accounts for as much of the variance in the outcome variable as possible but, for the sake of parsimony, we do not want to throw everything in to the model. We want our model to be elegant, including only the relevant variables. Relevant empirical and theoretical work will give you a good idea about which variables to include and which are irrelevant. It is possible to adjust a multiple regression model to account for this issue. If the model is created in step we can better estimate which of the variables predicts the largest change in the

outcome. Changes in r^2 can be observed after each step to find out how much the predictive power of the model improves after each new explanatory variable is added. This means a new explanatory variable is added to the model only if it explains some unique variance in the outcome that is not accounted for by variables already in the model. Decisions about the explanatory variables added to the model are made by the computer based entirely on statistical criteria as described below:

- Forward method:

The computer searches from the specified list of possible explanatory variables for the one with the strongest correlation with the outcome and enters that first. It continues to add variables in order of how much additional (unique) variance they explain. It only stops when there are no further variables that can explain additional (unique) variance that is not already accounted for by the variables already entered.

- Backward method:

The backward method does the opposite; it begins with all of the specified potential explanatory variables included in the model and then removes those which are not making a significant contribution.

- Stepwise method:

The stepwise option is similar to 1 and 2 but uses both forward and backward criteria for deciding when to add or remove an explanatory variable.

1.6 Geological setting of the study area and its Seismicity

Northeast part of India is seismically one of the six most active regions of the world, the other five being Mexico, Taiwan, California, Japan and Turkey. This part of the region lies at the junction of Himalayan arc to the north and Burmese arc to the east

(Tiwari, 2002). Northeast India lies in zone V (the highest level of seismic hazard in India) according to the seismic hazard zonation of India. The seismic zone map of India is shown in Fig. 1.15. The high seismicity in this zone is due to the collision tectonics between the Indian plate and the Eurasian plate in the north and Subduction tectonics along the Indo-Myanmar range (BIS, 1988). Geologically, Mizoram is a part of Surma Basin. This is an area of folded sediments and is characterized by westerly convex, sinuous structural ridges and valleys. This basin is wider to the north and narrower to the south. The NE–SW and NW–SE lineaments/faults are many in this basin. The tectonic map of Northeast India is shown in Fig. 1.16.

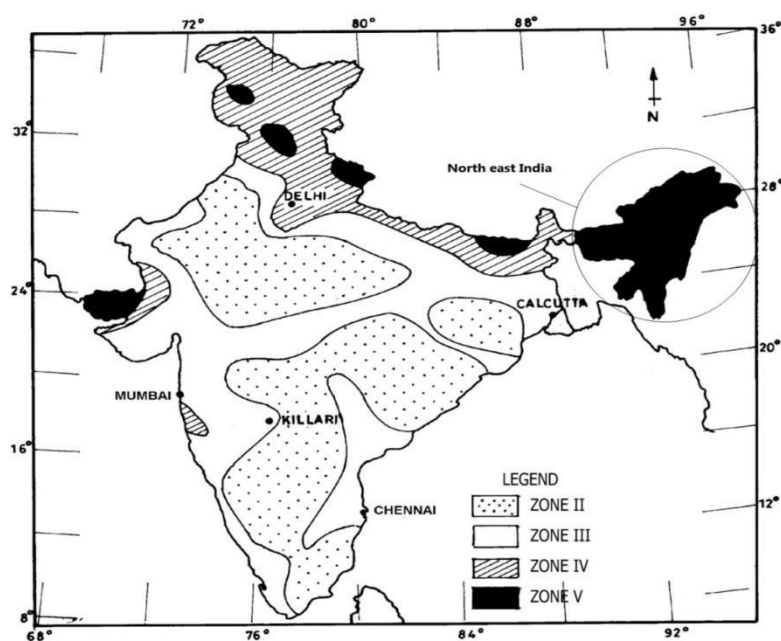


Fig. 1.15: Seismic zone map of India (BIS, 2002).

The geomorphologic map of Aizawl town forms a part of maridonal ridge (i.e. anticlines ridges and Tlawng synclines) and narrow valley (i.e. often controlled by faults). The Aizawl town and its surroundings are underlain by tertiary sedimentary rocks belonging to surma group of rocks of Oligocene- Miocene age. The rocks have been sub-divided into Middle Bhuban, upper Bhuban and Bokabil formation. The middle bhuban formation occupies the core of the Aizawl anticline. The lithological

aspects of this region are characterized by thinly bedded sandstones – siltstones/ shale in 50:50 ratios with mudstone, associated mainly with sandstones. In general, rock beds strike N15° E – S15° W with moderate to steep dips either toward east or west. The Aizawl anticline trend is N – S near Aizawl town, but toward south it becomes NNE – SSE where Tlawng syncline trend NNW – SSE. Both anticline and syncline plunge towards north (G.S.I., 1988; Tiwari *et al.*, 2011). The area has been affected by a number of faults of varying magnitude; they are longitudinal, transverse and oblique in disposition. The longitudinal faults having their imprints along the Chite river and Muthi river. The major transverse faults run along Siphui river, which dissects the ridge axis along the E – W segment of Tlawng river and the diagonal faults parallel to Sele river, Kurung river along the NE – SW segment of Tlawng.

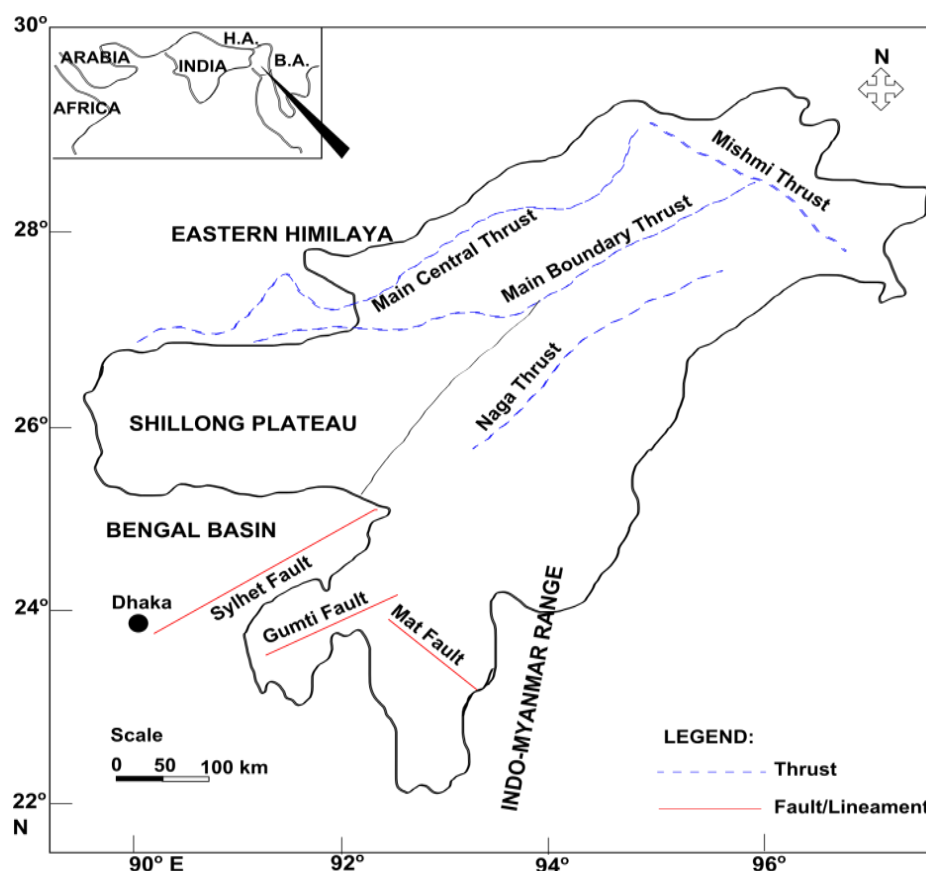


Fig. 1.16: Map of Northeast-India showing major lineaments/faults in Tripura-Mizoram fold belt.

The study area is along Chite valley; occur east of Aizawl anticline ridge. The Chite River, flowing between Aizawl and Zemabawk has formed broad valley, as shown in Fig. 1.17. The valley is approximately 600 m long and 45 to 60 m wide. Chite valley has 1.5 to 2.5 m thick saturated sand and gravel. From seismo-tectonic viewpoint, the northeast of India and its surrounding are tectonically complex and considered seismically active intra – continental region of the world (Rawat and Parihar, 2001). Seismicity in this region is related to plate subduction in the east of Mizoram and there is intra – continental adjustment along steep faults oriented oblique to the Himalayan trend. The east – west compressive stress field of Indo – Burmese arc has deformed the rocks by folding, strike faulting and adjustment along conjugate shear fractures (Deva and Rawat, 2006).

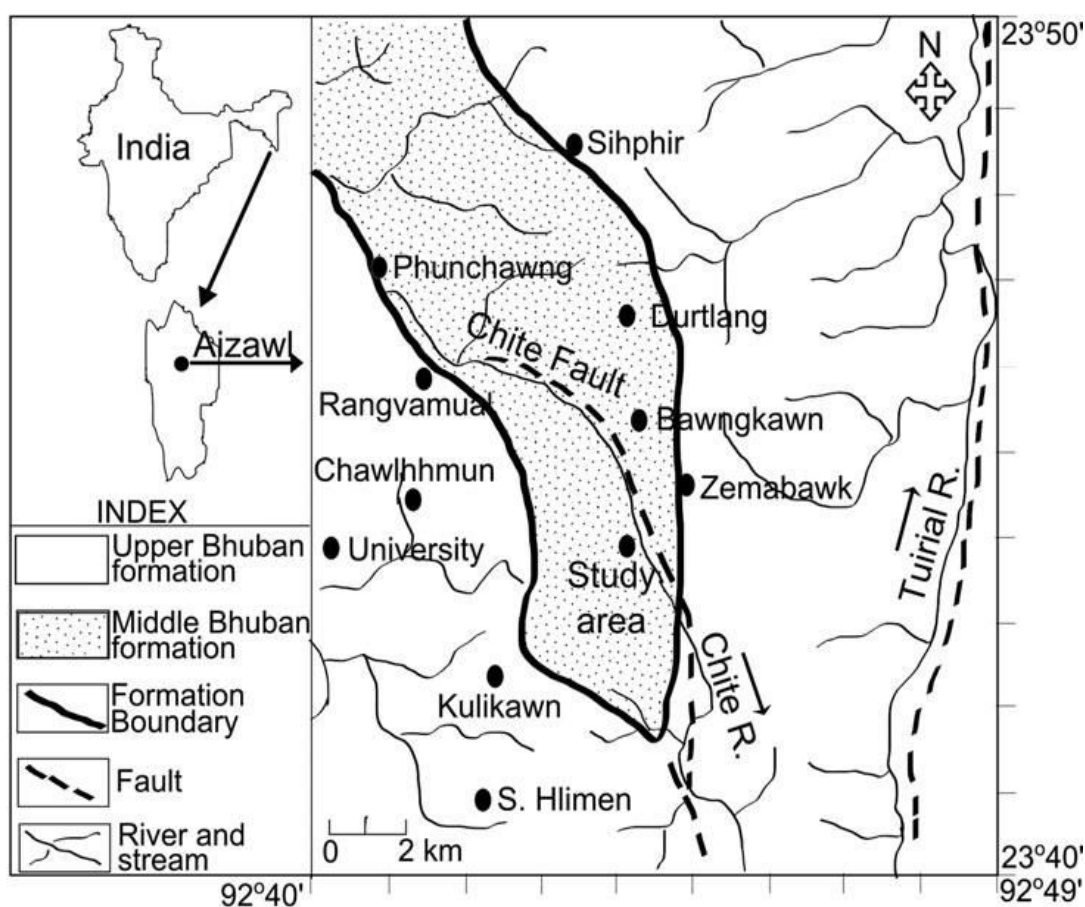


Fig. 1.17: Location map of study area showing the geology of the region.

1.7 Possible empirical relation of radon and earthquake

The precursory phenomena can be observed within the distance that is roughly the radius of the effective precursory manifestation zone. Several empirical relations have been proposed in the past between radon anomaly and seismic events parameters. Rikitake (1976) proposed a relation between precursor time (T) and earthquake magnitude (M),

$$\log T = 0.76M - 1.83 \quad (1.19)$$

Taking into consideration the case histories recorded in the Italian peninsula and the characteristics of the crustal structure in Italy the relation may be modified as follows (Hauksson and Goddard, 1981).

$$M = 2.4 \log D - 0.43 - 0.4 \quad (1.20)$$

Where D is in km and M is the magnitude of the earthquake.

On the basis of the radon data on variations in concentration of the gaseous components recorded in seismically active zone of Central Asia, Sultankhodzhayev (1984) proposed a relation between earthquake magnitude (M), precursor time (T) and the epicenter distance (D) as,

$$\log DT = 0.63 \pm 0.15 \quad (1.21)$$

Long term series analyses have revealed a relation between the amplitude and duration of the gaseous anomaly and the magnitude of the expected earthquake (Barsakov et al., 1984):

$$M = k\sqrt{s} \quad (1.22)$$

Where M is the magnitude, k is a correction factor and s is the area of the detected peak anomaly.

Taking into account the strain field model, Dobrovolsky *et al.* (1979) and Fleischer (1981) proposed empirical relation within which the earthquake preparation zone can be manifested.

$$R = 10 \exp 0.43M \quad (\text{Dobrovolsky } et al., 1979) \quad (1.23)$$

$$R = (10 \exp 0.48M) / 1.66 \text{ for } M > 3 \quad (\text{Fleischer, 1981}) \quad (1.24)$$

Where R is the epicenter distance in km and M is the magnitude of earthquake on the Richter scale. Virk (1996) modified the above relations considering 142 case studies in N-W Himalayas, India as

$$R = \left. \begin{array}{l} 10 \exp 0.32M \quad (10 < R < 50) \\ 10 \exp 0.43M \quad (50 < R < 100) \\ 10 \exp 0.56M \quad (100 < R < 500) \\ 10 \exp 0.63M \quad (500 < R < 1250) \end{array} \right\} \quad (1.25)$$

1.8 Background and the main scope of the study

Earthquakes have been a major threat and it is a great challenge to make efforts to prevent the disastrous consequences. All kinds of human activities are mostly sensible to and depend on seismo-tectonic and geo-dynamic conditions and events. The major problem of these events to be solved is it's forecasting i.e. determination of strength, place and time of possible future earthquake. During the last several decades a number of geo-chemical and hydro-chemical precursor in different seismo-tectonical regions were observed. But the number of precursors, which has constantly increased was hard to be monitored and nearly impossible to be interpreted. Perhaps lots of

evidences such as Rn, He, CO₂, CH₄, Ar, H₂, O₂, N₂, Na, Cl, Hg, Rb, Cs, SiO₂ are changing their concentration before, during and after an earthquake. Amongst these geo-gases, variations of radon concentration along the active fault region are most widely used as a possible precursor to earthquake. Besides, the northeast India has witnessed a mushroom growth of unplanned urban centre in last two decades, resulting into increasing vulnerability of human population and physical structures to the earthquakes. Therefore, it becomes essential to assess the status of seismicity in the northeast region realistically.

Radon variations might seem to be a better precursor of crustal motion resulting in earthquake. However seismic events are not always preceded by a geo-gas anomaly and not every radon increase/decrease is followed by an earthquake. But still the radon technique has successfully been applied in several seismic area of the world for the purpose of earthquake precursory research. The first monitoring of radon variation as a possible seismic in Mizoram, India began in 2011 at Mat fault in Serchhip district and the results of these studies have been reported. Encouraged with the trends observed for Mat fault, we extended the study over other active region of Mizoram.

The main objectives of the study is as follows-

- Study of variations in radon and thoron concentrations along Chite fault in Aizwal district.
- Study of possible correlation of radon and thoron concentration as a precursor to seismic events.

2

Review of literature

Radon emanations that are enhanced by forthcoming geophysical events as earthquake or volcanic activity have been observed all over the world. From last three decades we have seen an even increasing interest in studying the usefulness of radon measurements in earth sciences. For this purpose a number of active and passive methods have been proposed as an explanation of the experimental field data. The strain changes occurring within the earth's surface during an earthquake is expected to enhance the radon concentration in soil gas. This impressive development in the research of the earth's crust permits to estimate on probabilities for earthquake risks, which involves the prediction of precursor time, distance from epicenter, magnitude of incoming earthquake and other parameter. Moreover, the levels of radon concentration are strongly affected by geological and geophysical conditions, as well as atmospheric influences such as rainfall and barometric pressure.

In 1953, a study was performed by Z. Hatuda at an active fault zone for 2 years in Japan. Here he measured the radon concentration in soil gas and observed anomalous radon concentration change before the strong earthquake which occurred at Tonankai with a magnitude of 8.0 (Hatuda, 1953). S. Okabe observed in 1956, that there is a positive correlation between the daily change of atmospheric radon concentration near the ground surface and local seismicity occurring in Tottori, Japan. He also investigated that soil gas is enriched in radon in the fault zone. The daily measurements made by S. Okabe showed that the near surface air manifests significant increase in radon concentration at the time of earthquakes. In 1958, A.B. Tanner noticed that the

measurement of radon is very much influenced by different meteorological parameters. After some years, he cited that radon in soil gas could be used as a pointer to discover Uranium deposits or for prediction of earthquakes (Tanner, 1964). The first evidence of a correlation between radon and occurrence of seismic events come from Tashkent earthquake of $M = 5.3$ in 1966 (Ulomov and Mavashev, 1967). The wells were such chosen that they were situated on seismically active zone and at a depth interval of 0-7 km. The epicentral distance was within 5km and most of the anomalies were prominent precursor signals. This evidence encourage research work in this area soon afterward in many countries.

In Central California, C.Y. King (1978) performed a study in 1975 using the Track Etch Method to monitor soil gas radon activity in 0.7 m deep holes at 60 sites along several active faults. Since these anomalies occurred in different seasons and did not appear to be systematically related to meteorological changes, so ha inherent the anomalies to increased outgassing induced by some episodic strain changes. King and Slater (1978) compared the soil gas radon data recorded at two sites along the Calaveras fault in Hollister, California, with crustal strain data recorded on a two-color laser geodetic meter in the same area. They observed periods of higher radon emanation to coincide with periods of crustal compression, with a cross-correlation coefficient of 0.67. King and Wakita (1981) installed in 1978 a continuous ground-water radon monitor designed by Noguchi and Wakita (1977) at an artesian well in San Juan Bautista adjacent to the San Andreas fault and recorded a 7-month long decrease (of about 25%), beginning 4 months before the magnitude 5.7 Coyote lake earthquake on August 6, 1979, about 30km away on the Calaveras fault. These decreases may have been caused by admixing of radon poor water from another aquifer through cracks created by the earthquake-related strain changes.

Fleischer and Mogro-Campero perform their research regarding the correlation between radon concentration and seismic occurrence during the period 1981-1983 (Fleischer and Mogro-Campero, 1985) near Sand point, Alaska. They noticed a rise of radon concentration 6 weeks prior to the quake event of $M_s = 6.3$ at a distance of 180km from the radon measuring stations. In the Yakataga region, they detect both a decrease and an increase in radon concentration during seismic events such as the earthquake of May 2, 1982 with radon minimum, June- July 1980 with radon maximum, May 1981 with termination of large increase. They calculated the RSI (relative dislocation strain intensity) value and concluded that larger quakes are observable by radon, though smaller quakes is close to the maximum allowed by the uncertainty. They observed no significant correlation between radon and other meteorological effects such as rainfall, snow accumulation, temperature etc.

In Japan, Wakita *et al.* (1980) presented a radon anomaly that preceded the Izu-Oshima- Kinkai earthquake (1978) of magnitude 7.0. The data were collected using a continuous radon monitoring meter and revealed a complicated pattern of anomalous radon emission. Hauksson and Goddard (1981) in Iceland reported nine radon anomalies that preceded several different earthquakes in the magnitude range from 2.0 to 4.3. They operated a network of seven radon stations area. Their result indicated that the probability of observing radon anomalies in Iceland before small earthquake of magnitude larger than 2.0 was approximately 65%. Major earthquakes occurred during August 1983- July 1984, in Bhatsa dam, Maharastra, India. B. K. Rastogi and group in this region carried out radon measurement and they observed an increase in radon concentration during March – April 1984 (Rastogi *et al.*, 1986) when seismicity was high enough. Precursory phenomena of radon in earthquake sequence were noticed by B. K. Rastogi and other group at the Osmansagar reservoir, Hyderabad, India during

January – February, 1982 (Rastogi *et al.*, 1987). An earthquake of magnitude 3.5 occurred on 14 January, 1982 with subsequent events as well. There was an increase of radon concentration in soil gas during February due to those high seismic activities.

Liu *et al.* (1985) made weekly radon measurements of ground- water at four sites (a CO₂- rich cold spring, a hot spring and a 275m and a 30m deep geothermal well) in northern Taiwan between July 1980 and December 1983. They observed seven spike-like anomalies at three of the sites. Six of the anomalies were each followed by a shallow earthquake of magnitude 4.6 or larger within 4-51 days at epicentral distances of 14- 45 km, but only in certain directions. They also observed that gas bubbles in the water contained much more radon than expected from known equilibrium distribution between gas and water. Allegri *et al.* (1983) monitored weekly radon concentrations at two wells in central Italy during 1978-1980. They recorded some anomalous increases (25% and 170% above background) at both sites 1 and 5 months before the magnitude 6.5 Irpinia earthquake on November 23, 1980, about 250km to the southeast.

Friedmann (1985a) and his colleagues began in 1977 to continuously monitor groundwater radon concentrations at five springs in Austria with ionization chamber instruments. At one site they recorded an anomalous increase of a factor of 3 that lasts about 8 month, beginning 3 months before comparable anomaly that began shortly before several local earthquakes of about magnitude. He pointed out that the initial rate of increase of some radon anomalies tends to be smaller for larger epicentral distance and proposed a rheological model to explain this observation. In Spain, radon concentration in soil gas was studied by Duenas and Fernandez (1988). They observed both pre and post anomalies along with ‘no’ anomaly of radon concentration related to earthquake with magnitudes of 2- 4 at a distance of 90km from the monitoring site. In Turkey, H. Friedmann and his group monitored radon in soil gas at five sites along

200km at the North Anatolian Fault zone, Bolu (Friedmann *et al.*, 1988). They noticed the effect during the Biga earthquake of $M = 5.7$ on 5 July, 1983 and found an increase in radon concentration. Hirotake and group observed radon anomaly before the Nagano prefecture earthquake of $M = 6.8$ on 14 September, 1984 (Hirotake *et al.*, 1988) and the measuring site was about 65km away from the epicenter at the Atotsugawa fault. They observed a gradual increase in radon count before three month of the quake and a remarkable increase before 2 weeks of the shock.

B. F. Humanante *et al.* (1990), a radon concentration measurement survey was carried out in Ecuador using the SSNTD technique. Their measurements correspond to 15 days exposure in the soil and each recording corresponds to an average value of concentration during this time. Of the remaining 31 stations where radon concentration measurements were constantly performed and they observed that 14 produced clear abnormal signals prior to the March 6, 1987, $M6.1$ and $M6.9$ earthquakes. The stronger signals were found on 12 stations located some 200km from the epicenter. Weaker signals were found on 2 Lloa stations (site 12) out of 3. These stations are close to Quito, 90km the epicenter. Daily radon monitoring in soil-gas was performed in Amritsar (India) from 1984 to 1987 by M. Singh and group. They recorded several radon anomalies during the observation period: March 23, 1984 ($M = 5.0$); July 29, 1985 ($M = 6.8$); April 21, 1986 ($M = 5.7$); July10, 1986($M = 3.8$); March17, 1987($M = 4.3$) and May1, 1987($M = 5.0$). The anomalies occurred within 3 to 10 days; at an epicentral distance of 100- 400km (Singh *et al.*, 1991). M. Monnin and J. Seidal reported a finding on characteristics of radon in soil air during the earthquake in Mexico (Monnin and Seidal, 1991). They found that near surface radon fluctuation were mainly due to deeper fluid motion which supports the pore collapse (PC) model creating an upward motion of pore fluids that acts as radon carrier.

Y. Honkura and A.M. Isikara reviewed some results that were done along Izmit-Sapanca and Iznik- Mekece fault zones (Honkura and Isikara, 1991). Along with the magnetic and electric potential anomaly, radon anomaly in soil gas was also observed which was assumed as an effective way for detecting changes prior to fault. In Germany, radon in soil gas was measured by Heinicke and Koch in the vicinity of epicenters of earthquakes (Heinicke and Koch, 1993). In the same year, in China, Yang Yurong and Zhu Ziqiang (1993) studied the dependence of radon concentration on temperature, air pressure etc, in the first case.

Segovia along with his group measured radon concentration in soil along Guerrero coastal zone (Segovia *et al.*, 1995a, 1995b). A survey of radon and short lived daughter concentration in soil gas was carried out using SSNTD near Laguna Verda, Mexico. At Aeapulco stations, they observed weak radon anomaly during earthquakes of $M = 4.7, 5.5$ during 1990-1991, but significant radon increase during 1992-1994 earthquakes.

In Turkmenistan, Alekseev with other scientists performed a study on radon and metal contents measurements in soil as well as water. The measuring site area was chosen in the Ashkhabad and Kum-Dang region. They used nitrocellulose detector (SSNTD) which was placed inside the 70 cm deep pit and continuous radon measurement was carried out at intervals of 5-7 days. A simultaneous increase in radon concentration was observed during the devastating earthquake that occurred on 14 March, 1983 (Ashkseev *et al.*, 1995). A systematic study on radon measurements in soil gas at the region was performed by Wattananikorn and group at the region that is 65km N-NE of Chiang Mai City, Northern Thailand (Wattananikorn *et al.*, 1998). Using SSNTD (LR-115) at the depth of 50cm and 100cm below the surface, the data obtained during several earthquakes.

Garavaglia *et al.* (1998) performed a study on radon measurement in soil in seismic area of NE Italy. The monitoring site was in the cave in Villanova, which is one of the most seismically active regions of the Alps. Radon concentration variation was measured during the local seismicity occurred within 1996- March 1997 of $M = 2.5-4.2$. Along with the effects of seismic events, radon anomaly was also observed with pressure and temperature variation. Finkelstein *et al.* (1998) generalized an approach to remove noise components from the observed radon data to leave a residual component of radon concentration in underground cavity was derived taking into account a number of parameters such as: i) radon emanation from the soil, ii) variation of radon due to vertical warm convection arising shortly after sunrise, iii) variation of radon due to rain and radon dissolved in underground water, iv) variation due to fluctuation in air pressure, v) variation due to air movement, variation related to deep geodynamics, due to strong geodynamic storms in periods of solar chrome spherical bursts and vi) variation caused by the settling of aerosols following dust storms. The approach was demonstrated using data gathered in Israel at the time of the October 12, 1992 Giza earthquake in Egypt.

Temporal radon variation as well as barometric pressure, atmospheric precipitation and temperature were observed by Planinic *et al.*, (2000) at Croatia in 1998 using solid nuclear tract detector films (LR-115). They observed a negative correlation between the radon concentration in soil and barometric pressure. For two recorded earthquakes in 1998, the radon anomalies were observed about one month before each quake. Virk *et al.* (2000) carried out radon monitoring at Palampur and Dalhousie stations in Kangra and Chamba Valleys using emanometry for discrete measurement of time series radon data since 1992. They observed that the correlation between radon data and micro-earthquake during the time window 1992- 1997 shows a

rising trend both in micro seismicity as well as radon in Kangra and Chamba valleys of N-W Himalayan region under investigation. The correlation co-efficient of radon data and the meteorological parameters were studied; they suggested that temperature, rainfall and humidity have positive correlation, whereas wind velocity has negative correlation with radon.

H.S. Virk and his group observed the precursory nature of radon as well as helium in the NW Himalayas during the earthquakes that occurred on 20 October, 1991 and 29 March 1999 (Virk *et al.*, 2001) the Chamoli earthquake of $M = 6.5$ was associated with radon anomaly which was measured at Palampur about 393km from the epicenter. The radon anomaly started 19 days before the quake, 9 days before the quake it was minimum and 2 days before that quake the radon concentration reached at peak value ($> 2\sigma$). Tsvetkova *et al.* (2001) studied the variation of radon as precursor signal of earthquake in the Caucasus, Europe. Measurement of radon activity in soil gas with temperature and pressure variation at Krsko basin, Slovenia was performed by B. Zmazek along with his coworkers. They noticed changes in the correlation co-efficient between radon and barometric pressure before an earthquake at one place (Zmazek *et al.*, 2002).

A. Negarestani and group performed soil radon survey at Thailand (Negarestani *et al.*, 2002). A new method based on Layered neural network was employed by them to estimate radon concentration in soil related to environmental parameters. With the applied new method, they were able to differentiate time variation of radon concentration caused by environmental parameters from those arising by anomaly phenomena in the earth (e.g. earthquake). They conclude that the proposed method can give a better estimation of radon variation related to environmental parameters that may have a non-linear effect on the radon concentration in soil, such as rainfall.

The soil-gas radon concentration had been monitored almost continuously from June 1993 till November 1996 on Taal volcano, Luzon Island, the Philippines by P. Richon and his group. During the measurement period, a singular M_b 7.1 earthquake occurred on November 15, 1994, between Luzon and Mindoro, 48km south of the volcano, twenty-two days before the earthquake, an anomalies increase in soil- gas of Taal volcano appears to be strongly controlled by permeability variations correlated with the regional crustal stress.

During 2001-2002, Moussa and Arabi observed soil radon concentration along the fault line of Qena- Safaga fault, Egypt (Moussa and El Arabi, 2003). When performing a study on radon concentration variation with distance along the fault, they observed the radon peak 5- 10 times greater than the background on the fault trace. High radon peak on different dates in active fault zone have been noticed by using ALPHA GUARD. B. Zmazek and other workers on the basis of different environmental parameters and also seismic activity at the same place used regression method to predict radon concentration in soil gas (Zmazek *et al.*, 2003). They notice radon concentration with a correlation of 0.8 when it was influenced by environmental parameters and much lower correlation with seismic activity. Swakon *et al.* (2004) performed a study on radon in the vicinity of geologic fault zones within the Krakow region of Poland and to determine the influence of such formation on enhanced radon concentration in soil. The concentration of radon in soil gas and other radio- isotopes (radium, thorium, Potassium) was measured using ALPHA GUARD, diffusion chamber with CR-39 and Gamma ray spectrometry. High value of radon and thoron in soil gas was compared with those observed in an earlier survey. M. Burton and group performed a series of discrete measurement of radon concentration in soil with high spatial resolution (~ 5- 100m) in the Santa Venerina area on Mt Etna, Italy between July 2002- May 2003

(Burton *et al.*, 2004). Their measurement revealed well-defined linear anomalies that were interpreted as being caused by active faults whose higher porosity than surrounding soil allows an increased CO_2 flux, carrying radon from beneath. In October 2002 a series of earthquake shock, producing damage and soil fractures localized along the geometry of active fault revealed by their radon survey. They observed that thoron emissions appear to have a slightly different spatial distribution than radon, with increased contrast, coherent with the short half – life of thoron that limits its observation only to those areas which possess the highest flux of radon. Huang *et al.* (2004) observed the response to the devastating Chi- Chi earthquake of $M = 7.6$ that occurred on 21 September, 1999 at China. They measured radon concentration in around 52 wells at 5 different tectonic areas. They noticed pre-seismic changes in areas 1 just 5 day prior to the seismic event at a distance of 500km away from the epicenter. In contrast, in area 2,3,4,5 there seems to have some co- and pre- seismic changes, with the hypo- central distance of 800-2120km.

Llic *et al.* (2005) studied extensively regarding radon in Antarctica, during a yearly investigation they monitored an earthquake that happens on 4 August, 2003 of $M = 7.5$, in the Scotia Sea at a distance of 1176km from the measuring site Academician Vernadsky station. Using a model they made a prediction that an earthquake would happen on 30 October, 2003 of $M = 4.0$ and that was proved latter. V. Walia and his group carried out radon monitoring using emanometry technique at Palampur and Dalhousie station in the Kangra vally of Himachal Pradesh (India) from June 1996 to September 1999 (Walia *et al.*, 2005a). Discrete radon concentrations were recorded in soil-gas and ground-water at both the stations. The influence of meteorological parameters viz. temperature, rainfall, relative humidity and negative correlation with wind velocity has been identified.

S. Alparone and group performed continuous radon monitoring near southeast crater of Mt. Etna in September- November 1998, during a period of frequent eruptive episodes at that crater. They detected radon anomalies when eruptive episodes and the accompanying volcano tremor become increasingly intense. The device used to continuously record the radon activity in the soil by them was an alpha counter equipped with a 4cm² passive solid- state sensor (alpha METER^{cm} – alpha- NUCLEAR co., CANADA), placed at the bottom of a 1m deep sealed bore- hole (Alparous *et al.*, 2005). An experimental station for monitoring variation in radon and radon progeny concentrations in the gases from the thermal springs at Bakreswar, West Bengal, India was carried by Das and group (Das *et al.*, 2006). The electronic radon monitor SARAD DOSEman was used to determine the radon and progeny concentration. They observed distinct radon anomaly peak of $> 2\sigma$, before the devastating tsunami that occurred in Indonesia (M = 9.1) on the 26th December of 2004 and also the seismic events during January- February 2005 in Sumatra. Crockett *et al.* (2006) made an investigation with a RAD-7 detector during the period of June to December, 2002, at the University College Northampton Radon Research Group, UK. An earthquake occurred at Dudley on 22 September, 2002. Two spikes were observed on the 21st and 22nd of September 2002, preceded by two smaller spikes on the 20th and 21st of September 2002. They even notice a negative correlation during late October to mid November (Crockett *et al.*, 2006).

F.S. Erees and his group investigate the relationship between the earthquakes and radon concentrations in thermal waters along faults in the Denizli Basin, an area in Turkey known for its high seismic activity and thermal water. Measurement of radon concentration was performed by ZnS (Ag) scintillation counter in a collector chamber. They observed that at Pamukkale, an anomaly in radon concentration were over 1σ at

18-20 km distance 19 days before the $M = 3.8$ earthquake. At Tekke, an anomaly over 2σ was also noticed at 22km distance 28 days before the $M = 4.8$ earthquake. Ghosh *et al.* (2007) carried out an experiment on measuring radon concentration in soil gas with the use of CR-39 (SSNTD), at Kolkata, India. They observed radon anomaly for the earthquakes that occurred during the period of November 2005 - October 2006 within the range of 1000km from the measuring site and of $M \geq 4$. Measurement of ^{220}Rn , ^{222}Rn activity and of CO_2 flux in soil and fumaroles on Mount Etna Volcano in 2005-2006 was carried out by Giammanco *et al.* (2007) and his group, both in its Summit area and along active fault on its Flanks. They analyzed an empirical relationship between ($^{220}\text{Rn}/^{222}\text{Rn}$) and CO_2 efflux. They concluded that the empirical relationship provides perspective on the type and depth of the gas source and is more constrain than simply using the ratio between radon and thoron alone. Variation of helium and radon concentrations in soil gases was performed in the National Pingtung University of Science and Technology (NPUST) campus in southern Taiwan (Fu *et al.*, 2008). Soil gas samples were systematically collected from the 200-300m spacing grid in an area of about $1.2 \times 2.3 \text{ km}^2$. A total of 82 sample were collected using a hollow steel probe of 3cm diameter and 130cm length that was inserted into the soil at the depth of about 100cm. to monitor helium, radon and other gases, they have used helium leak detector (ASM100HDS, Alcatel), radon detector (RTM 2100, SARAD) and micro gas chromatography (CP4900, Varian) respectively. During their consecutive measurement for several months, a striking feature is that anomalously high concentrations appeared to be spike-like a few hours to a few days before the earthquakes. Plotting all the anomalous peaks with the earthquake events through time, they observed that about 90% of the events can be correlated to some precursory anomalous peaks a few hours to a few days before the event occurred.

Inan *et al.* (2008) measured physical and chemical properties of warm and hot spring water along with soil radon concentration continuously during 3 year period in the Marmara region; following the devastating Izmit earthquake of 17 August 1999 ($M_w=7.4$). Daily bottled spring water from the spring was collected monthly during site visits and 30 daily samples from each spring were brought to the laboratory where analyzed for anions and cations using Ion Chromatography instrument (Dionex Dx600). Soil radon was measured continuously at 15min. interval using alpha particle detectors (model 611 Alpha- meter). They observed promising and encouraging anomalies in ground radon emanation and were closely related to seismic activity. They noticed that during the absence of seismic activity, the radon data indicate random walk behavior of radon in soil and showed Rayleigh-type probability density function. During the earthquake build-up period, the data showed deviation from Rayleigh-type pdf, indicating the disturbance of the path of gas movement or gas release pattern prior to earthquake and multi parameter observation should be conducted with patience and for long time until sufficient data are acquired to develop a working model to convince the scientific community and reach a consensus.

V.M. Choubey and group perform continuous recording of different geophysical parameters, incorporated at a single location as a unified effort for earthquake precursory through geodynamical changes initiated for the first time in the Garhwal, Himalaya, India. For measurement a 68m deep borehole, penetrating into the water table is operated for continuous radon monitoring along with meteorological/geohydrological observations at two points, one at 10m (in the air column) and the second one at 50m (within water column) depths from surface. Preliminary studies reveal diagnostic short duration anomalies in radon concentration recorded few days before the occurrence of a nearby moderate M4.9 earthquake at Kharsali on the 23rd of

July, 2007 (Choubey *et al.*, 2009). S. Giammanco studied the comparison between different methodologies for detecting radon in soil along an active fault (Giammanco *et al.*, 2009). The first technique consisted of solid-state nuclear track detectors (SSNTD), CR-39 type and allowed integrated measurements. The second one consisted of a portable device for short time measurement. The last consisted of a continuous measurement device for extended monitoring, placed in selected sites. They investigated that the two different soil-gas horizontal transects across the Pernicana fault system from November 2006 to April 2007. The results obtained with the three methodologies are in a general agreement with each other and reflect the tectonic settings of the investigated study area. Kulahci *et al.* (2009) applied Artificial Neural Network approach concerning the relationship between radon and earthquake in the East Anatolian fault system (EAFS), Turkey. A three-layer Levenberg-Marquardt feedforward learning algorithm is used to model the earthquake prediction process. They employed individual training strategy with fixed-weight and supervised models leading to estimations. The average relative error between the magnitudes of the earthquakes acquired by ANN and measured data is about 2, 3%. They concluded that ANN approach is a potential alternative to other models with complex mathematical operations.

Pattama Pispak and group initiated to measure the radon concentration in soil over time and then to analyze possible variations of the radon data with respect to potential earthquake precursors for the Khlong Marui fault zone (KMFZ) and related faults in southern Thailand (Pispak *et al.*, 2010). They have used an automatic soil gas radon monitoring system (12 Feb.- 2 March, 2007) and a short-period seismometer (14 Jan.- 12 Apr., 2007), was installed in Thap Put district, Phang Nga province in the KMFZ. They observed two significant positive radon anomalies during the short period

of study, on 18 Feb. and 1 March, 2007. An increase in local and regional earthquake activity was noticed several days after each radon anomaly. They concluded that the seismic events and radon data indicates a relationship between the local and regional earthquakes, suggesting a possible (stress/strain) relationship between the Sunda subduction zone and the fault in southern Thailand.

Suleyman Baykut and his group carried out continuous monitoring of soil radon emanation along with other geophysical measurements in the seismically active Marmara region of Turkey over the past ten years for understanding the pre- earthquake crustal deformation. The soil radon gas emanation is measured via silicon detector based alpha- particle counting tools. And then the radon gas emanation time series were decomposed into intrinsic made via Empirical Mode decomposition (EMD) and the relationship between seismic activities and radon gas emanation is investigated (Baykut *et al.*, 2011).

M. Neri with his co-worker performed measurement of radon and thoron emissions from soil on the eastern flank of Mt. Etna, in a zone characterized by the presence of numerous seismogenic and aseismic faults (Neri *et al.*, 2011). They studied the statistical analysis on soil radon and thoron data which was useful to find the distribution trends, recognizing anomaly threshold value and to produce distribution maps that highlighted a significant spatial correlation between soil gas anomalies and tectonic lineaments. They concluded that mapping the distribution of radon and thoron in soil gas can reveal hidden faults buried by recent soil cover or faults that are not clearly visible at the surface.

Kumar *et al.* (2012) carried out continuous soil gas radon and daily monitoring of radon concentration in water at Amritsar (Punjab, India), a well known seismic zone to study the correlation of radon anomalies in relation to seismic activities in the study

area. For monitoring radon in soil they used barasol probe (BMC2) manufactured by Algade France and in case of radon content in water was recorded by using Rad7 radon monitoring system of Durrige company USA. The observed radon anomalies in the region had been correlated with the seismic events of $M \geq 2$ along the effects of meteorological parameters has been studied. They found that about 75% of the radon anomalies observed in soil gas and ground water correlates with the micro seismic events that occurred in the North - west Himalayas. Zoran *et al.* (2012) investigated temporal variations of radon concentration levels in air near the ground and in ground air using CR-39 and LR-115 (SSNTD) in relation with some seismic events at two seismic stations Vrancioaia (VRI) and Plostina (PLOR), located in Vrancea active region, Romania. Observation of radon concentration was done in the air near the ground at 1m height for the earthquake that encountered during the period of November 2010 – October 2011 in the range of magnitude $2.0 \leq M \leq 4.9$. They have identified that greater times between the start of the anomaly and the earthquake as well as longer durations of the radon anomalies appears to be associated with larger earthquake magnitude. Radon concentration in Jooshan hot spring complex were measured and investigated by Namvaran M. and Negarestani A. near Golbaf- Sirch fault system, SE of Iran from December 2011 until March 2012 (Namvaran and Negarestani, 2013). The main device used for their research was RAD7 (DURRIDGE company Inc, USA). They examined by considering and studying environmental parameters, the relationship between radon anomalies decline and all earthquakes with D/R that introduced by Dobrovolsky *et al.* 1979. Their research shows a good correlation between ground water radon variations and such earthquake parameters.

Li *et al.* (2013) measured the concentration of Hg, Rn, H₂, He and Co₂ in soil gas at 756 sites in the Tahgshan area, Northern China. They found that H₂ and He have

spatial congruence along the tectonic lines which they interpreted as being caused by deep source of gas and the migration path formed by the faults. A better spatial congruence was observed between Rn and Co₂ suggesting that Co₂ acts as a carrier gas for radon in the studied area. Padilla *et al.* (2013) performed continuous measurement of soil gas radon and thoron activities, during the period (2011-2012) of the recent volcanic unrest that occurred at El Hierro, Canary Island (Spain), at two different monitoring stations, namely HIEO2 and HIEO3. They identified that statistical analysis was competent to find relation between the long-term temporal trends of filtered radon to that of seismic energy release during the volcanic unrest.

Kulahci F. and Sen Z. (2014) carried out systematic measurements of ²²²Rn for earthquake prediction. Here, their measurements were obtained using active and passive radon detector systems in an earthquake-active region of Turkey. They proposed two new methods to explain the spatial behaviors and the statistical uncertainties in the radon emission measurements along fault lines in relation to earthquake occurrence. The applications of these methodologies were performed for 13,000 radon measurements that were deemed to be sufficient for the characterization of tectonics in the Keban Reservoir along the East Anatolian Fault System (EAFS) in Turkey.

Briestensky *et al.* (2014) has presented the result of fault displacement monitoring in central Europe at two caves in the Bohemian Massif. The fault displacement monitoring has been supplemented by radon monitoring at the Mladec caves and by carbon dioxide monitoring at the Zbrasov Aragonite caves. This period of tectonic instability was recorded around the time of the catastrophic M_w=9.0 Tohoku earthquake on 11 March 2011. They suggested that the Tohoku Earthquake in the Pacific Ocean and the unusual amount of geodynamic activity recorded in the Bohemian Massif and Western Carpathians report contemporaneous global tectonic changes.

Jaishi *et al.* (2014) performed continuous measurement of soil gas radon at two selected sites along Mat fault in Mizoram (India), which lies in the highest seismic zone in India. Their research was carried out during July 2011 to May 2013 using LR-115 Type- II films. Precursory changes in radon concentration were identified prior to some seismic events that occurred around the measuring sites. Statistical analysis of the radon data together with the meteorological parameters was performed using Multiple Regression method. The result obtained suggested that the method employed was useful for eliminating the effects of meteorological parameters and to identify radon maxima possibly caused by seismic activity. A. Piersanti and his group presented the results of a long term, continuous radon monitoring experiment in a seismically active area, affected during the 2010 – 2013 data acquisition time window by an intense micro-seismic activity and by several small seismic events. In their research, they employed both correlation and cross-correlation analysis in order to investigate possible relationships existing between the collected radon data, seismic events and meteorological parameters. Their results do not support the feasibility of a robust one-to-one association between the small magnitude earthquakes characterizing the local seismic activity and single radon measurement anomalies, but evidence significant correlation patterns between the spatio-temporal variation of seismic moment release and soil radon emanations, the latter being anyway dominantly modulated by meteorological parameters variations (Piersanti *et al.*, 2015).

Attanasio A. and Maravalli M. analyze the connection between radon emissions and earthquakes by developing statistical models. Taking into consideration the large amount of local data available in the period before and after the main shock, they decided to run their analysis on the recent earthquake which affected the Italian city of L'Aquila (Attanasio and Maravalli, 2016).

3

Materials and Method

3.1 Solid state Nuclear Track Detectors (SSNTD'S)

Solid state nuclear track detectors, one of the most fascinating nuclear particle detection techniques developed till date. SSNTD has been found to be equally useful in basic and applied research work, particularly for Scientists, engineers and technologists in the developing countries. It has applications in many distinguished fields like Nuclear Physics, Geochronology, Cosmology, Biology, Bird altimetry, Seismology, Elemental Analysis, Material Science, and Lithography etc. In the early days, mostly natural substances such as minerals were used as solid state nuclear track detectors. However as the passage of time many manmade materials were successfully developed for their use as track detectors. The pioneering work of Young, Silk and Barnes in 1959 encourage Fleischer, Price and Walker in 1961 to develop a new particle detector called Track Detector. SSNTD's are a class of dielectric materials which can be used to detect an energetic charged particle (Fleischer *et al.*, 1975). Numerous materials both Organic and Inorganic have been used as track detectors. The commonly used materials are listed in Table 3.1. In the beginning, crystalline minerals were used as detectors. For a better understanding in the registration and development properties of plastics and glass track-etch detectors have prominence the use of these detectors at the present time. Different materials have sensitivities to nuclear particles. Organic polymers are found to be the most sensitive track detectors, some of which produce etch able latent damage trials events for low energy protons, deuterons, alpha particles etc. Experiments carried out with heavy ion irradiations and cosmic rays have shown that each track detecting

materials has “a well defined threshold damage density”, below which no tracks are produced (Fleischer *et al.*, 1975; Flerov *et al.*, 1964).

Table 3.1: Commonly used Track-etch Materials.

Detectors	Atomic composition
<i>In organic</i>	
Quartz	SiO ₂
Phlogopite mica	KMg ₂ Al ₂ Si ₃ O ₁₀ (OH) ₂
Muscovite mica	KAl ₃ Si ₃ O ₁₀ (OH) ₂
Silica glass	SiO ₂
Flint glass	18SiO ₂ : 4PbO: 1.5Na ₂ O: K ₂ O
<i>Organic</i>	
Polyethylene terephthalate (Cronar, Melinex)	C ₅ H ₄ O ₂
Bisphenol A-polycarbonate (Lexan, Makrofol)	C ₁₆ H ₁₄ O ₃
Polymethylmethacrylate (Plexiglas, Lucite, Perspex)	C ₅ H ₈ O ₂
Cellulose triacetate (Cellit, Triafol-T, Kodacel TA-401 unplasticized)	C ₃ H ₄ O ₂
Cellulose nitrate (Daicell)	C ₆ H ₈ O ₉ N ₂
Allyl diglycol carbonate (CR-39)	C ₁₂ H ₁₈ O ₇

All entry taken from Fleischer *et al.* (1975), except the last entry (Lounis *et al.*, 2001).

When one compares the properties of SSNTD’s with the conventional detectors, it can be seen that the SSNTD’s have many advantages over other detectors in generals and over nuclear emulsions in particular. The fact that fission fragments can be recorded and distinguished in a mixed field of unwanted light charged particles has made these detectors extremely useful in experiments where fission reaction rate is very low and very high detection efficiency is required (Khan, 1972; Kleeman and Lovering, 1971). The most common plastic track- etch detectors used for alpha particle registration are CR-39 (Polyallyl-diglycol carbonate) and LR-115 (a member of cellulose nitrate

family). The plastic track-etch detectors are generally used for alpha particle and fission fragment registration. The alpha radiation emitting from radon and thoron, penetrates the surface of the plastic and causes radiation damage tracks along the entrance path. The number of tracks that penetrates is related to radon and thoron concentration (Valkovic, 2000). Track-etch monitors are of two types: open and closed types. In the open type, the SSNTD is exposed as a bare foil. Here, the detectors will register the alpha radiation from radon and thoron and their progenies. In case of closed type, the SSNTD is enclosed in a closed container into which radon/thoron diffuse through a filter. The filter prevents the entry of radon/thoron progenies and the dust particles into the chamber so that the foil is sensitive only to the alpha radiation from radon/thoron formed in the container (Valkovic, 2000). A typical closed type track-etch detector is shown in Fig 3.1.

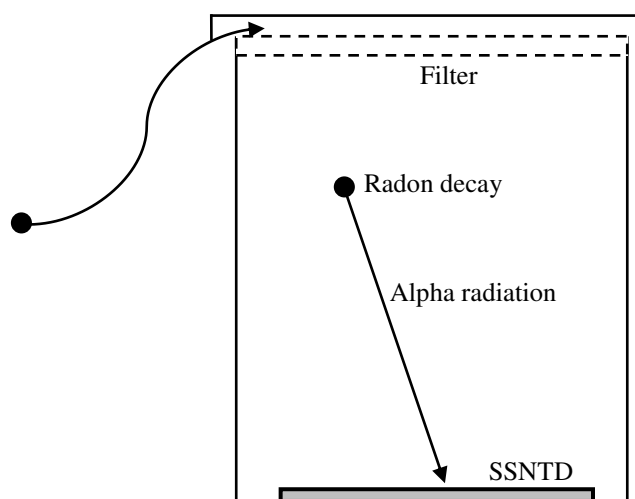


Fig. 3.1: Closed Track-etch monitor.

General description of LR-115 films:

Energetic heavy ions moving through some insulating materials leave damage trails that can be rendered visible in an optical microscope by suitable chemical etching.

The theories of track formation mechanisms are based in the means by which heavy ions energy as they slow down and come to rest in a solid. If the damage produced by the particles along their trajectories is greater than a critical value the track may be developed by etching with a chemical reagent and made visible in an optical microscope. The chemical etching preferentially attacks the damaged materials and less rapidly removes the surrounding undamaged matrix. The LR-115 film consists of a layer of cellulose nitrate strongly red colored and coated on an inert polyester base 100 μ m thick. Therefore only one of the surfaces is sensitive. In LR-115 type I film the cellulose nitrate layer is 6 μ m thick and this film is mainly recommended for alpha particles with energies between 0.5 and 2.0 Mev. Whereas in LR-115 type II film, the thickness of the layer is 12 μ m good for alpha particles with energies between 2 and 4 Mev. LR-115 detector film is sensitive to alpha particle such that when an alpha particle hits the film it causes localized damaged to the molecular structure of cellulose nitrate layer. The damage so registered can be observed visibly, when the exposed film is etched in a bath of diluted NaOH solution. These LR-115 film is insensitive to light, X and gamma rays and electrons (Fleischer *et al.*, 1975). As compared to LR-115, the poly carbonate detectors (i.e. CR-39 film) have thick detection film and shows high sensitivity to alpha radiation (Lounis *et al.*, 2001). The great disadvantageous of CR-39 film is that they produce larger tracks causing difficult to distinguish during the saturation level of the detector (i.e., the maximum density of tracks on the film in which a single track can be distinguished). The etching of LR-115 film leads to a controlled depletion of cellulose nitrate layer. This controlled loss is significant since its excess depletion of the cellulose nitrate layer may lead to an error in the results. After chemical etching, the etched films is viewed under the microscope each alpha particle that has been registered will show a bright spot of light. In case of other detectors, the film

absorbs light and hence the nuclear track appeared a dark spot. Therefore when viewed under a microscope, the tracks in LR-115 films are more easily distinguishable. The significant advantage in the film is that the dust particle which gets deposited in the film during manipulation is not counted as a nuclear track, where as in other detectors the dust particle deposition in the film may cause error. Moreover, the important feature about the etched LR-115 film is that it can be kept in stock for more than 10 years without any trouble and allows recalculation of the old films when needed. The etching time required for LR-115 film is far less (i.e. about 1 hour) than that of CR-39 (6 to 10 hours), which renders it more suitable for large scale measurements (Mayya *et al.*, 1998).

3.2 Principle and Salient features of the technique:

A massive charged particle passing through an electrical insulator produces a narrow region of radiation damaged materials, known as a 'latent damage trail' or simply as a 'track'. The process of track formation is discussed in detailed below.

3.2.1 Track registration and formation process

When an ionizing charged particle (for e.g., α -particle) passes through a medium, the transfer of energy to electrons results in a trail of damaged molecules along the track of the particle. The energetic charged particle interacts with the electrons of the atoms and molecules of the medium by means of coulomb interaction. The interaction with electrons results in ionization and excitation events along the particle trajectory. The damaged process can be divided into the following stages (Hepburn and Windle, 1980; see Fig. 3.2),

- I. Electrons are stripped from the penetrating particle.

- II. The region in which the particle is moving too fast to leave damage.
- III. The main region of the etch-able damage
- IV. The stage during which the particle still penetrates the solid but does not produce significant damage.
- V. The point at which the particle comes to rest which may be preceded by short second region of damage.

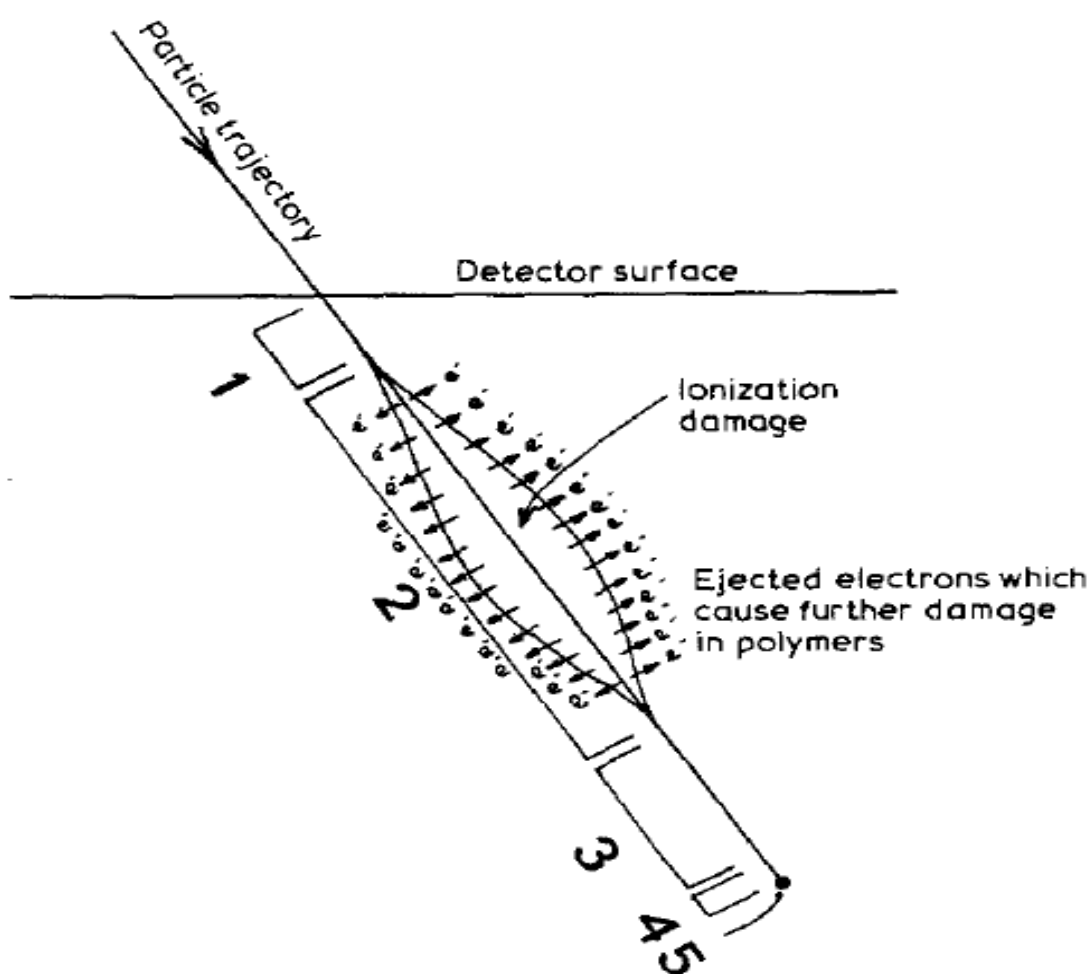


Fig. 3.2: Schematic diagram representing the different stages of penetration of a particle into a detector. Not all the stages are necessarily apparent for a given set of conditions. Stages: 1) Electrons are stripped from particle. 2) Particle moving too fast to leave etchable damage. 3) Main region of damage. 4) Particle regaining electrons and damage no longer etchable. 5) Some elastic collisions as particle come to rest which may cause damage if particle is heavy (after Hepburn and Windle, 1980).

It is to be noted that all the stages are necessarily perceived. Inclusion of stage II requires that the particle enters the detector at high energy. In case of polymers, stage IV cannot be observed and the main damage region merges with the characteristics of stage V.

Regarding the mechanism that led to the registration of tracks, several models have been put forward over the years. However, a complete satisfactory model does not yet exist (Knoll, 2010). Some of the model explaining track registration is discussed as follows.

3.2.2 Ion Explosion spike model

This model was first put forward by Fleischer and Price in 1965 (Fleischer *et al.*, 1975). When an energetic charged particle passes through a medium, it interacts with the atomic electrons via coulomb interaction. This interaction involves to the transfer of energy from the incident particle to the host material. The energy loss is characterized by a quantity called the *stopping power*. The stopping power of an ion penetrating into a solid is defined as the energy loss per unit length of the path. Ionization and radiation are the two important processes contributing to the total energy loss. At low ion energies, *Nuclear Stopping* dominates the energy loss. This corresponds to close encounters between the nucleus of the primary ion and the target nuclei. This process is characterized by large energy and angular momentum transfer, especially if the masses of the incident particle and the atom are not widely different. The nuclear stopping leads to abrupt changes of the projectile energy and direction (Fischer and Spohr, 1983). At high incident ion energies, the dominant part of energy loss is due to interaction between the primary ion and the electrons of the target material. This interaction is called *electronic stopping*. This type of collision leads to smooth, quasi-continuous

breaking process, leaving the projectile direction virtually unchanged. Electronic stopping increases at low energies approximately as \sqrt{E} and reaches a maximum depending on the penetrating ion between 1 and 10 MeV/nucleon and decreases beyond this maximum approximately as $1/E$. The total contribution to the stopping power can be written as (Varier, 2009),

$$\left[\frac{dE}{dx} \right]_{tot} = \left[\frac{dE}{dx} \right]_{nuc} + \left[\frac{dE}{dx} \right]_{el} \quad (3.1)$$

Where, $\left[\frac{dE}{dx} \right]_{nuc}$ and $\left[\frac{dE}{dx} \right]_{el}$ corresponds nuclear and electronic stopping respectively. In inorganic SSNTDs (crystals and glasses), secondary electron do not play significant role in latent track formation whereas in plastics both primary and secondary interactions contribute to the formation of tracks.

The necessary conditions for the formation of tracks (Fleischer *et al.*, 1975) by the ion explosion mechanism are listed below.

- Low mechanical strength, low dielectric constant and close inter atomic spacing.
- The incident particle should possess at its entry into the detector an energy and a mass such that its energy loss rate $\left[\frac{dE}{dx} \right]$ is larger than the critical value

$\left[\frac{dE}{dx} \right]_{crit}$ which is characteristic for each of the material used.

- There must be at least one ionization per atomic plane crossed by the incident particle. If they are discontinuous, the etch pit profile would be rough and shape would be irregular. This criterion is mostly imposed for tracks which are to be revealed by chemical etching.

- If other electrons replace those ejected by the incident charged particle before ionized atoms are forced into adjacent material, no track would be formed. The ions take around 10^{-4} nano seconds to get displaced from the normal sites. So, if electrons can be drained from a cylindrical region around the ionized core in less than this time, the track formation can be prevented.
- The hole mobility in a material at room temperature must be less than $0.2 \text{ cm}^2/\text{V sec}$. Otherwise, no tracks can be formed in the material. This criterion also leads to the conclusion that metals and most of semiconductors cannot be used as track storing materials.

The range R of the particle in a solid is the integral of the inverse stopping power (or the integral of the *penetrating power*) given by (Fischer and Spohr, 1983),

$$R = -\int_0^E \left(\frac{dE}{dx} \right)^{-1} dE \quad (3.2)$$

The range corresponds approximately to the length of generated nuclear track. Specific energy has a range in solids of about $1 \text{ }\mu\text{m}$ for a heavy ion of 0.1 MeV/nucleon , about $10 \text{ }\mu\text{m}$ for a heavy ion of 1 MeV/nucleon and approximately $100 \text{ }\mu\text{m}$ for a heavy ion of 10 MeV/nucleon .

3.2.3 Restricted energy loss model

This model was suggested by Benton (Benton and Nix, 1969). The model takes into account the combined effect of the primary and secondary electron events. The total stopping power is given by,

$$\frac{dE}{dx} = \left[\frac{dE}{dx} \right]_{W>W_0} + \left[\frac{dE}{dx} \right]_{W<W_0} \quad (3.3)$$

Where, $\left[\frac{dE}{dx} \right]_{W>W_o}$ is the energy loss in near interactions in which electrons with energy $W>W_o$ are knocked out and $\left[\frac{dE}{dx} \right]_{W<W_o}$ is the energy loss in distant interactions for which $W<W_o$. Here, the total stopping power is considered in two energy regimes separated by a characteristics energy W_o which determines the boundary between the electron energies that are not taken into account in track formation (Varier, 2009). The restricted energy loss is tied to the energy deposition rate, excluding that of long range delta rays (Benton and Nix, 1969). In this model, all events of electron ejected with energy transfer above W_o are completely ignored where events of electrons with energy below W_o are considered efficient.

3.3 Track etching

Several methods are employed (Monnin, 1980) to reveal the damaged tracks created by charged particles. The most common method is chemical etching. Etching transforms the latent tracks into an inerasable structure by supplying the required amount of energy for the enlargement process.

In chemical etching, the etching reagent attacks the damaged region and removes some material to enlarge the track. During this process, the bulk of the material is also attacked but at a much slower rate. The action of the etching process is characterized by the ratio V_T/V_G where, V_T is the track etch rate and V_G is the bulk etch rate. A track is enlarged only if the track etch rate exceeds the bulk etch rate. In a simple instance let us consider that the particle penetrates the detector normal to its original surface. Under these conditions, a cone shape pit is formed with an axis along the damaged track (Fig. 3.3). Further, assuming that V_T is constant along the track and V_G is

constant and isotropic, then V_T/V_G will be constant for short etching distances in isotropic non-crystalline solids (Hepburn and Windle, 1980). Both, l (length of the etched track) and d (the track diameter) depends on the competitive effect of V_T and V_G .

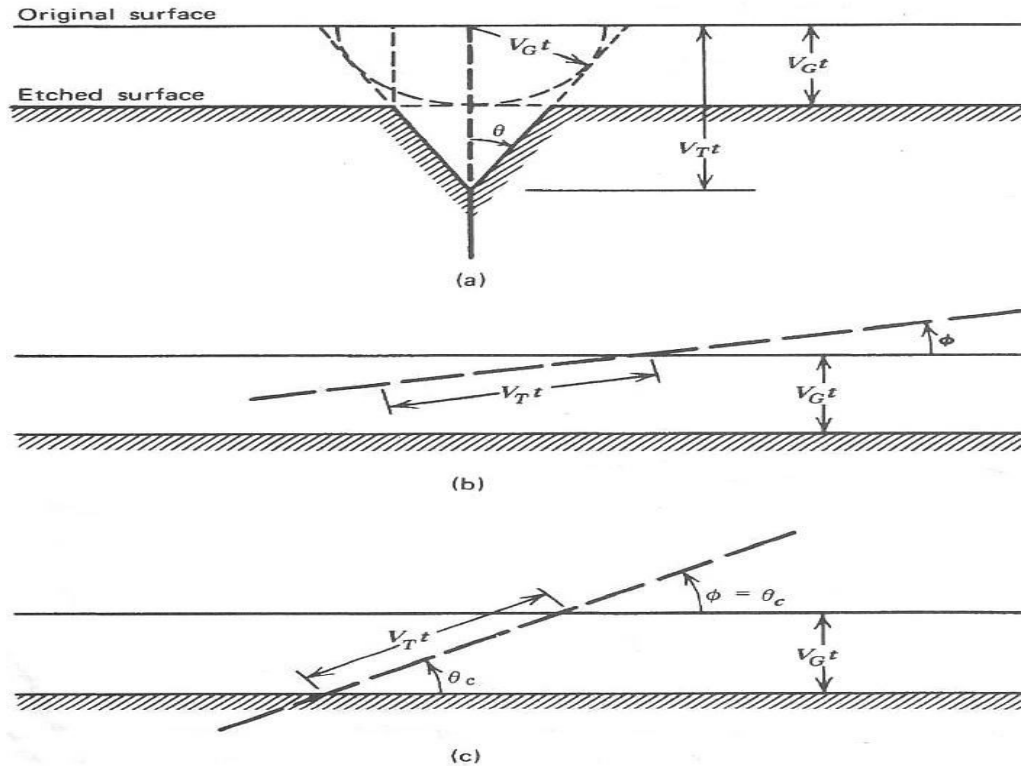


Fig. 3.3: (a) Model of track etching in which the normal surface is removed at a velocity V_G and the damaged track at a velocity V_T , leading to a cone-shaped pit. (b) Tracks formed at an angle ϕ less than the critical angle θ_c are not revealed because the normal surface advances faster than the etch rate along the track. (c) The case in which the particle enters at the critical angle θ_c . Tracks entering the surface at an angle greater than the critical angle will be visible after etching (after Fleischer *et al.*, 1975).

From Fig. 3.3 we can write,

$$l = (V_T - V_G) t \quad (3.4)$$

Where t is the etching time, and

$$d = 2V_G t \left[\frac{(V_T - V_G)}{(V_T + V_G)} \right]^{1/2} \quad (3.5)$$

When $V_T = V_B$, both l and d vanishes. For tracks incident on the surface at a dip angle (angle between track and surface), the component of V_T perpendicular to the surface ($V_T \sin \theta$) must exceed V_G for track registration to occur (Tommasino and Harrison, 1985).

$$V_T \sin \theta > V_G \quad \Rightarrow \quad \sin \theta > V_G / V_T$$

Hence using the above model, it can be shown that the angle of incidence must exceed the critical angle θ_c in order to produce a track. This critical angle is given by,

$$\theta_c = \arcsin \left(\frac{V_G}{V_T} \right) \quad (3.6)$$

Several parameters can play a significant role in the etching behavior. For example, the sensitivity of some plastic track-etch detectors depend on the presence or absence of oxygen during exposure (Fleischer *et al.*, 1975). Track formation may be enhanced through the application of electric field (Crannell *et al.*, 1969) or by exposure to ultraviolet radiation (Siegmon *et al.*, 1975). Besides the above mentioned parameters, the temperature (Piesch and Sayed, 1974) also plays an important role during etching. If the temperature is too high this may result in the inadvertent loss of the desired tracks.

3.4 Track counting

A number of schemes are available for the counting of etched tracks. The most direct and commonly used method is the manual observation through a microscope. This method is suitable when small number of samples is analyzed. In case of transparent material transmitted light illumination either in its light or dark field version is used whereas in opaque material the reflected light technique is used. To enhance the microscopic contrast several techniques are used (Hepburn and Windle, 1980) which

includes application of a dyed track recording material, metal evaporation of a thin metallic film on top of a track recorder and deposition of a thin metallic film on the total recorder surface or even inside the etched tracks. Scanning electron microscope and transmission electron microscope are used in cases where a higher resolution is desirable.

Although track counting through microscope is a commonly employed method, it suffers from the disadvantage of being slow. In cases where large number of detector foil is analyzed, track counting through microscope is a tedious and inaccurate process. The most successful method for rapid counting of tracks is the spark counting method (Cross and Tommasino, 1968). This method is useful for track densities up to about $3000/\text{cm}^2$. In this method the etched and dried film is placed on a flat electrode plate covered with a piece of aluminized mylar film. A positive voltage of about 500 V is applied to the thin aluminum layer which causes sparks to occur through perforations in the etched film. The spark pulses are then electronically counted with a scalar.

3.5 Monitoring Technique of Radon and Thoron in soil gas

For monitoring of radon/thoron concentration in soil gas concerning earthquake precursory studies, three different sites were established along Aizawl district, Mizoram (India). Continuous radon and thoron in soil gas were measured using LR-115 type II film, manufactured by Kodak Pathe, France. The study was carried out during March 2013 to May 2015 in this region. The cellulose nitrate films were loaded in the dosimeters which were cut into a size $3\text{cm} \times 3\text{cm}$. The dosimeter loaded with detectors films were kept inside metallic cylinders at 3 locations with 3 detectors each in two locations and 4 detectors in one. The final reading was the average of all the 10 detectors. The hollow metallic cylinders were 80 cm below the soil surface and 30 cm in

diameter as shown in Fig. 3.4. The detectors films were kept exposed for a period of 7 days and after the expose period; it was retrieved and chemically etched using 2.5N NaOH solution in a specially designed constant temperature bath model PSI-CTBI. The detectors films were etched at a stable temperature of 60° C for approximately 60 min.. After etching, the film were washed in running water and then kept in distilled water for about 2 hours. After this process, the films were stripped off and then dried. The etching is performed in order to enlarge the alpha track registered from the radon/ thoron within LR-115 films. The stripped LR-115 detectors films were further counted by using a spark counter to obtain the track densities in tracks per square centimeters.

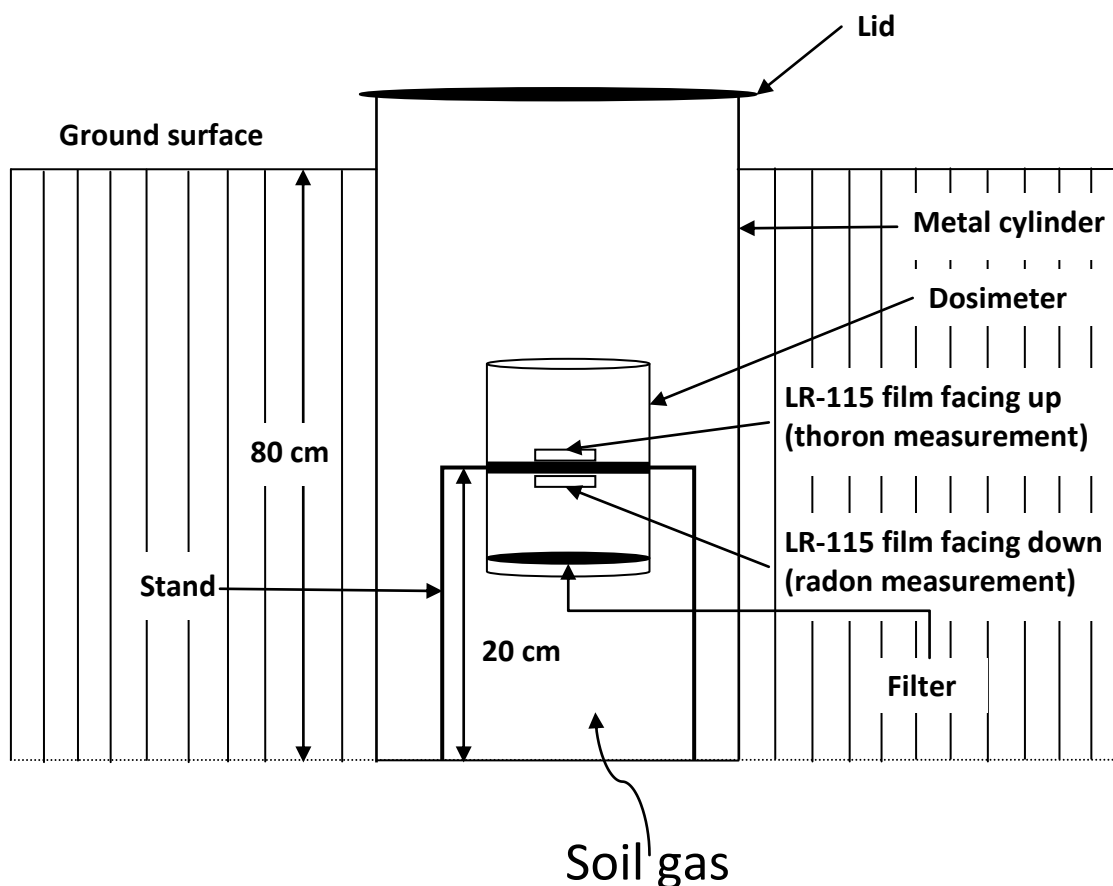


Fig. 3.4 Schematic representation of Radon and Thoron detection in soil.



Fig. 3.5: Methods of measurement in soil. (a) Bore hole at a depth of 80 cm below soil surface. (b) LR-115 loaded in the dosimeter. (c) Loaded dosimeter inserted in a metallic cylinder. (d) The metallic cylinder sealed by a plastic cover.

3.5.1 Description of Twin cup dosimeter

Twin cup radon/thoron discriminating dosimeter was employed for monitoring of radon and thoron in soil. The dosimeter were designed and fabricated at Bhabha Atomic Research Centre (BARC), Mumbai by Mayya and his group (Mayya *et al.*, 1998) as shown in Fig. 3.6. Each dosimeter has three compartments which are as follows

- I. The pinhole compartment measures radon only and allow more than 95% of radon gas to diffuse and suppress thoron gas to less than 1% (Arafa, 2002; Jansson, 1981; Ram Chandran *et al.*, 1987).
- II. The filter mode compartment allows both radon and thoron gas to diffuse into it and the entry of Progeny is blocked by placing a filter paper.

III. The bare mode allows the entry of both radon and thoron gas and their progenies

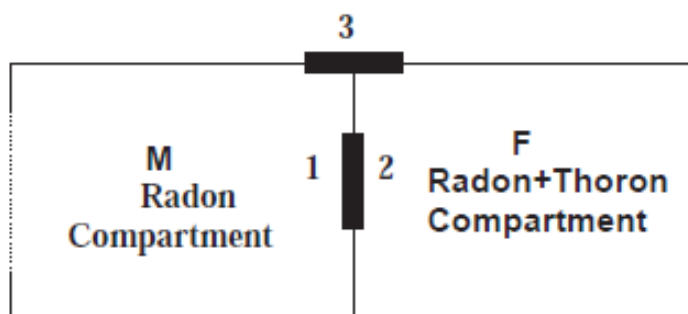


Fig. 3.6: Schematic representation of a twin-cup dosimeter: 1) Radon cup mode SSNTD film. 2) Radon + thoron cup mode SSNTD film. 3) Bare mode SSNTD film.

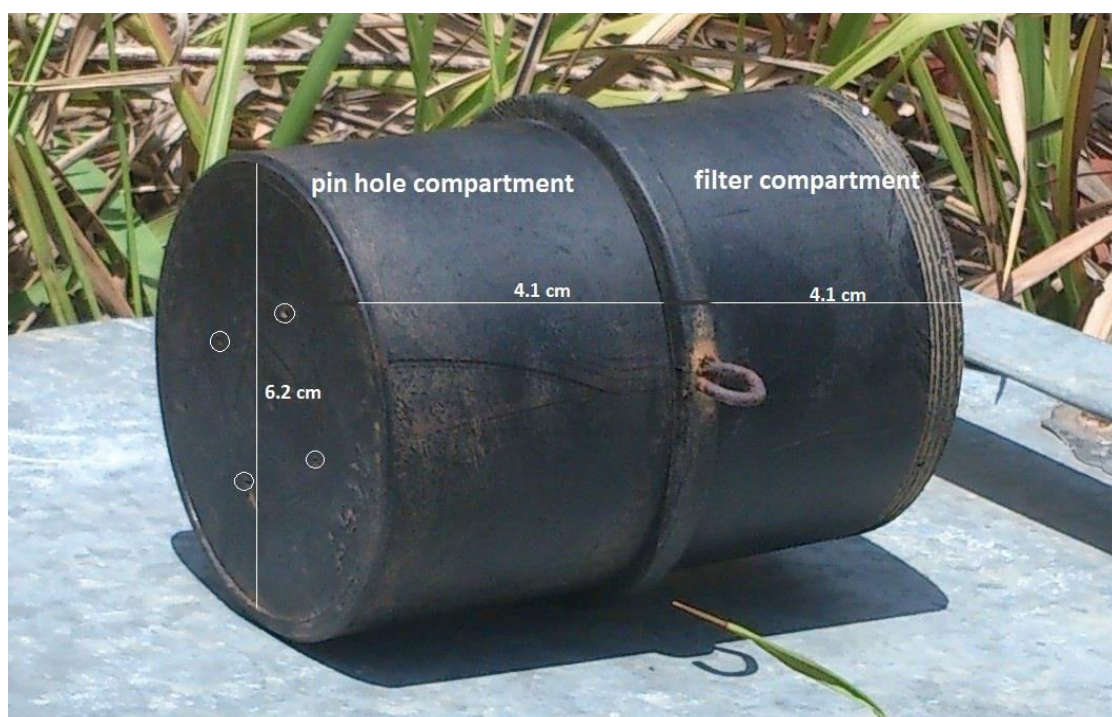


Fig. 3.7: Picture of radon thoron discriminating dosimeter. Oval shaped circles represent the pin holes.

In the present research study only two modes were used: Pinhole compartment to detect radon and filter mode compartment to detect radon and thoron concentrations. The spark counter provides track densities T_1 (Pinhole compartment) and T_2 (Filter

compartment) in Tracks/cm². The track densities were then converted to Becquerel per cubic meter using the following relation (Mayya *et al.*, 1998).

$$C_R \text{ (Bq/m}^3\text{)} = T_1/dK_R$$

$$C_T \text{ (Bq/m}^3\text{)} = T_2-T_1/dK_T$$

Where, C_R is the radon concentration, C_T is the thoron concentration is the exposure period in days, $K_R = 0.021$ tracks/cm² per Bq d m⁻³ for radon and $K_T = 0.019$ tracks/cm² per Bq d m⁻³ for thoron (Eappen and Mayya, 2004).

3.5.2 Constant Temperature bath

The constant temperature bath, a product from Polltech instruments Pvt. Ltd. It is a specially designed water bath suitable for chemical etching of SSNTD films used for measurement of radon/thoron exposure. The bath has been designed for precise temperature control so as to attain temperature stability of the etchant within $\pm 0.5^\circ\text{C}$ to overcome the fluctuations in etching rates which may be caused by variations in temperature. This is achieved by using a proportional electronic temperature controller and RTD sensor. A water circulating pump provides fast dynamic response to achieve the stability. The water bath is double-walled with glass wool insulation for the inner vessel. Water inside the bath is heated at pre-set temperature using an immersion heater and then circulated inside the tank for uniform heating. There are 3 etching vessels, placed inside the water bath from the top lid. Water circulating inside the bath maintained to a pre-set temperature keeps the etching solution at the desired temperature. Each etching vessel has a rod with 10 slots for hanging 10 cartridges, making a total of 30 films processing at one time. The system automatically switches off the power to the heater after pre-set time and also gives an audio signal indicating completion of the etching process.



Fig. 3.8: (a) Picture of a constant temperature bath. (b) LR-115 films loaded in cartridges before etching. (c) Loaded films in NaOH solution inside the etching vessels.

3.5.2.1 General recommendations

- The strength of the etching bath affects heavily the results obtained. The bath must therefore be prepared exactly and be maintained at correct strength.
- Care must be taken to allow for the effects of evaporation, especially when processing at 60 °C and also for that of absorption from the air carbon dioxide,

which will combine with the sodium hydroxide to form less-alkaline sodium carbonate.

- The etching bath should not be agitated. A uniform temperature should be maintained. The mean temperature during the whole etching process has a very high effect on the etching efficiency (tracks number).
- Surface-active reagents, such as detergents, organic solvents, adhesive tapes, iron or bad stainless steel, ball-point or felt-pen inks may lead to adverse reaction and should therefore not be allowed. They can contaminate the etching bath and sometimes destroy the cellulose nitrate.

3.5.3 Spark Counter

After the process of chemical etching and the detector films were dried, holes are produced along the tracks of the detector film. The holes were then electronically counted by employing a spark counter model PSI-SC1, manufactured by Polltech Instruments, Mumbai. The picture of the spark counter used is illustrated in Fig. 3.9. The spark counter is developed for easy operation using electronic control panel with display and provision for data storage and data transfer facilities. The operating voltages are stored in a microprocessor for operational ease. The pre-sparking and count voltages are adjustable from 100V to 1000V DC through digital potentiometers. The spark counting time called the Gate window time is adjustable from 1 to 10 seconds. The data from the spark counter can be transferred to a PC through the in-built RS-232 serial communication link. The spark detectors film is mounted rigidly on top of the instrument box. This consists of two parts viz. the acrylic detector base and the S.S. counter weight. The acrylic detector base has a fixed S.S. disc of 1 cm² area and a spring loaded S.S. contact. The positive high voltage is applied to the disc and the

optically plane and polished to a high degree of flatness. The counter weight has a flat circular glass window to press the film during spark counting the detector is mounted on a tripod stand which can be easily moved.

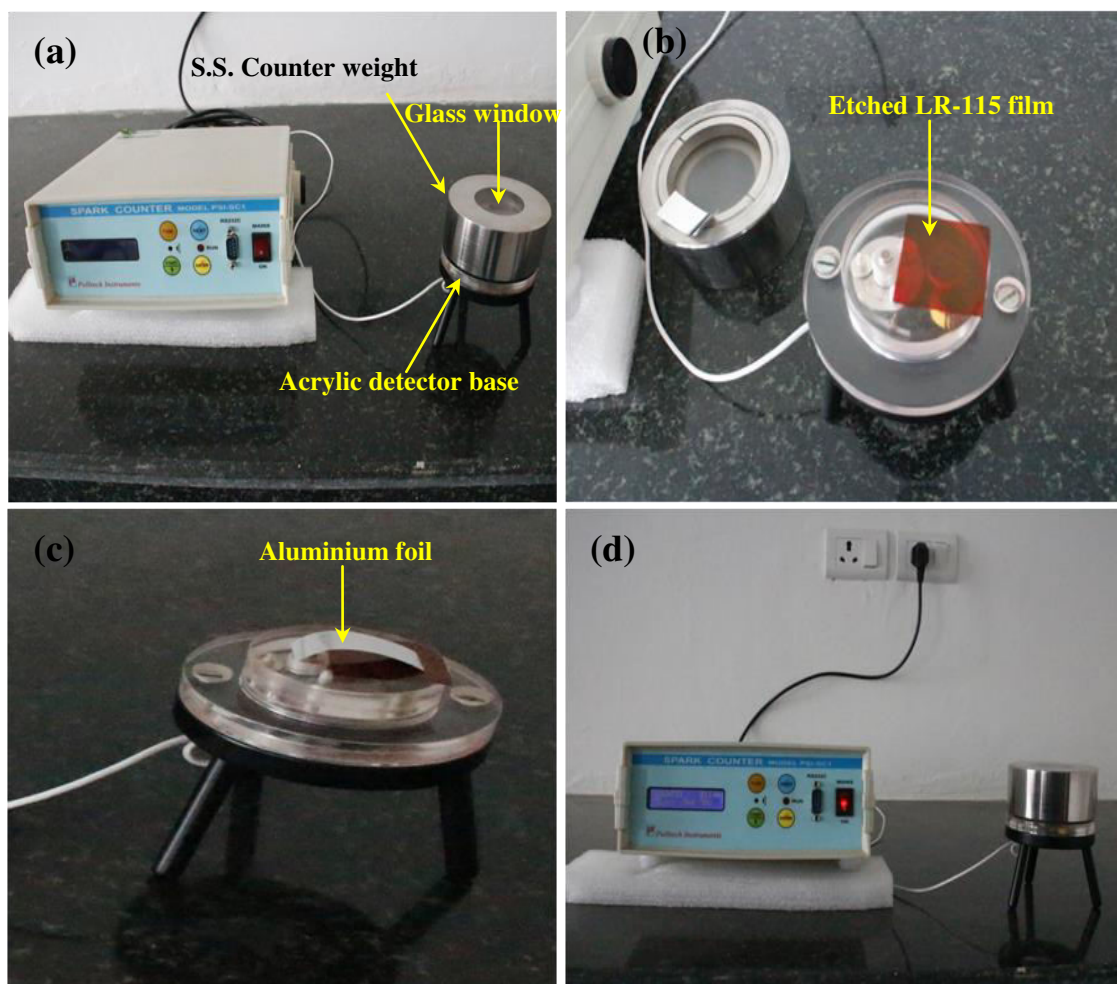


Fig. 3.9: (a) Spark counter model PSI-SC 1. (b) Etched LR-115 film placed on top of a thick conductive electrode. (c) Film covered by aluminium foil. (d) Track counting.

The spark detector cable has a matching amphenol connector for providing high voltage and measurement of count pulse. The dried and stripped LR-115 film is placed on top of a thick conductive electrode (area 1 cm^2) commonly made of brass or stainless steel and covered by a plastic foil namely a very layer of aluminum evaporated into a Mylar backing. The thin film is in contact with the aluminized side of the foil. This whole assembly forms a capacitor with LR-115 film as a dielectric medium between them. The

schematic diagram of a spark counter is shown in Fig.3.10. In addition an RC circuit is used to remove the applied voltage at the time of sparking in order to avoid spark propagation in the neighboring holes.

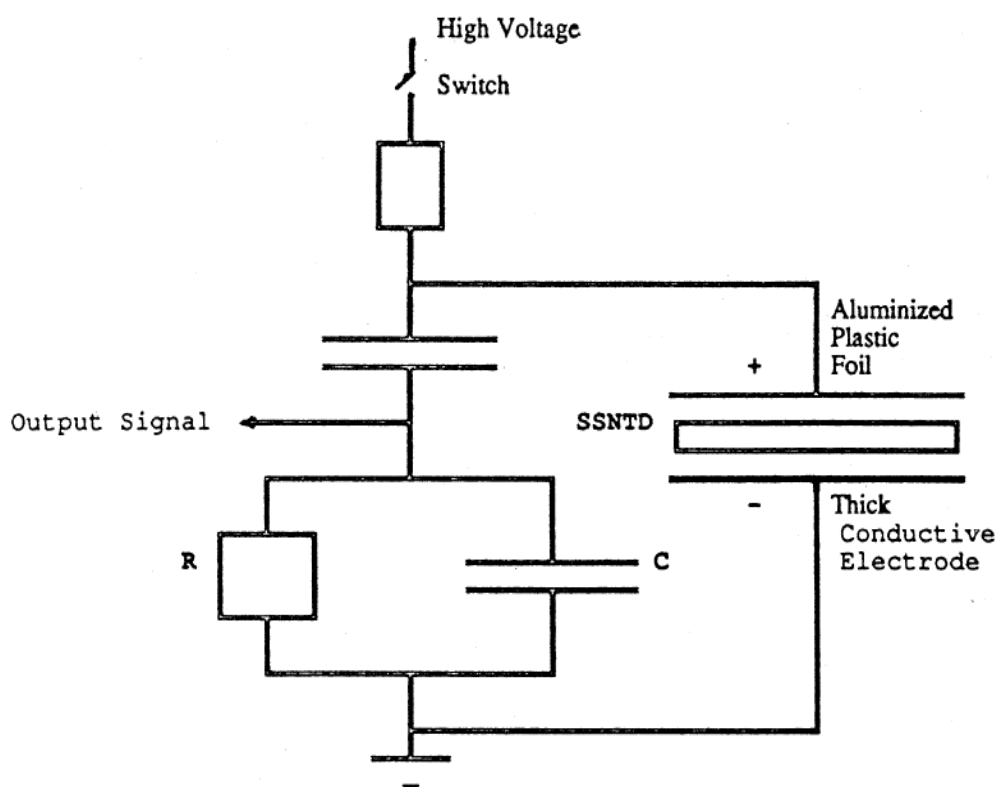


Fig. 3.10: Schematic diagram of a spark counter. The SSNTD placed between the electrode forms a capacitor. When high voltage is applied across the capacitor C, an electric spark takes place through a track hole. The voltage pulse produced across the resistor R can easily be counted electronically (after Azimi-Garakani, 1990).

When a high voltage is applied across the capacitor C, an electrical discharge takes place through the track hole. The voltage pulse produced across a load resistor can easily be counted electronically by a counter. The spark passing through the track hole evaporates the thin layer of aluminum, which produces larger circular spot on the aluminum electrode. After the short circuit, the spark is stopped, the capacitor C is charged again but a second spark cannot occur on the same track hole because of the evaporation of aluminum of the electrode. Therefore the spark jumps randomly from

one track hole to other until all the tracks are counted. The stripped LR-115 films were first pre-sparked by the actual count at a voltage of 900V (Azimi- Garakani, 1990). Pre-sparking is performed in order to convert any partially developed holes into full ones if any residual thickness is remaining after etching, as it is expected due to the difference in the energies of the incident alpha particles. After the completion of pre-sparking, the Mylar film is replaced by a new one without disturbing the pre-sparked area. The voltage between the electrodes is set at an operating voltage and the counts are recorded. The operating voltage for track counting is usually around 400-600 V. To find out the operating voltage, the voltage was first set at 100V (minimum voltage) and the count was noted. The voltage was then increased by 50V at each step and the corresponding counts were recorded. It should be remembered that the applied voltage in this process should not exceeds the pre-sparking voltage (i.e. 900V) as shown in the Fig. 3.11.

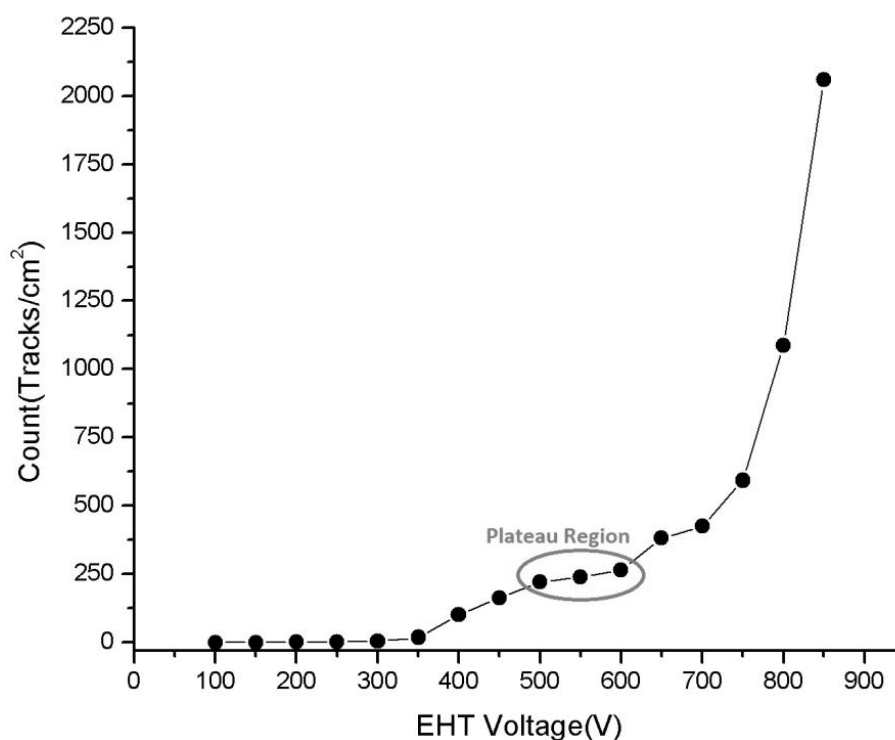


Fig. 3.11: Applied voltage vs. counts, showing the plateau region. The plateau region depicts the operating voltage

The curve in the figure shows similar trend to that of a Geiger tube with an optimum operating voltage at the centre of the plateau (Malik and Durrani, 1974). So, the operating voltage for track counting was set at 500V and the counting was recorded in tracks per square centimeters.

4

Result and Discussion

In defining an underlying theoretical physical model regarding the interaction of the mechanical processes preceding an earthquake within a radon domain, various theories concerning radon release and its relation with earthquake occurrence have been developed from time to time. But none is complete in itself. Each theory assumes different parameters which sometimes fit into the observed data and at other times is a complete failure. For identifying the patterns in radon variation that characteristically occur prior to earthquakes, some empirical relations have been proposed in the past relating precursor time of radon anomalies to earthquake magnitude and epicentral distance. On the basis of strain field models, Dobrovolsky *et al.* (1979) and Fleischer (1981) had given relations between earthquake magnitude and the radius of the effective precursory manifestation zone, where radon anomaly occurs, as follows

$$\left. \begin{aligned}
 D &= 10 \exp 0.43 M, && (\text{Dobrovolsky et al., 1979}) \\
 D &= \frac{(10 \exp 0.813 M)}{1.66} \text{ for } M < 3 \text{ and} \\
 D &= \frac{(10 \exp 0.480 M)}{1.66} \text{ for } M > 3, && (\text{Fleischer 1981})
 \end{aligned} \right\} \quad (4.1)$$

Where, D is the epicentral distance in km and M is the magnitude of the earthquake on the Richter scale. In the present investigation, the relation given by Fleischer (1981) has been used for the selection of earthquakes that occurred around the study area during the observation period. The details of earthquakes (source: [http:// www.imd.gov.in](http://www.imd.gov.in)) fulfilling Eq. 4.1 is summarized in Table 4.1 and the spatial distribution of the earthquake is depicted in Fig. 4.1.

Table 4.1: Details of earthquakes occurred around the measuring site during the investigation period (source: www.imd.gov.in)

Date (MM/DD/YYYY)	Lat	Long	Depth (km)	Magnitude (M)	Region	Epicenter distance(km)
03/02/2013	24.8°N	92.2°E	10	5.2	India (Karimganj) Bangladesh Border Region	138
12/30/2013	24.3°N	93.2°E	10	4.5	Churachandpur (Manipur)	68
01/29/2014	23.9°N	93.9°E	33	5.1	Myanmar – India(Manipur) Border Region	120
11/20/2014	23.8°N	93.5°E	33	5.6	Myanmar – India (Mizoram) Border Region	76
11/21/2014	23.6°N	93.4°E	46	4.7	India (Mizoram) – Myanmar Border Region	71
02/12/2015	24.2°N	94.0°E	90	5.0	Manipur (Chandel)	141

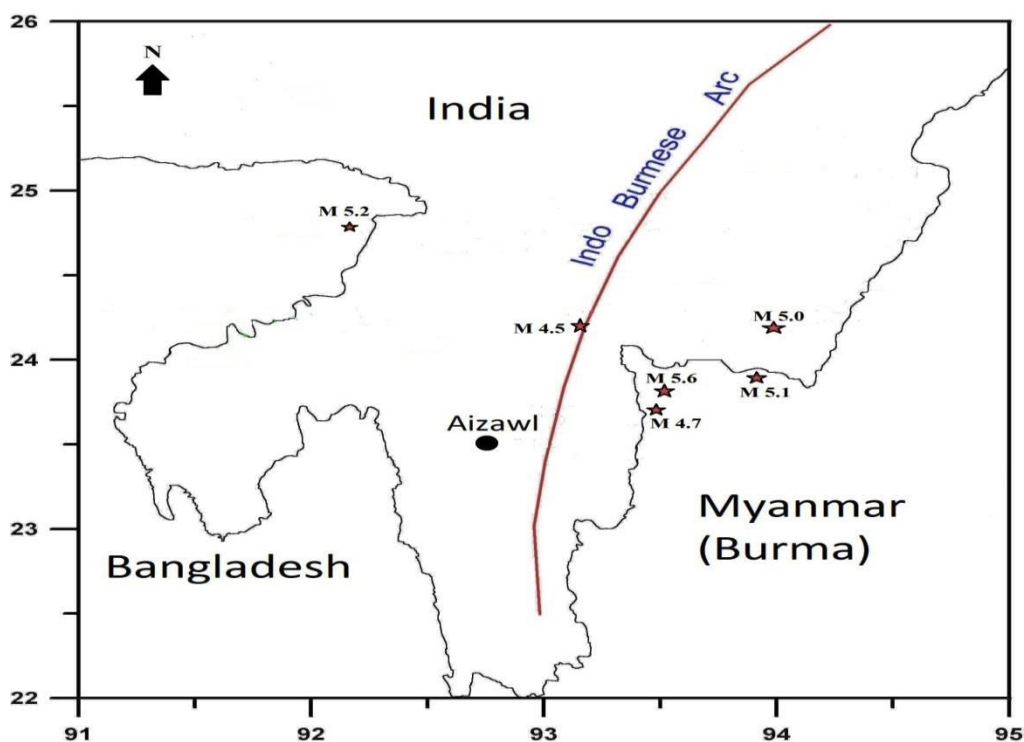


Fig. 4.1: Spatial distribution of the earthquakes that occurred around the study areas during the observation period.

The meteorological data for the investigated area were obtained from Indian Meteorological Department (IMD) regional meteorological centre, Guwahati, Assam, India. Daily recorded rainfall data, air temperature, relative humidity and barometric pressure were obtained from the observatory and the integrated measurement for 7 days was calculated for each parameters. Total rainfall is calculated for one week, temperature, pressure and relative humidity are the moving average of one week.

4.1 External influence of meteorological parameters on radon emanation

Soil gas radon concentrations have been measured continuously during March 2013 to May 2015. The measurements were carried out at ten different bare holes and the average of all the ten pits was considered as the final reading. The measured radon concentrations were plotted with the meteorological in order to examine the effect of these parameters on radon emission. The correlations of meteorological parameters with radon concentration were presented in Fig. 4.2 respectively. From Table 4.2, the measured radon concentration show positive correlation with rainfall, relative humidity and temperature. The correlation co-efficient between radon and rainfall was found to be 0.21, i.e. the increase in rainfall tends to increase the measured radon concentration and vice versa. This increase in radon concentration may be due to capping effect of wet soil layers at the surface which further prevents escaping of these gases into the atmosphere. As a result the radon values initially falls and then start rising over a period of time (Kraner *et al.*, 1964; Jaacks, 1984; Virk *et al.*, 2000). A low positive correlations was found between radon and relative humidity ($r = 0.12$). This increase in radon emanation with an increase in soil moisture has been reported elsewhere (Damkjaer and Korsbech, 1985; Lindmark and Rosen, 1985). The increase moisture in soil might increase the fraction of radon produced in rocks to migrate into pore fluids, thus

increases the radon content of soil gas (Tanner, 1964; Fleischer, 1983). Radon shows high positive correlation with temperature, i.e. the value of radon concentration increases as temperature increase and decreases with decrease in temperature. The correlation coefficient between radon and temperature was found to be 0.52 (Table 4.2). It suggests that an increase in surface temperature not only causes the soil gas to expand and escape but it tends to release the vapor species absorbed to the surface soil particles (Virk, 1993).

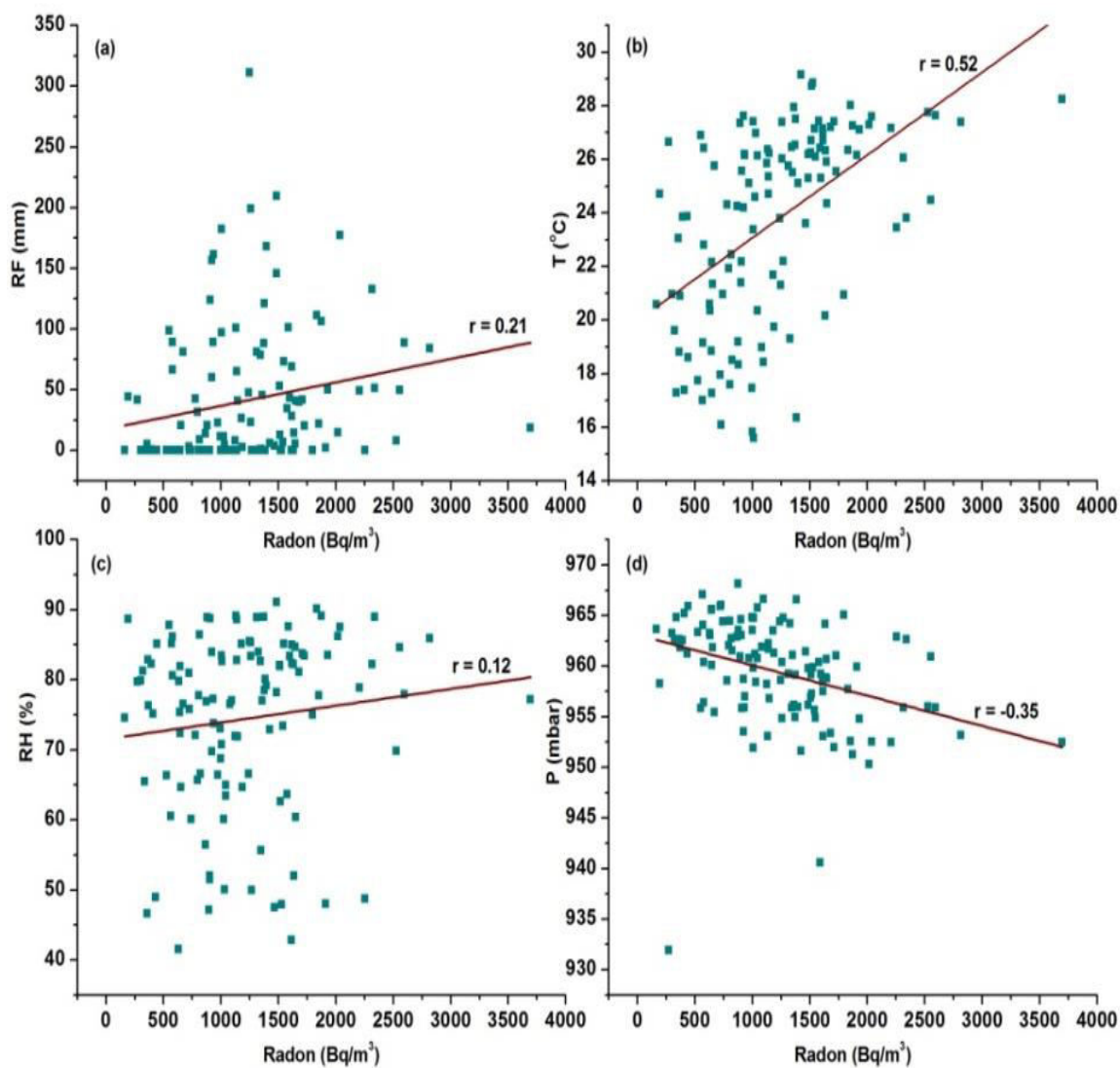


Fig. 4.2: Linear fitting of radon data with meteorological parameters at Chite fault: (a) rainfall, (b) temperature, (c) relative humidity and (d) pressure.

Negative correlation co-efficient of -0.35 between radon and pressure has been found i.e. radon decreases with increase in pressure and vice versa. This may be due to the pumping effect which induces vertical flow of soil-gas, whose component concentration varies with depth (King, 1986). An increase in atmospheric pressure tends to push the radon poor atmospheric air into the ground resulting in the fall of radon concentration. While the decrease in pressure lets the radon rich soil-gas escape from the deeper layers of the ground (Virk, 1993).

Table 4.2: Descriptive statistics of radon concentration and the meteorological parameters during the observation period

Parameters	No. of Observation	Average	Standard Deviation	Correlation Coefficient	Significance (P-value)
Radon(Bq/m ³)	118	1204.63	613.26	-	-
Rainfall (mm)	118	40.76	56.92	0.208	0.024
Temp. (°C)	118	23.71	3.63	0.52	0.00
RH (%)	118	74.41	12.65	0.12	0.21
Pressure (mb)	118	959.48	5.25	-0.35	0.00

RH (Relative Humidity)

To test the significance of the relations between the measured radon concentration and the meteorological parameters, we have performed the two-tailed test of significance (Snedecor and Cochran, 2009) at 95% confidence interval for each correlated case and the probability have been reported in the significance column of Table 4.2. The test indicates that there is no significant evidence for the correlation co-efficient observed between radon and relative humidity (P-value is 0.21 which is > 0.05level). In other words, the effect of relative humidity on the measured radon is not clearly understood. Whereas rainfall, temperature and relative humidity seems to have a significant effect on the measured radon concentration (P-values < 0.05 levels).

4.2 Meteorological parameters influence on Thoron emanation

The exhalation of thoron from soil is more dependent on soil conditions and meteorological factors than in the case for radon, because of the short half-life of thoron, the effective exhalation depth is only a few centimeters and the thoron exhalation decreases rapidly when moisture content increases. Investigating the correlation of thoron data with different meteorological parameters provides useful information about the dependence of these parameters on thoron emission. Soil thoron concentrations shows very much similar trends compared to radon concentration with different meteorological parameters. Fig.4.3, presents the correlation plot of thoron with different meteorological parameters.

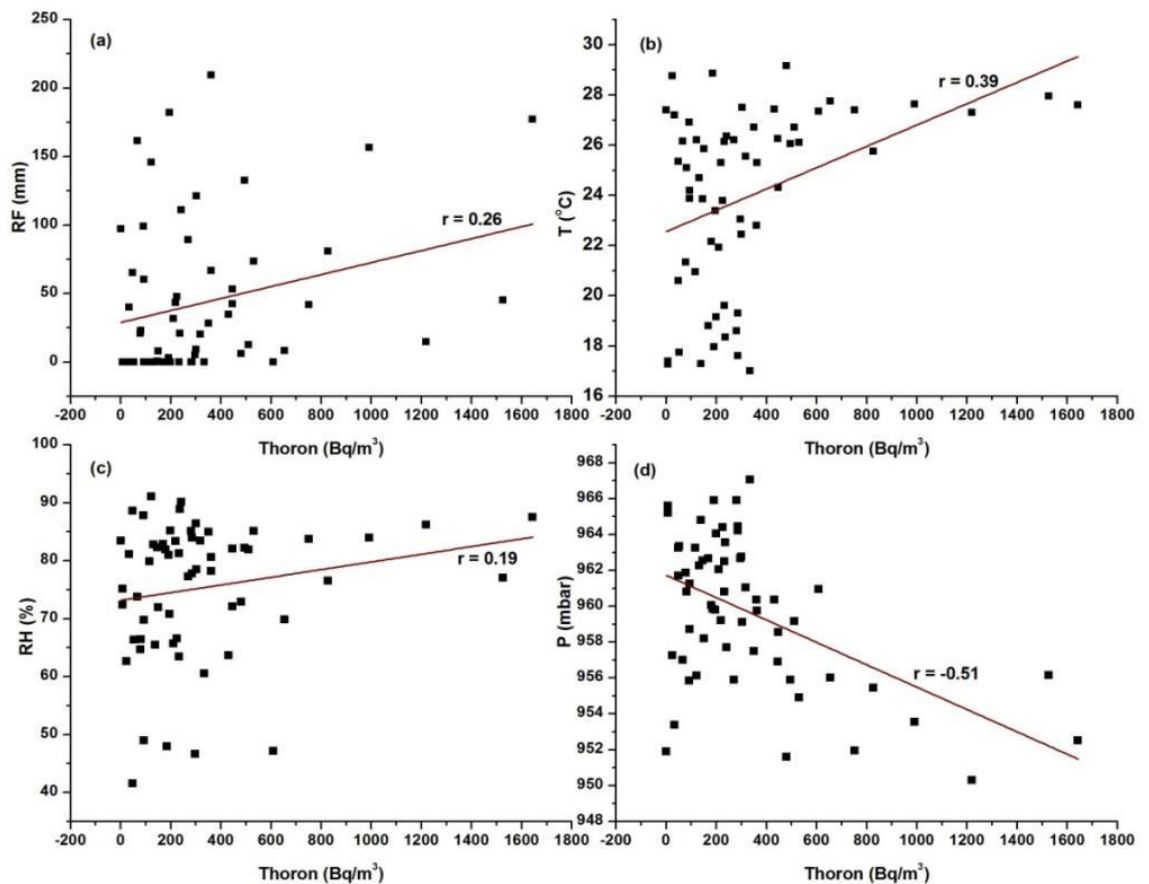


Fig. 4.3: Linear fitting of Thoron data with meteorological parameters at Chite fault: (a) rainfall, (b) temperature, (c) relative humidity and (d) pressure.

The measured thoron data shows a moderate positive correlation with rainfall. The correlation coefficient was found to be $r = 0.26$. This positive correlation suggests that the increase in rainfall tends to increase the measured thoron concentration. From Table 4.3, it is clear that thoron values show similar trend with temperature, i.e. with an increase in temperature, the thoron value increases. For a given time window, the correlation co-efficient between thoron and temperature was observed to be $r = 0.39$. The relative humidity shows a low positive correlation with thoron concentration i.e. $r = 0.19$. Low positive correlation was observed in radon as well. The measured thoron concentration shows an inverse correlation with barometric pressure.

Table 4.3: Descriptive statistics of Thoron concentration and the meteorological parameters during the observation period.

Parameters	No. of observation	Average	Standard Deviation	Correlation Coefficient	Significance (P-value)
Thoron (Bq/m ³)	60	326.32	336.75	-	-
Rainfall (mm)	60	43.12	55.86	0.26	0.042
Temperature (°C)	60	23.94	3.63	0.39	0.002
Relative Humidity (%)	60	75.34	11.80	0.19	0.148
Pressure (mb)	60	955.45	4.11	-0.51	0.000

The correlation coefficient between thoron and barometric pressure was found to be $r = -0.51$, indicating the increasing in barometric pressure tends to decrease the thoron concentration and vice-versa. Similarly, we have tested the significance for measured thoron with different meteorological parameters. We have performed the two- tailed test of significance at 95% confidence interval for each correlated case. The probability has been summarized in Table 4.3. It have been noticed that rainfall, temperature and pressure shows significant effect on measured thoron data (P-value are 0.042, 0.002 and 0.000 all of which were <0.05 level). In case of thoron, only relative humidity do not

have significant effect on measured thoron concentration (P-value is 0.148 which is >0.05 level).

4.3 Radon concentration associated with seismic events (using standard deviation from related mean value)

Numerous criteria have been used by different authors in order to evaluate the soil radon anomalies which include mean plus 'n' standard deviation (SD) (Fu *et al.*, 2005; King *et al.*, 1996; Price *et al.*, 1994; Rannou, 1989). The deviation of radon concentration by more than ± 2 SD are generally accepted as anomaly caused by seismic events and not by meteorological parameters (Guerra and Lombards, 2001; Virk *et al.*, 2002; Walia *et al.*, 2005b, Zmazek *et al.*, 2002). Moreover, the variation in radon concentration due to various meteorological parameters are well below +1SD (Singh *et al.*, 1991). In the present study for those anomalous changes in radon and thoron concentrations which are $\approx \pm 1$ STD or slightly more than ± 1 STD, a careful examination was done by observing the variations in meteorological parameters during the period of occurrence of anomaly and accordingly and anomaly is assumed. Fig. 4.4 presented the integrated value of radon concentration over 7 day along with the meteorological parameters viz., rainfall (Rf), Relative humidity (Rh), air temperature (T) and barometric pressure (P).

The average value of radon concentration during the investigation period was recorded to be 1204.63 Bq/m^3 with a standard deviation of 613.26 Bq/m^3 (Table 4.2). During the observation period, a total of nineteen radon peaks were perceived which were as follows:

- Four positive peaks crossing +2 SD
- Seven positive peaks crossing +1SD

- Eight negative peaks beneath $-1SD$

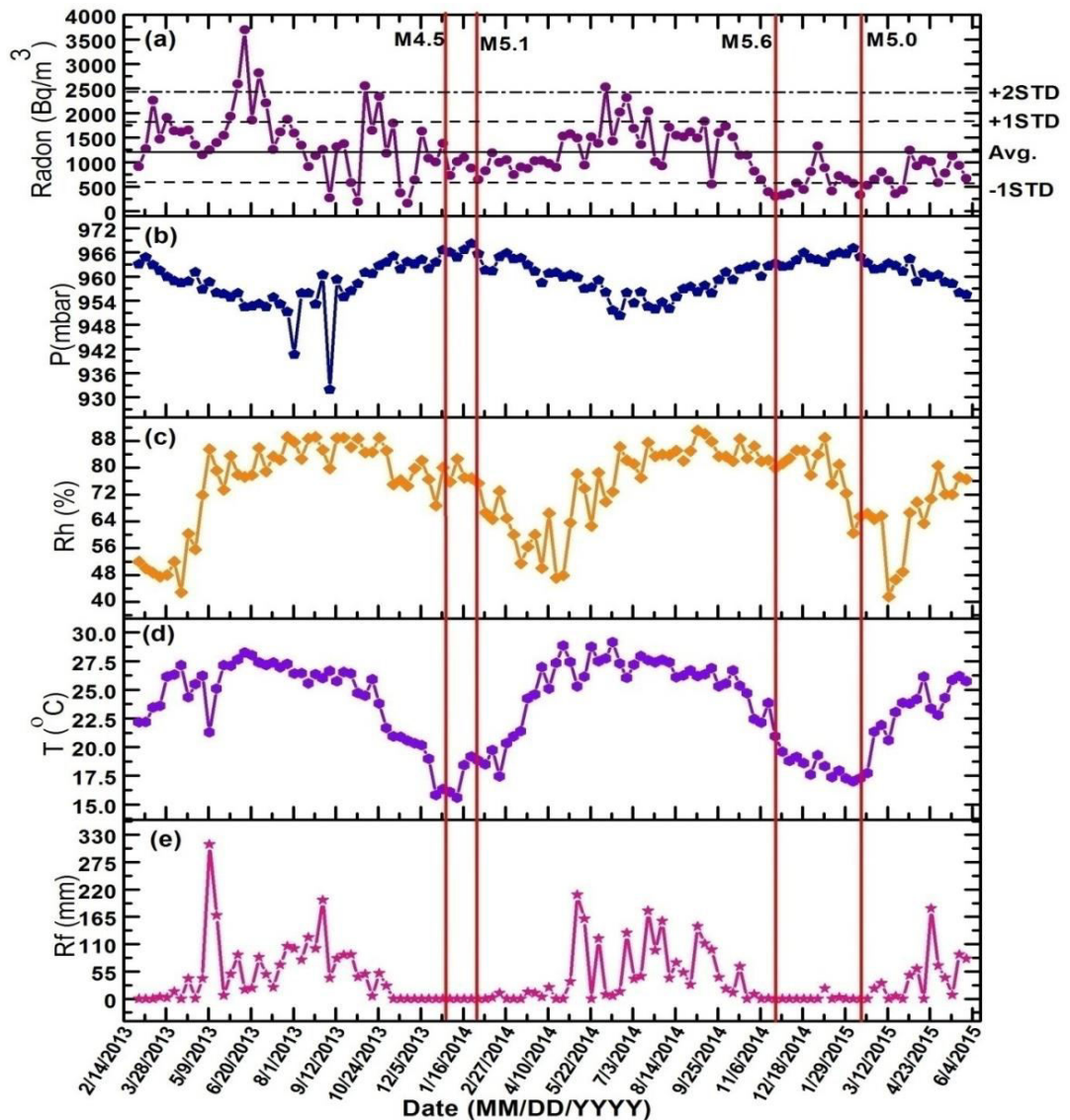


Fig. 4.4: (a) Radon concentration variation in the soil along with the; (b) pressure, (c) relative humidity, (d) temperature and (e) rainfall. The vertical bands passing through all the diagrams represent the earthquakes along with their magnitude that occurred during the observation period. The solid horizontal lines in (a) represents the average value of radon and the dotted lines indicate the standard deviations (+1 SD, +2 SD and -1SD) from the average values.

From Fig. 4.4, it is clear that those increase in radon peaks which crosses +1SD and +2SD, during that period there was no signature of any seismic events. Perhaps, all these increase in radon peaks may have occurred due to ongoing crustal deformation in

the region which was not mature enough to produce an earthquake (Walia *et al.*, 2009). Moreover, these increments in radon peaks occurred during rainy seasons, where the water filters through a porous surface and affects the gas emanation thus prevent gas to migrate toward the surface. As a result radon values initially falls and then start rising over a period of time (Kraner *et al.*, 1964; Jaaks, 1984; Virk *et al.*, 2000). Therefore, all these increments in radon concentration were considered as false anomalies or may cause due to meteorological parameters. Whereas for those decrease in radon concentration (i.e. below -1SD), out of eight radon peaks we could possibly three of them with that of the relevant seismic event. The remaining peaks were further examined along with the meteorological parameters during the observation period. It was found that pressure seems deviating from its mean value when low radon was recorded. Since, the correlation co-efficient between pressure and radon shows negative correlation. Therefore, these decreases in radon concentration could have been due to the influence of pressure on radon concentration.

The first noticeable radon anomaly (i.e. below -1SD) was observed on 11/22/13 (MM/DD/YY). This anomalous decrease in radon concentration may be correlated with two relevant seismic events of magnitude M4.5 and M5.1 which occurred on 12/30/13 and 1/29/14 (i.e. 38 days and 68 days after the anomaly was observed). The M4.5 and M5.1 quake occurred at a distance of 68km and 120km from the monitoring site. Next impulsive change in radon concentration (i.e. less than -1SD) was recorded on 11/21/14 during the investigation period. An earthquake of M5.6 and M4.7 occurred on 11/20/14 and 11/21/14 at a distance of 76km and 71km from the measuring site. The hypocentral depth of the earthquake was 33km and 46km. The third decrease in radon concentration was registered on 2/6/15 which was followed by an event on magnitude M5.0 occurred on 2/12/15 i.e., the observed anomaly was observed 6 days prior to the event. So, the

observed noticeable radon anomaly may be considered as a precursor signal since the two quakes occurred 1 day before the anomaly and the other occurred on the same day. Nevertheless, it is very difficult to directly correlated radon anomalies with those of relevant seismic activities. Since the effect of meteorological parameter on radon concentration play a significant role in perturbing the variation (or behavior) of soil gas radon concentration. Therefore, in order to have a much better or precise results an approach such as Multi linear regression and Artificial neural network has been implemented.

4.4 Correlation of Thoron anomalies with relevant earthquakes (using standard deviation method)

In contrast, measurement of thoron concentration was carried out from 4/11/2014 to 5/29/2015. Variation of soil gas thoron concentration after every 7 days along with the meteorological parameter is presented in Fig. 4.5. The average value of thoron during the investigation period was found to be 326.32 Bq/m^3 with a standard deviation 336.75 Bq/m^3 (Table 4.3). From Fig. 4.5, it is clear that the variation in thoron concentration seems to follow similar trend with that of radon concentration.

During investigation period only three thoron peaks were observed, two peaks which crosses +2 SD and one thoron peaks which was above +1 SD. The first peak was observed on 6/20/14 crossing +2 SD, the second peak was recorded on 7/18/14 and the last one was registered on 8/1/15 (crossing +1SD). However, for each particular thoron peaks during the time period there was no signature of any seismic events. While inspecting the behavior of meteorological parameters, there was noticeable deviation in rainfall, temperature and relative humidity in increasing mode from its average value whereas pressure seems to be deviating down from mean value.

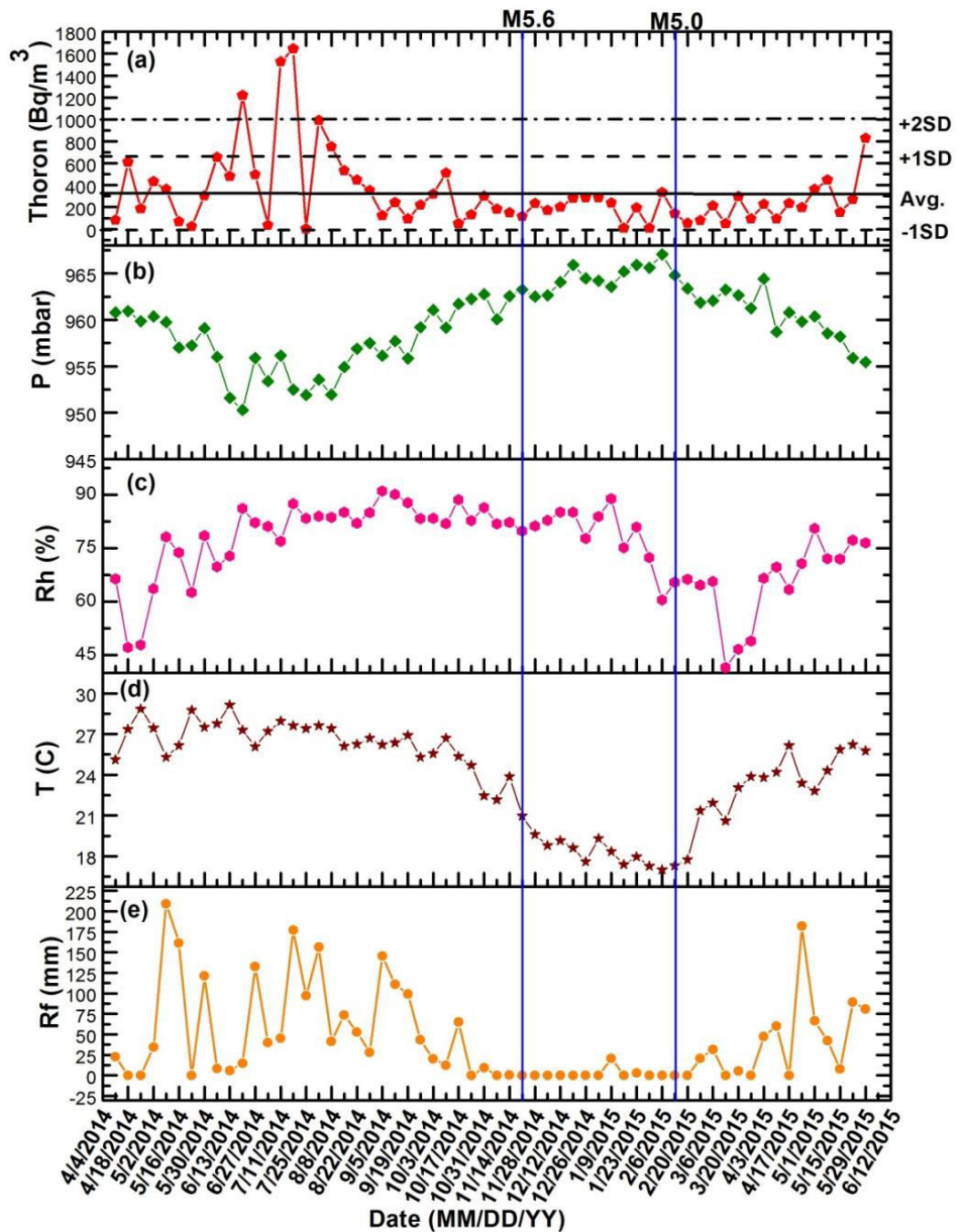


Fig. 4.5: (a) Thoron concentration variation in the soil along with the; (b) pressure, (c) relative humidity, (d) temperature and (e) rainfall. The vertical bands passing through all the diagrams represent the earthquakes along with their magnitude that occurred during the observation period. The solid horizontal lines in (a) represents the average value of radon and the dotted lines indicate the standard deviations (+1 SD, +2 SD and -1SD) from the average values.

Therefore all the registered peaks were considered as false anomaly caused due to the influence of meteorological parameters. Furthermore, for better result we made an attempt to analysis thoron data using two statistical approaches i.e. Multiple linear regressions (MLRs) and Artificial neural network (ANN).

4.5 Statistical analysis of soil radon and thoron data at Chite fault, Aizawl using Artificial Neural Network (ANN) and Multiple Linear Regressions (MLRs):

4.5.1 Artificial Neural Network

The ANNs architecture are generally classified as (1) Single-layer feedforward, (2) multi- layer feedforward, (3) recurrent and (4) Lattice structure (Haykin, 1994). Among this topology, multi- layer feedforward neural networks, commonly referred to as multilayer perceptrons (MLPs) have been used and applied successfully to solve some of the difficult and diverse problems in several domains including prediction and forecasting. MPL has a layered architecture consisting of input, hidden and output layers. The input signals propagate through the network in a forward direction on layer-by-layer basis. The output of each layer is transferred to the input of neurons in the next layer through weighted links. The hidden layer aids in performing useful complex computation by extracting progressively more meaningful features from the input layer. In case of training and weight adaptation, MLPs is done in supervised manner with a highly popular algorithm known as the error back propagation algorithm. The algorithm provides an established action for changing the weights in a back propagation network to assign the given input pattern, correctly for a given training set of input-output pairs (Kulachi *et al.*, 2009; Sen and Bispenera, 2004). In this study, Levenberg- Marquardt algorithm is applied as one of the back propagation training methods, as it has the

fastest convergence for medium size ANNs (Zurada, 1992). This method is a modification of the classic newton algorithm which is as follows

$$\chi_{k+1} = \chi_k - [J^T J + \mu I]^{-1} J^T e \quad (4.2)$$

Here, Newton's method applied the approximate Hessian matrix, the scalar μ is zero, but when μ is large this become gradient descent with a small step size. Therefore, μ is decreased after each successful step (reduction in performance function) and it is increased only when a tentative step would increase the performance function (The Mathworks Inc. USA, 2007). In the present study, a total of 118 dataset was trained, which were divided into three sets: the training set (70%), the cross-validation set (15%) and the test set (15%). The training set has been used to train the network, the validation set has been used for the purpose of monitoring the training process and to guard against overtraining and the testing set has been used to judge the performance of the trained network. Furthermore, the training was stopped just below threshold cross-validation error i.e. when the cross-validation error was lowest. Fig. 4.6 represents the ANN topology for learning radon concentration dependency on environmental parameters.

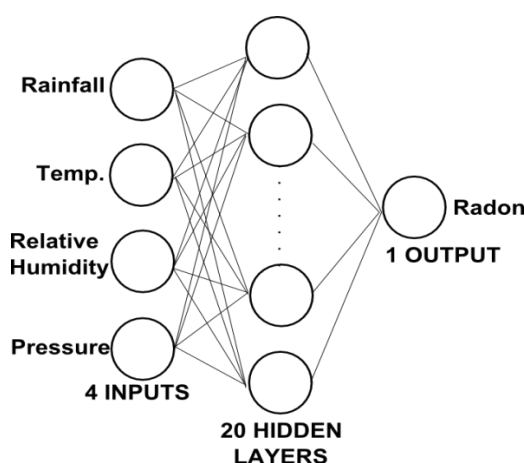


Fig. 4.6: The ANN topology for learning radon concentration dependency on environmental parameters.

During the investigation period, a total of 16 radon peaks were observed. Amongst these radon peaks there are two peaks of radon concentration which crosses above +2SD, five peaks crossing +1SD and nine peaks were beneath -1SD. From the Fig.4.7, it can be seen that all those positive radon peaks crossing +2SD and +1SD could not be correlated with the seismic activity, since there was no such signature of any seismic events during that time window. Instead all these increments in radon concentration appeared at the time of heavy rainfall; where the water filters through a porous surface and perturb the gas emanation thus prevent gas to migrate toward the surface. As a result the radon values initially falls and then start rising over a period of time (Krener *et al.*, 1964; Jaacks, 1984; Virk *et al.*, 2000). Therefore, these positive peaks may be considered as false anomaly.

Whereas, the radon peaks which were recorded below -1SD out of nine peaks only five of them could be correlated with the relevant seismic event. The first two decreases in radon concentration were observed on 11/29/13 and 12/13/13; these radon minima could be correlated to the earthquake on magnitude M4.5 which occurred on 12/30/13 of the observation period (i.e. 31days and 17 days prior to the seismic events). The third decrease in radon concentration was registered on 2/4/14 and this may be correlated to the earthquake of M5.1 which occurred on 1/29/14 (i.e. 6 days before the anomaly was observed or we can consider this peak as post-cursor anomaly). The fourth anomalous change in radon concentration (-1STD) was recorded on 11/7/14 which was followed by two seismic events taking place on 11/20/14 and 11/21/14 with a magnitude of M5.6 and M4.7. This is considered as precursor anomaly with a precursor time of 13 days and 14 days prior to the events. Their epicentral distances from the monitoring site were 76 km and 71 km. The fifth anomaly was registered on 2/6/15 followed by an earthquake of M5.0 (on 2/12/15 i.e. 6 days after the observed anomaly).

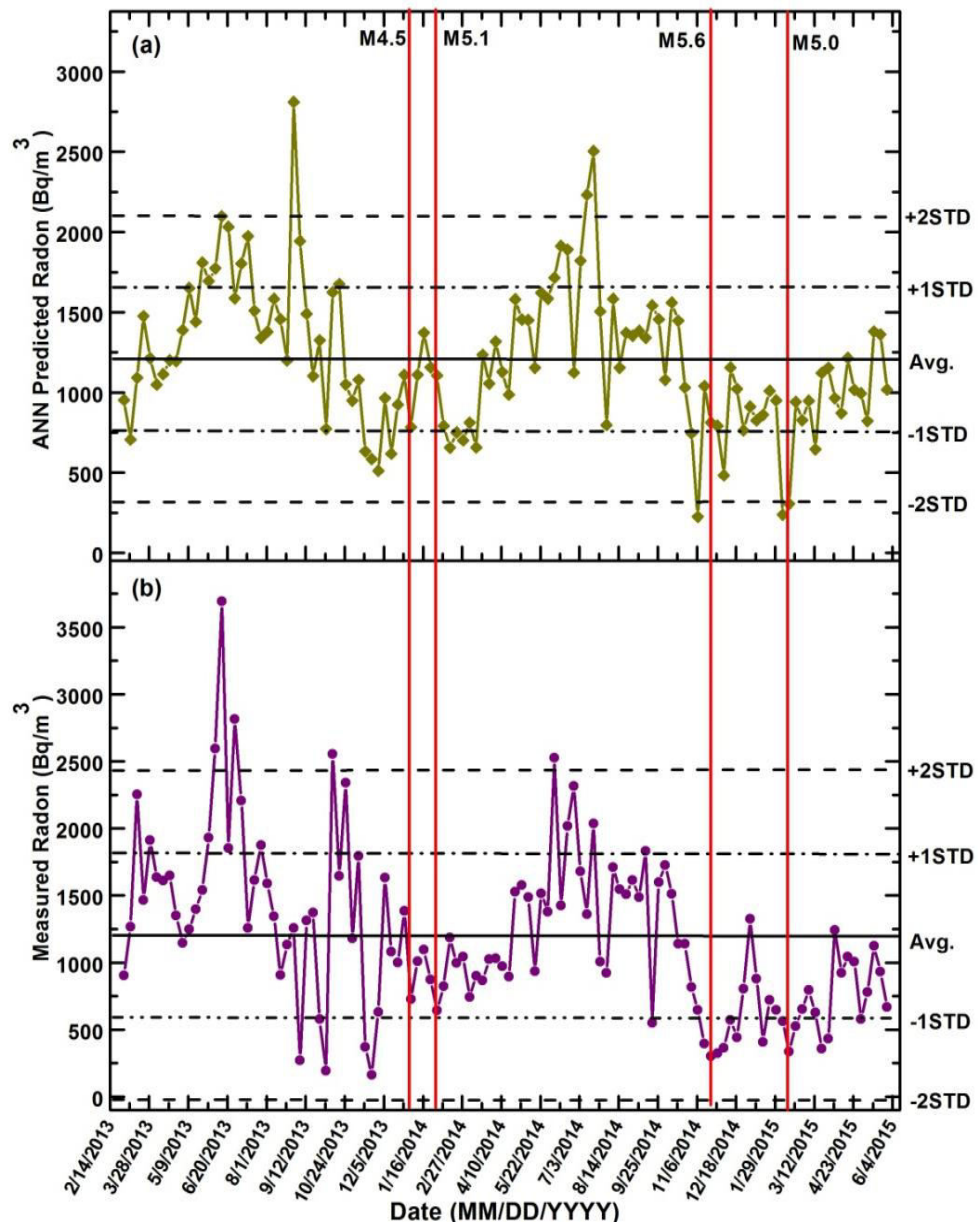


Fig. 4.7: Variation of (a) Predicted radon concentration (ANN) and (b) Measured radon concentration during the Investigation period at Chite fault. The solid vertical lines represent the earthquakes along with their magnitudes (M).

As in case of thoron data, there were 10 thoron peaks recorded during the observed period (i.e. from 4/11/14 to 5/29/15). From Fig.4.8, it can be seen that only one thoron peak was found to be crossing +2SD. Five of the thoron peaks were recorded to be above +1SD and four of them were beneath -1SD. During the investigation period, only three peaks could possibly be correlated with the relevant

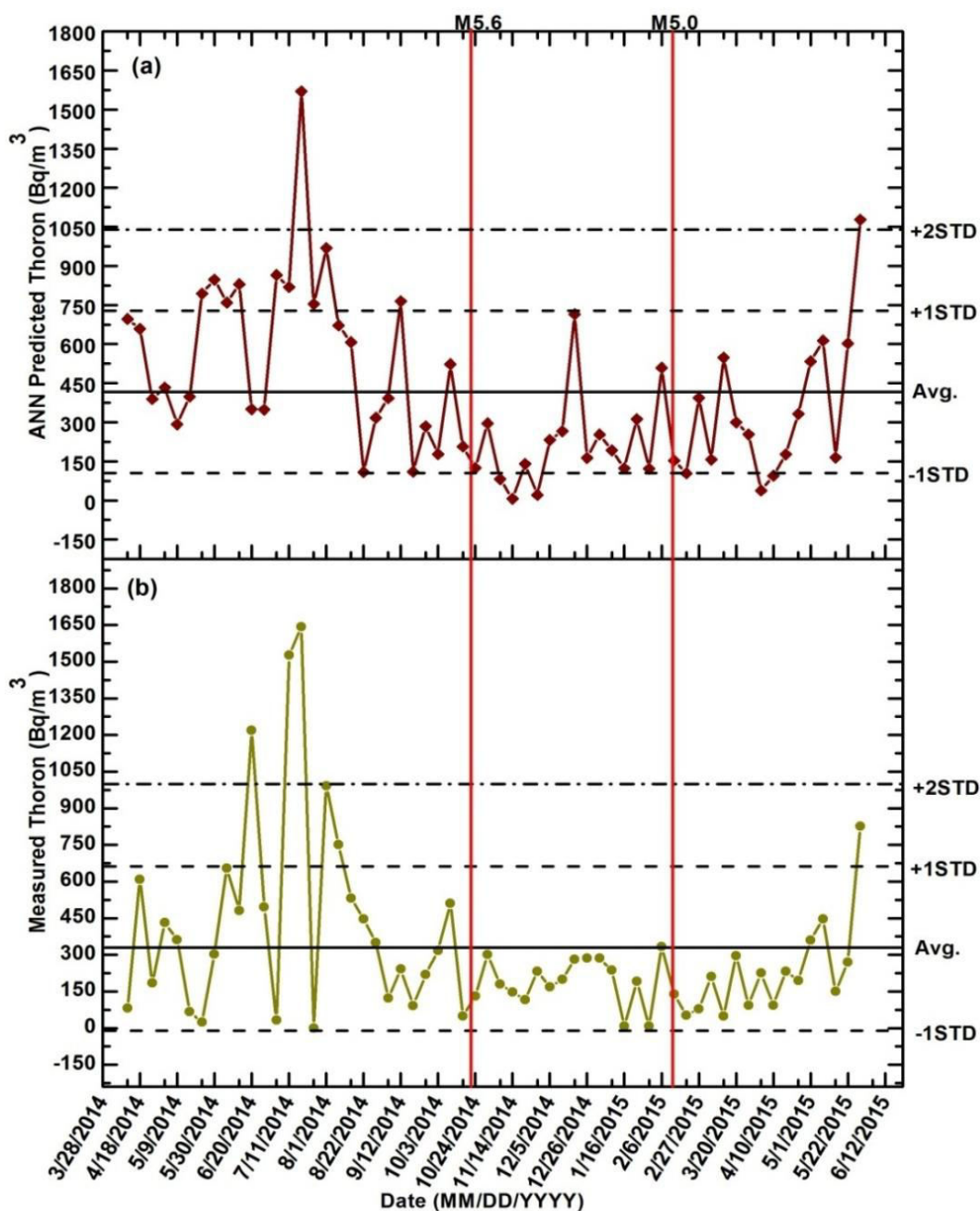


Fig. 4.8: Variation of (a) Predicted thoron concentration (ANN) and (b) Measured thoron concentration during the Investigation period at Chite fault. The solid vertical lines represent the earthquakes along with their magnitudes (M).

seismic events. Similar as that of radon, this remaining thoron peaks were observed during summer season (i.e. during heavy rainfall). Moreover, no such seismic activity occurred during this period. Therefore these thoron peaks were considered as false anomaly or may be due to influence of meteorological parameters. The first thoron

anomaly (i.e. decrease in thoron below -1SD) was recorded on 11/14/14 and the second thoron anomaly was observed on 11/28/14. At this time period, there were two events which occurred on 11/20/14 and 11/21/14 at epicentral distances 76 km and 71 km from the measuring site. For the first anomaly the two events occurred after 6 days and 7 days. And for the second thoron anomaly the two events occurred before 8 days and 7 days. The third thoron anomaly was found on 2/20/15. An event of magnitude M5.0 (2/12/15) occurred at an epicentral distance of 141 km from the monitoring site. The anomaly was recorded 8 days after the event.

All the anomalies correlated with the relevant seismic events in both radon and thoron concentration was found to be in decreasing from its average level. These decreases in radon and thoron concentration may have been caused either by admixing of radon-poor water from another aquifer through cracks created by the earthquake related strain changes or else may be due to accumulation of tectonic strain and a slow, steady increase of stress under geological condition. These types of decrease in radon concentration have been reported by certain authors in the past (King and Wakita, 1981; Kuo *et al.*, 2010).

4.5.2 Multiple Linear Regressions

In the present investigation we had performed MLRs analysis taking into account soil radon concentration (Rn) as the dependent variable and the meteorological parameters viz. rainfall (Rf), relative humidity (Rh), temperature (T) and Pressure (P) as independent variables. Here Rn has been regressed with Rf, Rh, T and P. All the predictor variables mentioned may not be a significant predictor of the dependent variables. To sort out this problem and to build a better model we performed backward regression method using SPSS statistical package. The backward regression method

starts with all the predictor variables, test the significance of each predictor variable using t-test and then delete the variable (if any) that improve the model the most by being deleted. This process is repeated until the maximum number of steps is reached or no more independent variable qualifies for removal (Hocking, 1976). The coefficients of the backward regression output for Radon are presented in Table 4.4.

Table 4.4: Coefficients of the Backward Regression output of Radon.

	Model	Unstandardized		Standardised	T	Sig.
		Coefficients		Coefficient		
		B	Std. Error	Beta		
1	Constant	-13892.422	14260.112		-0.974	0.332
	Rf	-0.323	1.032	-0.030	-0.313	0.755
	T	102.204	20.410	0.605	5.008	0.000
	RH	5.714	4.464	0.118	1.280	0.203
	P	12.780	14.399	0.109	0.888	0.377
2	Constant	-14214.377	14166.511		-1.003	0.318
	T	100.783	19.819	0.596	5.085	0.000
	RH	5.183	4.112	0.107	1.260	0.210
	P	13.178	14.286	0.113	0.922	0.358
3	Constant	-1152.375	415.438		-2.774	0.006
	T	87.335	13.416	0.517	6.510	0.000
	RH	3.849	3.847	0.079	1.001	0.319
4	Constant	-888.444	320.955		-2.768	0.007
	T	88.283	13.838	0.522	6.597	0.000

From the radon data, the backward regression output has four distinct models (Model 1, Model 2, Model 3 and Model 4). In the first model, it includes all the predictor variables (Rf, Rh, T and P). Now, to check the significance of the predictor variables a t-test is performed at 95% confidence interval (i.e. the alpha value is set at 0.05) and its corresponding probability is shown in significance column of the table (Table 4.4).

Looking at the significance of each predictor variable in model 1, three predictor variables (Rf, Rh and P) are non-significance predictors of the dependent variable as the p-value (significance) is more than α -value (0.05). In backward regression method, only one predictor variable are eliminated at a time (the predictor variable with the highest p-value is deleted first). Therefore, rainfall having the highest p-value (0.755) is removed from the model 1 and a second model is constructed with T, Rh and P as independent variables. Model 2 shows that P is a non significant predictor (i.e. the p-value is more than 0.05). So, P is removed from the model and a third model is constructed with T and Rh as predictor variable. It can be seen in Model 3 that Rh is a non significant predictor (since the p-value is much more than 0.05). For that reason Rh is removed from the model and a fourth model is built with T as a single predictor variable. It is now clear that T is a significant predictor (p-value <0.05) of Rn. Therefore the raw score regression equation for model 4 can be written as

$$Rn' = - 888.444 + 88.283(T) \quad (4.3)$$

We calculated the predictor value of measured radon concentration (Rn') and temperature using the above equation. The graphical representation of the predicted radon concentration and measured radon concentration during the observation period is shown in Fig 4.9. The first radon anomaly was observed on 12/20/13. This anomaly was found to be below -1SD. This anomaly was followed by an event of M4.5 which occurred on 12/30/13(i.e. the anomaly was seen 10 days prior to the event). Its epicentral distance from the measuring site was 68 km and a depth of 10 km. The second anomaly was recorded on 1/10/14 (decrease in radon concentration below -1SD). An earthquake of magnitude M5.1 was recorded on 1/29/14 and this event take place just 19 days after the anomaly was seen. The third decrease in radon concentration (i.e. below -1 SD) was registered on 12/26/14. There were two seismic events of M5.6

and M4.7 which occurred on 11/20/14 and 11/21/14 i.e. 36 days and 35 days before the anomaly was seen. Their epicentral distances from the monitoring site was 76 km and 71 km with a hypocentral depth of 33 km and 46 km. the fourth decrease in radon concentration was recorded on 2/6/15 which was followed by an event of M5.0 and this event occurred on 2/12/15, which is 6 days after the anomaly was observed. It can be clearly seen from the Fig 4.9., that there were 10 radon peaks and we could correlate only 4 of the peaks with relevant seismic events. The remaining five radon peaks were considered as false anomaly since there were no seismic events during the registered radon peaks.

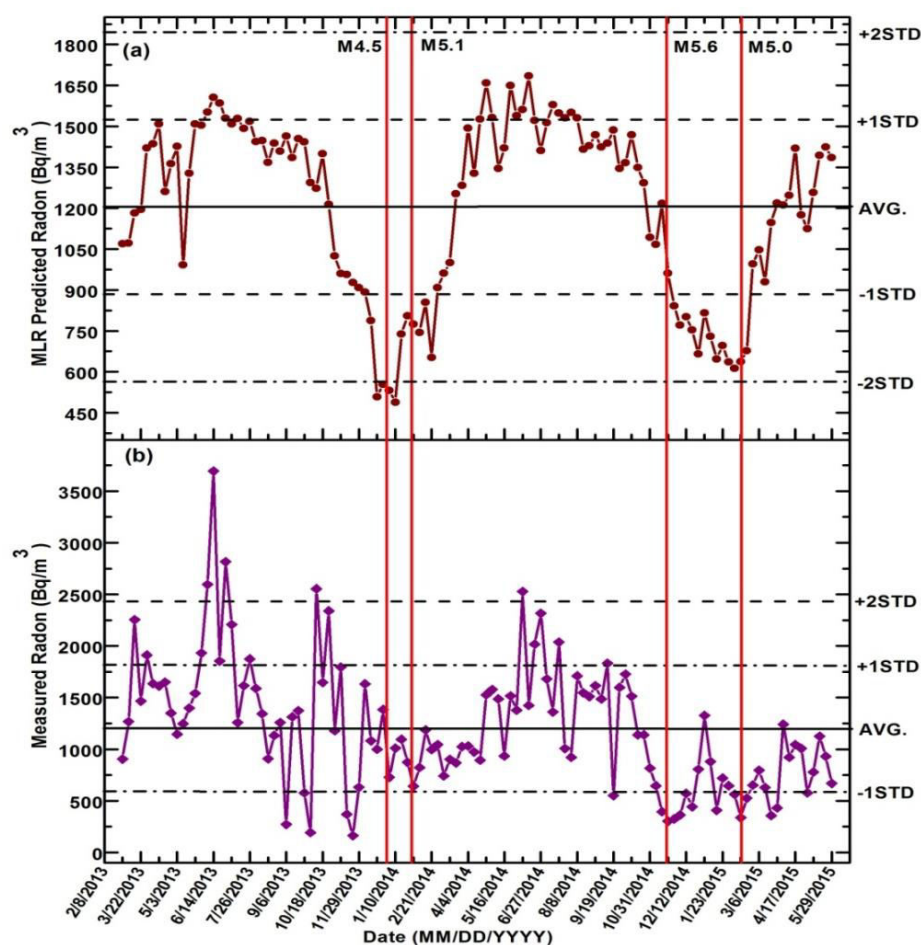


Fig. 4.9: Variation of (a) Predicted radon concentration (MLR) and (b) Measured radon concentration during the Investigation period at Chite fault. The solid vertical lines represent the earthquakes along with their magnitudes (M).

In contrast, thoron data was also regressed with Rf, Rh, T and P and even performed backward regression method using SPSS statistical package. Table 4.5 represents the coefficients of the backward regression out. Similarly the backward regression output has four distinct models (Model 1, Model 2, Model 3 and Model 4). The first model includes all the predictor variables (Rf, Rh, T and P). We even check the significance of each predictor variable in Model 1 and find out that all the predictor variable variables (i.e. Rf, Rh, T and P) are non-significant predictors of the dependent variables as the P-value (Significance) is more than the α -value (0.05) in all the cases.

Table 4.5: Coefficients of the Backward regression output of Thoron.

Model		Unstandardized		Standardised	T	Sig.
		Coefficients		Coefficient		
		B	Std. Error	Beta		
1	(Constant)	43053.744	18236.766		2.361	.022
	RF	.034	.828	.006	.041	.968
	T	-5.097	19.929	-.055	-.256	.799
	RH	1.122	3.757	.039	.299	.766
	P	-44.484	18.487	-.543	-2.406	.020
2	(Constant)	43175.383	17829.112		2.422	.019
	T	-5.005	19.625	-.054	-.255	.800
	RH	1.160	3.606	.041	.322	.749
	P	-44.615	18.044	-.544	-2.473	.016
3	(Constant)	39320.662	9380.218		4.192	.000
	RH	1.464	3.375	.051	.434	.666
	P	-40.747	9.697	-.497	-4.202	.000
4	(Constant)	40551.312	8878.381		4.567	.000
	P	-41.914	9.251	-.511	-4.531	.000

The backward regression method eliminates one predictor variable at a time (the predictor variable with the highest P-value is deleted first). So, rainfall (Rf) having the

highest P-value (0.968) is removed from Model 1 and a second model is build with Rh, T and P as independent variables. In Model 2, T and Rh is a non-significant predictor (since the P-value is more than 0.05). Therefore, T is removed from the model and a third model is built with Rh and P as predictor variables. Model 3 shows that Rf is a non-significant predictor (i.e. the P-value is much more than 0.05). Rf is therefore removed from the model and a fourth model is constructed with P as a single predictor variable. Clearly, P is a significant predictor (P-value <0.05) of thoron. So, the raw score regression equation for Model 4 can be written as

$$\text{Th}' = 40551.312 - 41.914 (P) \quad (4.4)$$

Here, we have calculated the predicted value of measured thoron concentration using the above equation. Detailed examination of thoron data using MLR shows that there were seven thoron peaks (i.e. one peak crossing +2SD, 3 peaks crossing +1SD and 3 peaks was below -1SD) registered during the measuring period. Out of these seven peaks, only two peaks which were below -1SD could be correlated with relevant earthquake (see Fig. 4.10). The first thoron anomaly was observed on 12/19/14, during this time period two events have occurred on 11/20/2014 and 11/21/2014 of magnitude M5.6 and M4.7. The epicentral distances were 76 km and 71 km. The second thoron anomaly was recorded on 2/6/2015 followed by an event of M5.0. The events occurred on 2/12/2015 which was 6 days after the anomaly was observed. The remaining five thoron peaks was considered as false anomaly. The reason for these false anomalies has been discussed elsewhere (section 4.3 and 4.4).

4.6 Comparisons of the results with different statistical approaches

The results of all the three approaches i.e. (1) Standard deviation from the related mean value, (2) MLR and (3) ANN used for the identification of radon

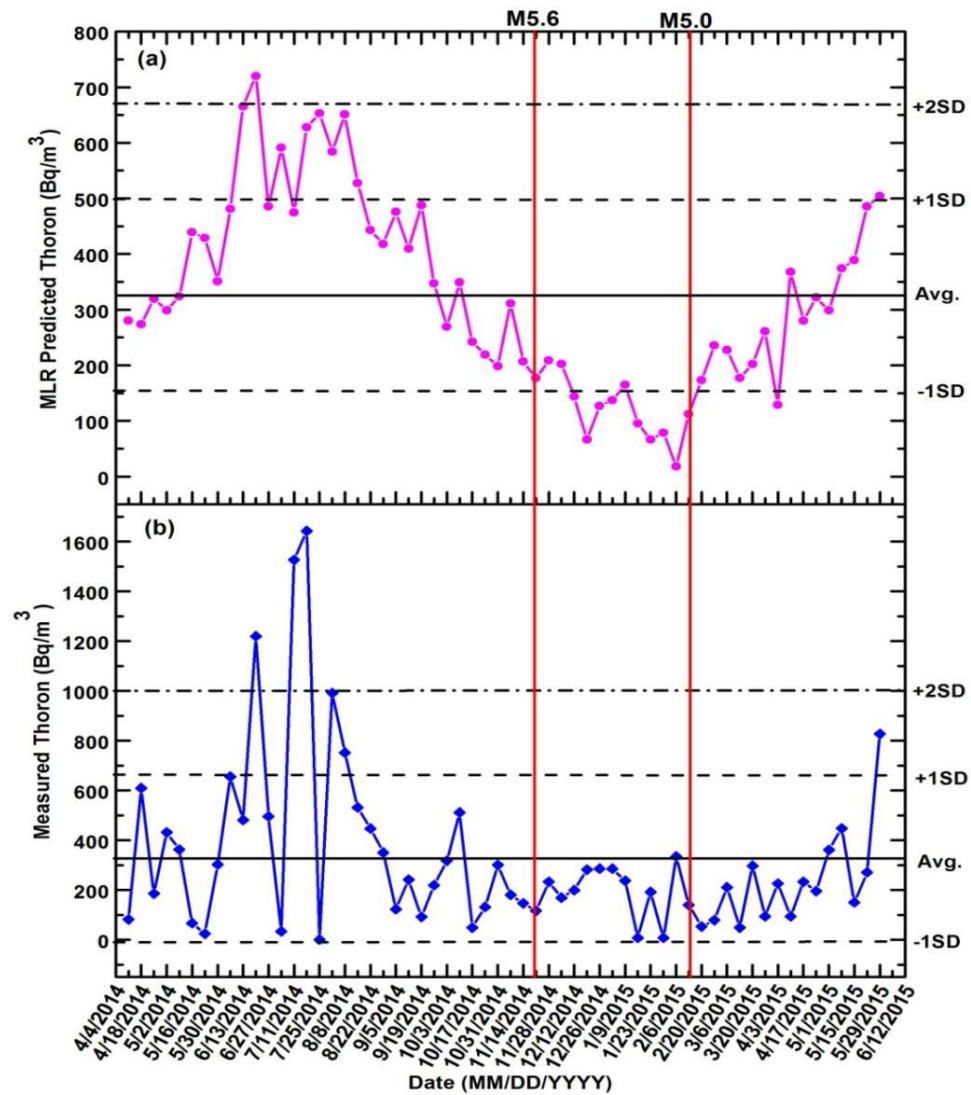


Fig. 4.10: Variation of (a) Predicted thoron concentration (MLR) and (b) Measured thoron concentration during the Investigation period at Chite fault. The solid vertical lines represent the earthquakes along with their magnitudes (M).

anomalies caused by seismic events in soil gas radon at Chite fault are shown in Fig.4.11. The statistical approach of ANN, it can be noticed from Fig. 4.11 (a) that there were four radon peaks crossing $\pm 2SD$ (2 peaks exceeding $+2SD$ and 2 peaks which is below $-2SD$). But we could correlate only 2 peaks which were below $-2SD$ with the relevant seismic activities. These two peaks may be considered as an anomaly caused by seismic events. Moreover the precursor time between the occurrence of anomaly and earthquake seems to take place at short time period. While the other two radon

anomalies which were correlated with the relevant seismic events was well below -1SD. In contrast, the statistical MLR approach shows that two radon peaks (below -2SD) was correlated with the seismic events of magnitude M4.5 and M5.1. There were also two radon peaks recorded during the observation period which were below -1SD. These two anomalies were seen to be correlated with the relevant earthquakes of magnitude M5.6 and M5.0 (Fig.4.11b).

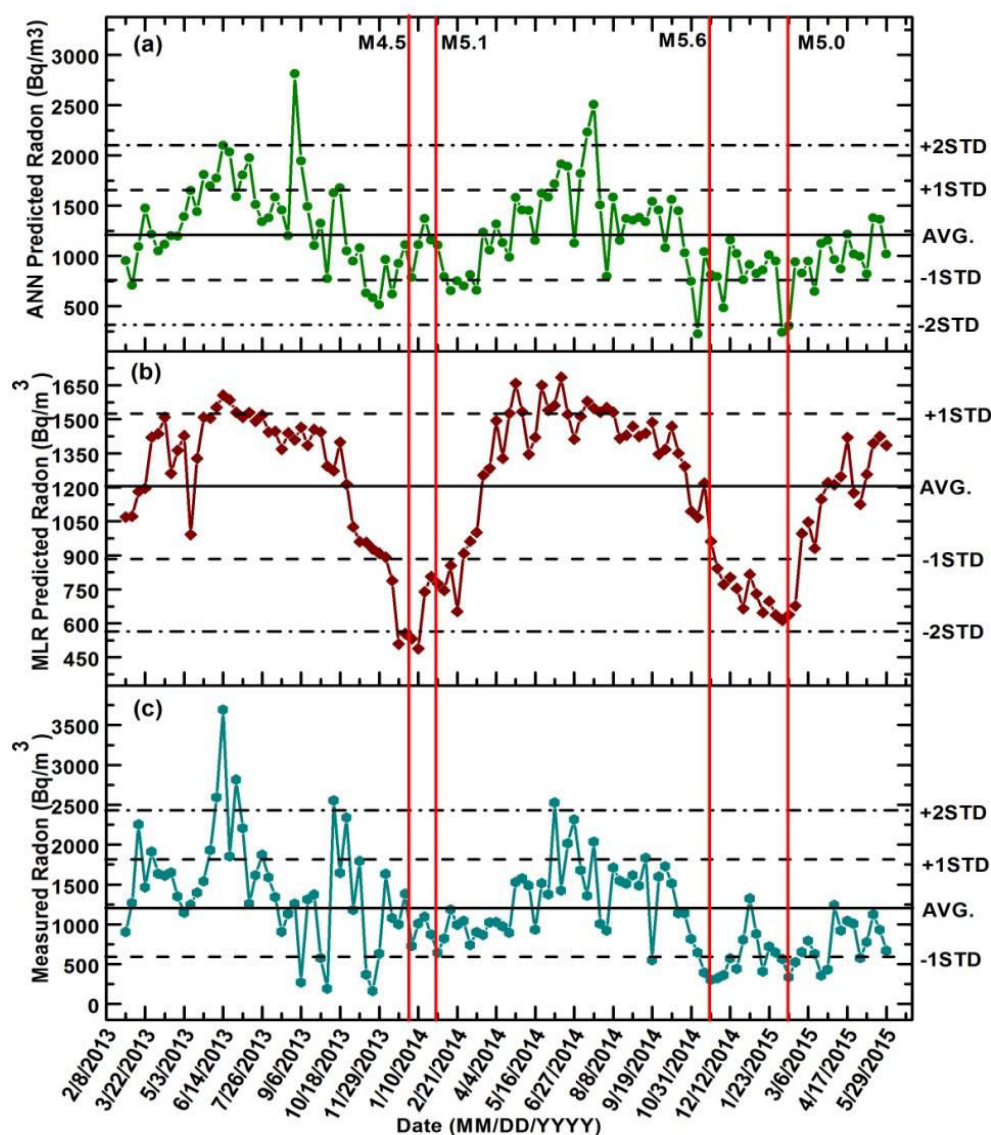


Fig. 4.11: Variation of (a) Predicted radon concentration (ANN), (b) Predicted radon concentration (MLR) and (c) Measured radon concentration during the Investigation period at Chite fault. The solid vertical lines represent the earthquakes along with their magnitudes (M).

There were no radon peaks crossing +2SD during the investigation period. Five radon peaks could be seen from Fig. 4.11 which was above +1SD but no seismic activity occurred during that time period. From Fig. 4.11 (c), analysis by standard deviation from the related means value shows that there were four positive peaks crossing +2SD and during that period there was no signature of any seismic events taking place. Even there were several radon peaks crossing +1SD but no occurrence of seismic activity. These increases in radon concentration may be considered as false anomaly or could have arisen due to the effect of meteorological parameters on radon. Only those decreases in radon concentration which was well below -1SD could be correlated with the relevant earthquakes.

Table 4.6: Descriptive statistics of Measured Radon concentration, predicted Radon (ANN) and Predicted Radon (MLR)

Parameters	No. of Observation	Mean	Standard Deviation	Maximum	Minimum	Correlation Coefficient
Measured Radon (Bq/m ³)	118	1204.63	613.26	3693.00	164	-
ANN	118	1208.26	446.25	2811.01	224.45	0.57
Predicted Radon (Bq/m ³)						
MLR	118	1204.63	320.31	1685.00	488.33	0.52
Predicted Radon (Bq/m ³)						

In conclusion, all the three statistical approaches used gives very similar results. During the investigation period, the relevant earthquakes were correlated only with the decrease in radon concentration which were well below -1SD and -2SD in all the three approaches. Amongst these three analyses, the ANNs seem to gives much better results as compared to the other two. The correlation coefficient between measured radon and

predicted radon using ANN is much larger than the correlation coefficient between measured radon and predicted radon using MLR (Table 4.6). The precursor time in all the three approaches, between observed anomaly and occurrences of seismic events was between 0 to 40 days. But in ANN, most of the anomaly was observed prior to the events. From Fig. 4.12, the statistical analysis of thoron data using the three approaches shows that ANN and MLR gives very similar characteristics.

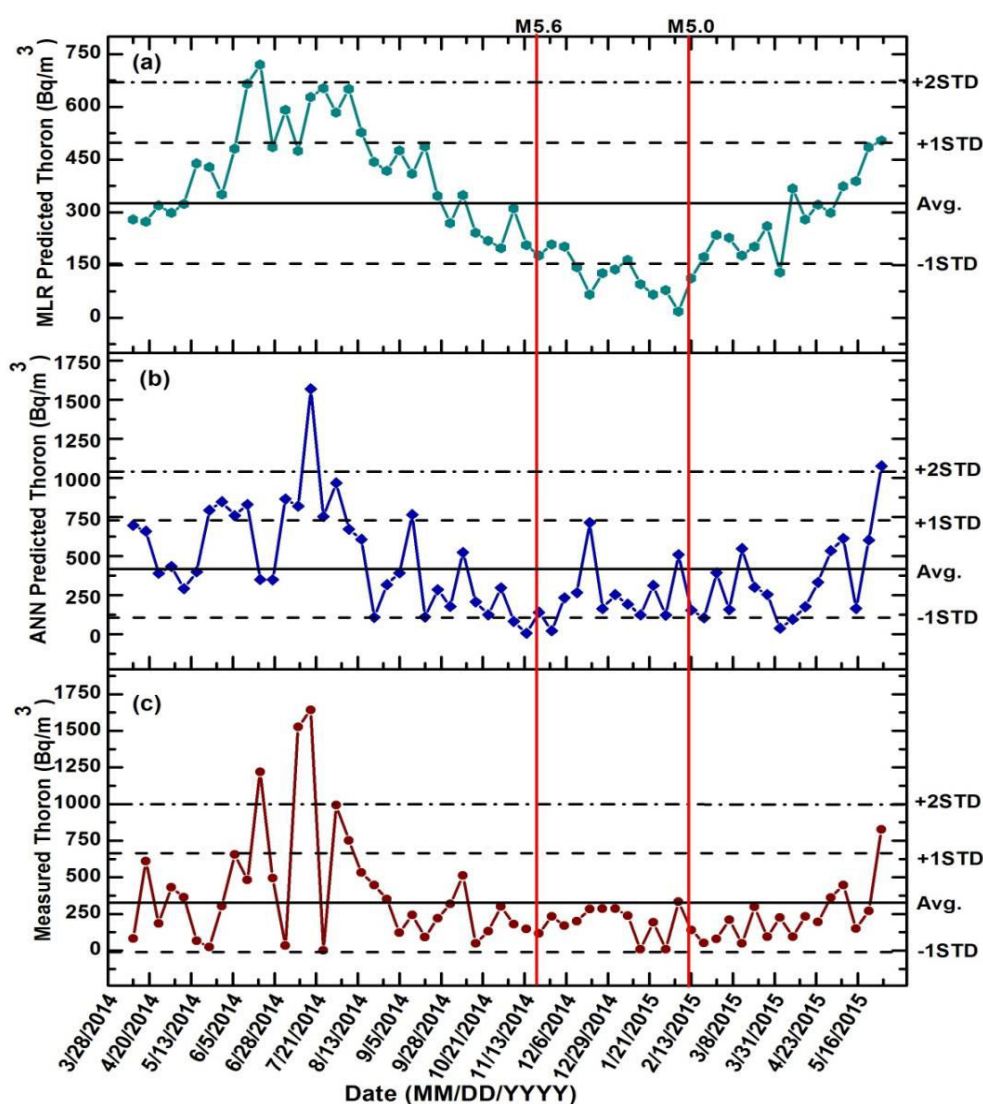


Fig. 4.12: Variation of (a) Predicted thoron concentration (ANN), (b) Predicted thoron concentration (MLR) and (c) Measured thoron concentration during the Investigation period at Chite fault. The solid vertical lines represent the earthquakes along with their magnitudes (M).

Whereas in case of the standard deviation approach, there was no anomaly noticed that could be correlated with the seismic events. From Fig. 4.12 (a), (b) and (c), it is clear that the positive peaks crossing +2SD and +1SD were considered as false anomaly or caused due to meteorological effects. Moreover, there were no seismic events occurred during that time period. Rather there were two seismic events of Magnitude M5.6 and M5.0 which was found to be correlated with the decreasing in thoron concentration (i.e. below -1SD). For Magnitude M5.6, a post anomaly could be observed in MLR approach, but in case of ANN thoron anomaly was noticed prior to the event. Regarding M5.0, MLR shows that thoron anomaly was seen prior to the event and for ANN approach, post anomaly was registered after the events. It has been observed that lesser number of thoron anomalies was detected as compared to radon data. The reason may be due to relatively short half-life of thoron (56 sec.) as compared to radon (3.823 days) which makes it difficult to detect.

5

Summary and Conclusion

Correlations between gas-geochemical and distant earthquakes have attracted re-establish interest in India due to large scale disaster caused by several major earthquakes in recent years. Emission of radon and thoron is strongly influenced by day to day meteorological conditions as well as seasonal. Different authors have attempt to tackle seasonal variation by normalizing the raw emission value over a local time period observation as a way of tackling the periodic variations in the mean emitted value. An appropriate interpretation of field measurement plays a significant role in any research. The main purpose of this work was to combine and evaluate the different approaches applied for differentiating the radon anomalies caused by increased seismic activities from those caused by environmental parameters.

The purpose of the present investigation is to generate radon/thoron database and to evaluate the possible correlation between soil radon/thoron concentration and earthquake along Chite fault, Mizoram, India which lies in seismic zone v according to the seismic zonation map of India. The study was performed during March 2013 to May 2015 at Chite in Aizawl district (Mizoram). Measurement was carried continuously over 7 day's period for collecting soil radon and thoron. Three different statistical approaches such as Standard deviation, Multiple linear regression and Artificial neural networking has been utilized to correlate the measured soil radon and thoron data to the seismic events that occurred in and around the study area during the period of investigation.

Effects of meteorological parameters on radon and thoron data have been analyzed during the observation period. The result obtained shows that both soil radon

and thoron data were positively correlated with rainfall, humidity and temperature whereas negative correlation was obtained with barometric pressure. It can be observed that both soil radon and thoron data seems to be affected by variation in the meteorological parameters. Radon and thoron data were less affected by variation in rainfall and relative humidity, since their correlation co-efficient with radon were found to be very weak. The correlation coefficient between temperature and radon/thoron show moderate positive correlation (i.e. 0.52 for radon and 0.39 for thoron). In case of pressure, its correlation shows moderate negative for both radon and thoron (i.e. -0.35 for radon and -0.51 for thoron). From Fig. 4.4 and Fig. 4.5, it can be clearly observed that seasonal analysis of soil radon and thoron data provides useful information on radon and thoron emission under variety of weather condition. High value of radon and thoron were found during summer whereas it was low during spring season. Generally, the soil radon and thoron concentrations changes seasonally but the effect on these gas emission has not been fully understood. This indicate that the soil gas emission are more likely to be caused by geophysical process though the effect of meteorological parameters cannot be neglected because these parameters may change the physical characteristics of the soil and thus influence the variation caused by geophysical process.

For better interpretation, the effect of meteorological parameters on measured radon and thoron data has been reduced by employing standard deviation approach. Each correlated events were analyzed carefully and then accordingly an anomaly was assumed. Several peaks of radon and thoron anomalies (both positive and negative peaks) were observed prior to the earthquake. Five events within the range of M4.5 to M5.6 occurred around the study area during the observation period. The epicenter

distance of the seismic events varies from 68 to 141 km. Three radon anomalies could be correlated to the events of M4.5, M5.1, M5.6, M4.7 and M5.0. The remaining radon peaks were considered as false anomalies (probably caused by variation in meteorological parameters). The precursor time between the occurrence of radon anomalies and the seismic events varies from 1 to 68 days. Moreover, most of the correlated events occurred along the Indo-Myanmar ranges (see Fig. 4.1) indicating that the study regions are active to the seismic events generated along the Indo-Myanmar subduction tectonics. In case of thoron, three thoron peaks were observed. But there was no seismic events occurred during the time period of observed anomaly. Therefore, the three registered peaks were considered as false anomaly. The reason may be due to the effect of meteorological parameters or else due to relatively short half-life of thoron as compared to radon which makes it difficult to detect.

Statistical analysis of soil radon data during the entire period of observation by employing artificial neural network (ANN) approach gives useful evidence to extract a radon anomaly caused by seismic events. The result obtained from ANN approach shows that there were 16 radon peaks registered during the investigation period. And only five radon anomaly could successfully correlate with the relevant earthquakes. Where as in case of thoron data, 10 thoron peaks were observed during the measurement period, only three of the thoron anomaly were correlated with the relevant seismic events.

Analysis of radon and thoron data using multiple linear regression approach shows that there were 10 radon peaks observed and out of these peaks, we could possibly correlate 4 of the radon anomalies with the relevant seismic activities. While in case of thoron, there were 7 thoron peaks and we could correlate only two thoron

anomalies with that of the relevant earthquake. In all the three approaches, the anomalies correlate with seismic events were decrease in its concentration (i.e. below -1STD and -2STD) in both radon and thoron data. These types of decreases in radon and thoron concentration have been reported by certain authors in the past (King and Wakita, 1981; Kuo et al., 2010).

Future scope of the study:

The present study represents an initial effort of monitoring soil radon and thoron variations along Chite fault, Aizawl district (Mizoram), India. Although, periodical soil radon and thoron measurements at weekly intervals do not appear to be frequent enough to interpret a possible direct relation with certain seismic events. The result of this study has proved the usefulness of using such data for setting the range of normal soil radon and thoron variations above or below which radon and thoron values could be considered anomalous. The estimated range is regarded to be an important step at this stage of our radon and thoron monitoring program as it may assist the distinction of usual soil radon and thoron variation in the study from other unusual values which might be caused by tectonic disturbance. However, the result obtained would have been much promising and interesting with shorter sampling period of time. Further for better prospective, we would like carried out this research with online radon/thoron analysis along with simultaneous measurement of carrier gases like CO_2 and CH_4 which play a dominant role in controlling the transport of radon gas toward the earth surface.

References

- Alekseev V.A., Alekseeva N.G., Jchankuliev (1995). On relation between fluxes of metals in waters and radon in Turkmenistan region of seismic activity. *Radiation Measurements*, **25**, 637-639.
- Allegri L., Bella F., Della Monica G., Ermini A., Improta S., Sgrigna V. and Biagi P. F. (1983). Radon and tilt anomalies detected before the Irpinia (south Italy) earthquake of November 23, 1980, at great distance from the epicenter. *Geophysical Research Letters*, **10**, 269-272.
- Alparone S., Behncke B., Giammanco S., Neri M. and Privitera E. (2005). Paroxysmal summit activity at Mt. Etna (Italy) monitored through continuous soil radon measurements. *Geophysical Research Letters*, **32**, doi: 10.1029/2005GL023352,
- Anderson D.L. and Whitcomb J.H. (1973). The dilatancy-diffusion model of earthquake prediction. In: Proc. Conf. on Tectonic problems of the San Andreas Fault systems (Kovach R.L. and Nur A., Eds.). *Stanford University Press*, **13**, 417-425.
- Anderson O.L. and Grew P.C. (1977). Stress corrosion theory of crack propagation with application to Geophysics. *Reviews of Geophysics*, **15**, 77-104.
- Andrews J.N. and Wood D.F (1972). Mechanism of radon release in rock matrices and entry into groundwaters. *Applied Earth Sciences*, **81**, 198-209.
- Arafa W. (2002). Permeability of radon-222 through some materials. *Radiation Measurements*, **35**, 207-211.

- Arjun C.R. and Kumar A. (2009). Artificial Neural network- based estimation of peak ground acceleration. *ISET Journal of earthquake technology*, **46**, 19-28.
- Atkinson B.K. (1984). Subcritical crack growth in geological materials. *J. Geophysical Research*, **89**, 4077-4114.
- Attanasio A. and Maravalli M. (2016). Some considerations between radon and earthquakes in the crater of L'Aquila. *Natural Hazards*, **81(3)**, 1971-1979.
- Azimi-Garakani D. (1990). Spark counter for alpha particle registration. In: Proc. of the international workshop on Radon monitoring in Radioprotection, Environmental Radioactivity and Earth Sciences (Tommasino L., Furlan G., Khan H.A. and Monnin M., Eds.), ICTP, Trieste, 3-14 April 1989, 164-170.
- Barsukov V.L., Varshal G.M., Garanm A.B. and Serebrennikov V.S. (1984). Hydrochemical Precursors of Earthquakes. In: Earthquake Prediction, UNESCO, Paris 169-180.
- Baykut S., Akgul T. and Inan S. (2011). Seismic activity-rekated anomaly detection in soil radon emanation, 19th European signal processing conference (EUSIPCO 2011), Barcelona, Spain, August 29-September 2, 2011, 908-912.
- Benton E.V. and Nix W.D. (1969). The restricted energy loss criterion for registration of charged particles in plastics. *Nuclear Instruments and Methods*, **67**, 343-347.
- Bernard P., Herrero A. and Berge C. (1996). Modeling directivity of heterogeneous earthquake ruptures. *Bull. Seismol. Soc. Am.*, **10**, 1149-1160.
- Bossus D.A.W. (1984). Emanating power and specific surface area. *Radiat. Prot. Dosim.*, **7**, 73-76.

- Brace W.F. and Bombolakis E.G. (1963). A note on brittle crack growth in compression. *J. Geophys. Res.*, **68**, 3709-3713.
- Brace W.F. and Byerlee J.D. (1966). Stick-slip as a mechanism for earthquake. *Science*, **153**, 990-992.
- Briestensky M., Thinnova L., Praksova R., Stemberk J., Rowberry M.D. and Knejflová Z. (2014). Radon, carbon dioxide and fault displacements in central Europe related to the Tōhoku earthquake. *Radiat. Prot. Dosim.*, doi:10.1093/rpd/ncu090.
- Burton M., Neri M. and Condarelli D. (2004). High spatial resolution radon measurements reveal hidden active faults on Mt. Etna. *Geophys. Res. Lett.*, **31**, doi:10.1029/2003GL019181, 2004.
- Burridge R. and Knopoff L. (1967). Model and theoretical seismicity. *Bull. Seismol. Soc. Amer.*, **57**, 341-371.
- Carlson J.M., Langer J.S. and Shaw B.E. (1994). Dynamics of earthquake faults. *Rev. Mod. Phys.*, **66**, 657-670.
- Carlson J.M., Langer J.S., Shaw B.E. and Tang C. (1991). Intrinsic properties of Burridge-Knopoff model of an earthquake fault. *Physical Review A*, **44**, 884-897.
- Chng E.S., Chen S. and Mulgrew B. (1996). Gradient radial basis function networks for nonlinear and nonstationary time series prediction. *IEEE Transactions on Neural Networks*, **7(1)**, 190-194.

- Choubey V.M., Kumar Naresh, Arora B.R. (2009). Precursory signatures in the radon and geohydrological borehole data for M4.9 Kharsali earthquake of Garhwal Himalaya. *Science of the total environment*, **407**, 5877-5883.
- Cicerone R. D., Ebel J.E. and Britton J. (2009). A systemic compilation of earthquake precursors. *Tectonophysics*, **476**, 371-396.
- Crannell H., Crannell C.J., Kline F.J. and Battist L. (1969). Particle track enhancement in cellulose nitrate by application of an electric field. *Science*, **166**, 606-607.
- Crockett R.G.M., Gillmore G.K., Phillips P.S., Denman A.R. and Groves-Kirkby C.J. (2006). Radon anomalies preceding earthquakes which occurred in the UK, in summer and autumn 2002. *Science of the Total Environment*, **364**, 138-148.
- Cross W.G. and Tommasino L. (1968). Electrical detection of fission fragment tracks for fast neutron dosimetry. *Health Phys.*, **15**, 196.
- Dahlen F.A. (1977). The balance of energy in earthquake faulting. *Geophysical Journal International*, **48**, 239-261.
- Damkjaer A. and Korsbech U. (1985), Measurement of the emanation of radon-222 transport from Danish soils. *Science of the Total Environment*, **45**, 343-350.
- Das N.K., Choudhury H., Bhandari R.K., Ghose D., Sen P. and Sinha B. (2006). Continuous monitoring of ²²²Rn and its progeny at a remote station for seismic Hazard surveillance. *Radiation Measurements*, **41**, 634-637.
- Deva, Y. and Rawat, U.S.A *feasibility study for urban tunnelling in soft tertiary sedimentary rocks of Mizoram, India*. Proceedings of the 10th International Congress of the IAEG at Nottingham, IAEG – 168, 1 – 8(2006).

- Dieterich J.H. (1979). Modeling of rock friction: 1. Experimental results and constitutive equations. *J. Geophys. Res.: Solid Earth*, **84**, 2161-2168.
- Dongarra G. and Martinelli G. (1993). Migration process of radon towards the earth surface: implications for the prediction of seismic and volcanic events. In: Proceedings on Scientific Meeting on the Seismic protection, Venice, 12-13 July 1993, 141-147.
- Duenas C. and Fernandez M.C. (1988). Temporal variations in soil gas radon: any possible relation to earthquakes? *Tectonophysics*, **152**, 137-145.
- Eappen K.P. and Mayya Y.S. (2004). Calibration factors for LR-115 (type II) based radon thoron discriminating dosimeter. *Radiation Measurements*, **38**, 5-17.
- Erees F.S., Aytas S., Sac M.M., Yener G. and Salk M. (2007). Radon concentrations in thermal waters related to seismic events along faults in the Denizli Basin, Western Turkey. *Radiation Measurements*, **42**, 80-86.
- Etiopie G. and Martinelli G. (2002). Migration of carrier and trace gases in the geosphere: an overview. *Physics of the Earth and Planetary Interiors*, **129**, 185-204.
- Ferguson C.D., Klein W. and Rundle J.B. (1998). Long-range earthquake fault models. *Computers in Physics*, **12**, 34-40.
- Finkelstein M., Brenner S., Eppelbaum L. and Ne'eman E. (1998). Identification of anomalous radon concentrations due to geodynamic processes by elimination of Rn variations caused by other factors. *Geophys. J. Int.*, **133**, 407-412.

- Fischer B.E. and Spohr R. (1983). Production and use of nuclear tracks: imprinting structure on solids. *Reviews of Modern Physics*, **55**, 907-948.
- Fleischer R.L. (1981). Dislocation Model for radon response to distant earthquakes. *Geophys. Res. Lett.*, **8**, 477-480.
- Fleischer R.L. (1983). Theory of alpha recoil effects on radon release and isotopic disequilibrium. *Geochimica et Cosmochimica Acta*, **47**, 779-784.
- Fleischer R.L. and Mogro-Campero A. (1985). Association of subsurface radon changes in Alaska and the northeastern United States with earthquakes. *Geochimica et Cosmochimica Acta*, **49**, 1061-1071.
- Fleischer R.L., Price P.B. and Walker R.M. (1975). Nuclear Tracks in Solids. *University of California Press*, Berkeley.
- Flerov G.N., Oganesyon Yu T., Lobanov Yu V., Kuznetsov V.I., Druin V.A., Perehlyng V.P., Gavrilov K.A., Tretiakova S.P., Platko V.M. (1964). Synthesis and Physical Identification of the Isotope of element 104 with Mass near 260. *Phys. Letters*, **13**, 73-75.
- Friedmann, H. (2012). Radon in earthquake prediction research. *Radiat. Prot. Dosim.*, **149**, 177-184.
- Friedmann H. (1985). Anomalies in the radon content of spring water as earthquake precursor phenomena. *Earthquake Prediction Research*, **3**, 179-189.
- Friedmann H., Aric K., Gutdeutsch R., King C.Y., Altay C. and Sav H. (1988). Radon measurements for earthquake prediction along the North Anatolian Fault Zone: a progress report. *Tectonophysics*, **152**, 209-214.

- Fu C.C., Yang T.F., Du J., Walia V., Chen Y.G., Liu T.K. and Chen C.H. (2008). Variations of helium and radon concentrations in soil gases from an active fault zone in southern Taiwan. *Radiation Measurements*, **43**, S348-S352.
- Fu C.C., Yang T.F., Walia V. and Cheng C.H. (2005). Reconnaissance of soil gas composition over the buried fault and fracture zone in southern Taiwan. *Geochemical Journal*, **39**, 427-439.
- Garavaglia M., Braitenberg C. and Zadro M. (1998). Radon monitoring in a cave of North- Eastern Italy. *Physics and Chemistry of the Earth*, **23**, 949-952.
- Geological Survey of India. (1988). *Geoenvironmental appraisal of Aizawl town and its surroundings, Aizawl district, Mizoram*. Unpublished Report, Field Season 1985 – 1986.
- George A.C., Paschoa A.S. and Usler F.S. (2008). World history of radon research and measurement from the early 1900's to today. In: AIP Conference Proceedings, **1034**, p.20.
- Ghosh D., Deb A., Sengupta R., Patra K.K. and Bera S. (2007). Pronounced radon anomaly—precursor of recent earthquakes in India. *Radiation Measurements*, **42**, 466-471.
- Ghosh D., Deb A. and Sengupta R. (2009). Anomalous radon emission as precursor of earthquakes. *J. Applied Geophysics*, **69**, 67-81.
- Giammanco S., Immè G., Mangano G., Morelli D. and Neri M. (2009). Comparison between different methodologies for detecting radon in soil along an active fault:

- The case of the Pernicana fault system, Mt. Etna (Italy). *Applied Radiation and Isotopes*, **67**, 178-185.
- Giammanco S., Sims K. W. M. and Neri M. (2007). Measurement of ^{220}Rn , ^{222}Rn and CO_2 emission in soil and fumaroles gases on Mt. Etna volcano (Italy): Implications for gas transport and shallow ground fracture. *Geochem. Geophys. Geosyst.*, **8**, doi:10.1029/2007GC001644.
- Grammakov A.G. (1936). On the influence of some factors in the spreading of radioactive emanations under natural conditions. *Zeitschrift für Geofizik*, **6**, 123-148.
- Guerra M. and Lombardi S. (2001). Soil-gas method for tracing neotectonic faults in clay basin: the Pisticci field (southern Italy). *Tectonophysics*, **339**, 511-522.
- Hatuda Z. (1953). Radon content and its change in soil air near the ground surface. *Memoirs of the College of Science, University of Kyoto, Series B* 20, 285-306.
- Hauksson E. and Goddard J.G. (1981). Radon earthquake precursor studies in Iceland. *Journal of Geophysical Research*, **86**, 7037.
- Haykin S. (1994). *Neural Network: A comprehensive foundation*. Prentice-Hall, Inc., New Jersey, U.S.A.
- Heaton T.H. (1990). Evidence for and implications of self-healing pulses of slip in earthquake rupture. *Physics of the Earth and Planetary Interiors*, **64**, 1-20.
- Heinicke J. and Koch U. (1993). Experiences with radon measurements for earthquake prediction and landslides. *Nuclear Tracks and Radiation Measurements*, **22(1-4)**, 345.

- Hepburn C. and Windle A.H. (1980). Solid state nuclear track detectors. *J. Materials Science*, **15**, 279-301.
- Hirota U., Moriuchi H., Takemura Y., Tsuchida H., Fujii I. and Nakamura M. (1988). Anomalously high radon discharge from the Atotsugawa fault prior to the western Nagano Prefecture earthquake (M 6.8) of September 14, 1984. *Tectonophysics*, **152**, 147-152.
- Honkura Y. and Isikara A.M. (1999). Multidisciplinary research on fault activity in the western part of the North Antolian fault zone. *Tectonophysics*, **193(4)**, 347-357.
- Huang F., Jian C., Tang Y., Xu G., Deng Z. and Chi G. (2004). Response changes of some wells in the mainland subsurface fluid monitoring network of China, due to the September 21, 1999, Ms 7.6 Chi-Chi earthquake. *Tectonophysics*, **390**, 217-234.
- Humanante B.F., Giroletti E., Idrovo J., Monnin M., Pasinetti R. and Seidel J.-L. (1990). Radon signals related to seismic activity in Ecuador, March 1989. *PAGEOPH*, **132(3)**, 506-520.
- Ilic R., Rusov V.D., Pavlovyh V.N., Vaschenko V.M., Hanzic L. and Bondarchuk Y.A. 2005. Radon in Antarctica. *Radiation Measurements*, **40**, 415-422.
- Imme G. and Morelli D. (2012). Radon as earthquake precursor, In: Earthquake Research and Analysis-Statistical Studies, Observation and Planning (Dr. Amico S.D., Ed.), ISBN: 978-953-51-0134-5, In Tech, Available from: <http://www.intechopen.com/books/earthquake-research-and-analysis-statistical-studies-observations-and-planning/radon-as-earthquake-precursor>.

- İnan S., Akgül T., Seyis C., Saatçılar R., Baykut S., Ergintav S. and Baş M. (2008). Geochemical monitoring in the Marmara region (NW Turkey): A search for precursors of seismic activity. *J. Geophysical Research*, **113**, doi:10.1029/2007JB005206, 2008.
- Jaacks J.A. (1984), Meteorological influence upon mercury, radon and helium soil gas emission, Ph.D. Thesis, Colorado School of mines.
- Jacobi W. and Andre K. (1963). The vertical distribution of radon-222, radon-220 and their decay products in the atmosphere. *J. Geophys. Res.*, **68**, 3799-3814.
- Jaishi H.P., Singh S., Tiwari R.P. and Tiwari R.C. (2014). Analysis of soil radon data in earthquake precursory studies, *Annals of Geophysics*, doi:10.4401/ag-6513.
- Jönsson G. (1995). Radon gas-where from and what to do? *Radiation Measurements*, **25**, 1-4.
- Jonsson G. (1981). The angular sensitivity of Kodak LR-film to alpha particles. *Nuclear Instruments and Methods in Physics Research*, **190**, 407-414.
- Kanamori H. and Heaton T.H. (2000). Microscopic and macroscopic physics of earthquakes. *Geophysical Monograph Series*, **120**, 147-163.
- Kanamori H. and Brodsky E.E. (2001). The physics of earthquakes. *Physics Today*, **54**, 34-40.
- Kanamori H. and Brodsky E.E. (2004). The physics of earthquakes. *Reports on Progress in Physics*, **67**, 1429-1496.

- Kawamura H., Hatano T., Kato N., Biswas S. and Chakrabarti B.K. (2012). Statistical physics of fracture, friction, and earthquakes. *Reviews of Modern Physics*, **84**, 839-884.
- Khan H. A. (1972). Development and Applications of Solid State Nuclear Track Detectors, Ph D. Thesis, University of Birmingham (U.K).
- King C.Y. (1986). Gas geochemistry applied to earthquake prediction: an overview. *J. Geophysical Research*, **91**, 12269-12281.
- King C.Y. and Slater L.E. (1978). A comparison of soil-gas radon and crustal strain data (Abstract). *Earthquake Notes*, **49(4)**, 44.
- King C.Y. and Wakita H. (1981) Anomalous radon changes in an artesian well and possible relation to earthquakes (Abstract). *Earthquake Notes*, **52(1)**, 71.
- King C.Y. (1978). Radon emanation on San Andreas fault. *Nature*, **271**, 516-519.
- King C.Y., King B.S., Evans W.C. and Zhang W. (1996). Spatial radon anomalies on active faults in California. *Applied Gechemistry*, **11**, 497-510.
- King C.-Y. and Wakita H. (1981). Anomalous radon changes in an artesian well and possible relation to earthquake (abstract). *Earthquake Notes*, **52(1)**, 71.
- Kleeman J. D. and Lovering J. F. (1971). A determination of the Decay Constant for Spontaneous Fission of Natural Uranium Using Fission Track Accumulation. *Geochim Cosmochim Acta*, **35**, 637-640.
- Knopoff L. (1958). Energy release in earthquakes. *Geophysical Journal of the Royal Astronomical Society*, **1**, 44-52.

- Kraner H.W., Schroeder G.L. and Evans R.D. (1964). Measurement of effects of atmospheric variables on ^{222}Rn flux and soil gas concentration. In: Symposium Proc., Natural Radiation Environment (Adams J.A.S and Lowder W.M., Eds.), Houston, Texas, 10-13 April 1963, University of Chicago Press, Chicago, 191-215.
- Kristiansson K. and Malmqvist L. (1984). The depth dependence of the concentration of $^{222}_{86}\text{Rn}$ in soil gas near the surface and its implication for exploration. *Geoexploration*, **22**, 17-41.
- Kristiansson K. and Malmqvist L. (1982). Evidence for non-diffusive transport of $^{222}_{86}\text{Rn}$ in the ground and a new physical model for the transport. *Geophysics*, **47**, 1444-1452.
- Külahci F., İnceöz M., Doğru M., Aksoy E. and Baykara O. (2009). Artificial neural network model for earthquake prediction with radon monitoring. *Applied Radiation and Isotopes*, **67**, 212-219.
- Kulahci F. and Sen Z. (2014). On the correction of spatial and statistical uncertainties in systematic measurements of ^{222}Rn for earthquake prediction. *Surv. Geophys.*, **35**, 449-478.
- Kumar A., Walia V., Singh S., Bajwa B.S., Mahajan S., Dhar S. and Yang T.F. (2012). Earthquake precursory studies at Amritsar Punjab, India using radon measurement techniques. *International Journal of Physical Science*, **7(42)**, 5669-5677.

- Kuo T., Su C., Chang C., Lin C., Cheng W., Liang H., Lewis C. and Chiang C. (2010). Application of recurrent radon precursors for forecasting large earthquakes (Mw > 6.0) near Antung, *Taiwan. Radiat. Meas.*, **45(9)**, 1049–1054.
- Li Y., Du J., Wang X., Zhou X., Xie C. and Cui Y. (2013). Spatial Variations of Soil Gas Geochemistry in the Tangshan Area of Northern China. *Terr. Atmos. Ocean. Sci.*, **24**, 323-332.
- Lindmark A. and Rosen B. (1985). Radon in soil gas exhalation tests and in Situ measurements. *Science of the total Environment*, **45**, 397-404.
- Lounis Z., Djeflal S., Morsli K. and Allab M. (2001). Track etch parameters in CR-39 detectors for proton and alpha particles of different energies. *Nuclear Instruments and Methods in Physics Research*, **179**, 543-550.
- Lui K.K., Yui T.F., Yeh Y. H., Tsai Y.B. and Teng T.L. (1985). Variation of radon content in ground waters and possible correlation with seismic activities in northern Taiwan. *Pure and Applied Geophysics*, **122**, 231-244.
- Malik S.R. and Durrani S.A. (1974). Spatial distribution of uranium in meteorites, tektites and other geological materials by spark counter. *Applied Radiation and Isotopes*, **25**, 1-4.
- Mayya Y.S., Eappen K.P. and Nambi K.S.V. (1998). Methodology for mixed field inhalation dosimetry in monazite areas using a twin-cup dosimeter with three track detectors. *Radiat. Prot. Dosim.*, **77**, 177-184.
- Markkanen M. and Arvela H. (1992). Radon emanation from soils. *Radiat. Prot. Dosim.*, **45**, 269-272.

- Megumi K. and Mamuro T. (1974). Emanation and exhalation of radon and thoron gases from soil particles. *J. Geophys. Res.*, **79**, 3357-3360.
- Mjachkin V.I., Brace W.F., Sobolev G.A. and Dieterich J.H. (1975). Two models for earthquake forerunners. *Pure and Applied Geophysics*, **113**, 169-181.
- Mojtaba N. and Negarestani A. (2013). Measuring the radon concentration and investigating mechanism of decline prior an earthquake. *J. Radioanal. Nucl. Chem.*, **298**, 1-8.
- Monnin M.M. and Seidel J.L. (1992). Radon in soil-air and in ground water related to major geophysical events: a survey. *Nuclear Instruments and Methods in Physics Research Section A: Accelerators, Spectrometers, Detectors and Associated Equipment*, **314**, 316-330.
- Monnin M.M. (1980). Methods of automatic scanning of SSNTDs. *Nuclear Instruments and Methods*, **173**, 63-72.
- Monnin M.M. and Seidel J.L. (1991). Radon and geophysics: recent advances. *Int. J. Radiat. Appl. Instrum., Part D, Nucl. Tracks Radiat. Meas.*, **19**, 375-382.
- Morawska L. and Jeffris C. (1994). Distribution of radium mineral sand grains and its potential effect on radon emanation. *Radiat. Prot. Dosim.*, **56**, 199-200.
- Mori T. and Kawamura H. (2005). Simulating study of Spatiotemporal correlations of earthquakes as a stick slip frictional instability. *Phys. Rev. Lett.*, **94**, doi: 10.1103/PhysRevLett.94.058501

- Moussa M.M. and El Arabi A.M. (2003). Soil radon survey for tracing active fault: a case study along Qena-Safaga road, Eastern Desert, Egypt. *Radiation Measurements*, **37**, 211-216.
- Muir wood D., Belkheir K. and Lui D.F. (1994). Strain softening and state parameter forsand modeling. *Geotechnique*, **44**, 335-339.
- Nazaroff W.W. (1992). Radon transport from soil to air. *Rev. Geophys.*, **30**, 137-160.
- Negarestani A., Setayeshi S., Ghannadi-Maragheh M. and Akashe B. (2002). Layered neural networks based analysis of radon concentration and environmental parameters in earthquake prediction. *J. Environmental Radioactivity*, **62**, 225-233.
- Neri M., Giammanco S., Ferrera E., Patanè G. and Zanon V. (2011). Spatial distribution of soil radon as a tool to recognize active faulting on an active volcano: the example of Mt. Etna (Italy). *J. Environmental Radioactivity*, **102**, 863-870.
- Nur A. (1972). Dilatancy, pore fluids and premonitory variations of t_s/t_p travel times. *Bull. Seismol. Soc. Amer.*, **62**, 1217-1222.
- Nur A. and Simmons G. (1969). The effect of saturation on velocity in low porosity rocks. *Earth and Planetary Science Letters*, **7**, 183-193.
- Olami Z., Feder H.J.S. and Christensen K. (1992). Self-organized critically in a continuous, non conservative cellular automation modeling earthquakes. *Phys. Rev. Lett.*, **68**, 1244-1247.
- Padilla G.D., Hernandez P.A., Padron E., Barrancos J., Perez N.M., Melian G., Nolasco D., Dionis S., Rodriguez F., Calvo D. and Hernandez I. (2013). Soil gas radon

- emission and volcanic activity at El Hierro (Canary Island): the 2011–2012 submarine eruption. *Geochem. Geophys. Geosyst.*, **14**, 432-447.
- Park J. and Sandberg I.W. (1993). Approximation and radial basis function network. *Neural Computation*, **5**, 305-316.
- Piersanti A., Cannelli V. and Galli G. (2015). Long term continuous radon monitoring in a seismically active area. *Annals of Geophysics*, doi: 10.4401/ag-6735.
- Piesch E. and Sayed A.M. (1974). Latent fading in solid-state track etching detectors. *Nuclear Instruments and Methods*, **119**, 367-371.
- Pispek P., Durrast H. and Bhongsuwan T. (2010). Soil-gas radon as a possible earthquake precursor: A case study from the Khlong fault zone, southern Thailand. *Kasetsart J. (Nat. Sci.)*, **44**, 1079-1093.
- Planinic J., Radolic V. and Culo D. (2000). Searching for an earthquake precursor: temporal variations of radon in soil and water. *FIZIKA B*, **9(2)**, 75-82.
- Price J.G., Christensen L., Hess R., La Pointe D.D., Ramelli A.R., Desilets M., Hopper R.D., Kluesner T. and Marshall S. (1994), Radon in outdoor air in Nevada, *Health Physics*, **66**: 433-438.
- Ramachandran T.V., Lalit B.Y. and Mishra U.C. (1987). Measurement of radon permeability through some membranes. *Int. J. Radiat. Appl. Instrum., Part D, Nucl. Tracks Radiat. Meas.*, **13**, 81-84.
- Rannou A. (1989). The bare detector and results of indoor radon survey in France, In: Proc. of international workshop on *Radon monitoring in Radioprotection, Environmental Radioactivity and Earth Science*, 145-222.

- Rastogi B.K., Chadha R.K. and Raju I.P. (1986). Seismicity near Bhatsa reservoir, Maharashtra, India. *Physics of the Earth and Planetary Interiors*, **44**, 179-199.
- Rastogi B.K., Ramakrishna Rao C.V., Chadha R.K. and Gupta H.K. (1987). Precursory phenomena in the microearthquake sequence near the Osmansagar reservoir, Hyderabad, India. *Tectonophysics*, **138**, 17-24.
- Rawat, U.S. and Parihar, C.P.S. *Geoenvironment of Mizoram and its implication in development*. In: Proceedings of National Symposium-Role of Earth Sciences in Integrated Development and Related Societal Issues, GSISP – **65 (I)**, 185 – 190(2001).
- Reilly D.L. and Cooper L.N. (1990). An overview of neural networks: early models to real world systems. In: Zornetzer S.F., Davis J.L., Lau C. (Eds.). An introduction to neural and electronic networks. Academic Press, 227-248.
- Richon P., Sabroux J.C., Halbwachs M., Vandemeulebrouck J., Poussielgue N., Tabbagh J. and Punongbayan R. (2003). Radon anomaly in the soil of Taal volcano, the Philippines: A likely precursor of the M 7.1 Mindoro earthquake (1994). *Geophys. Res. Lett.*, **30**, doi:10.1029/2003GL016902, 2003.
- Rikitake T. (1976), Earthquake Prediction, *Elsevier*, New York.
- Rundle J.B., Turcotte D.L., Shcherbakov R., Klein W. and Sammis C. (2003). Statistical physics approach to understanding the multi scale dynamics of earthquake fault systems. *Reviews of Geophysics*, **41**, doi:10.1029/2003RG000135.
- Scholz C.H., Sykes L.R. and Aggarwal Y.P. (1973). Earthquake prediction: a physical basis. *Science*, **181**, 803-810.

- Scholz C.H. (1990). The mechanics of earthquake faulting. Cambridge University Press, New York, 1-438.
- Segovia N., Mena M., Seidel J.L., Monnin M., Tamez E. and Pena P. (1995a). Short and long term radon in soil monitoring for geophysical purposes. *Radiation Measurements*, **25**, 547-552.
- Segovia N., Maciel R., Pena P., Tamez E., Rosas J. and Mena M. (1995b). Radon in soil studies in Jalisco state, Mexico. *Radiation Measurements*, **25**, 617-620.
- Sen Z. and Beshpenera M. E. (2004). Water resources assessment, IACWRA 2004. Lecture Notes. Water Engineering Research and Development Center, Istanbul, 100.
- Shin Y. and Ghosh J. (1995). Ridge polynomial networks. *IEEE Transactions on Neural Networks*, **6(3)**, 610-622.
- Siegmon G., Bartholomä K.P. and Enge W. (1975). The enhancement of the charge resolution of Lexan applying UV-irradiation. *Nuclear Instruments and Methods*, **128**, 461-472.
- Singh M., Ramola R.C., Singh B., Singh S. and Virk H.S. (1991). Subsurface soil gas radon changes associated with earthquakes. *Int. J. Radiat. Appl. Instrum., Part D, Nucl. Tracks Radiat. Meas.*, **19**, 417-420.
- Singh S., Kumar A., Bajwa B.S., Mahajan S., Kumar V. and Dhar S. (2010). Radon monitoring in soil gas and ground water for earthquake prediction studies in north- west Himalayas, India. *Terr. Atmos. Ocean. Sci.*, **21(4)**, 685-695.

- Snedecor G. W. and Cochran W. G. (1989). *Statistic Methods*. 8th Edn. Iowa State University Press .
- Stranden E., Kolstad A.K. and Lind B. (1984). The influence of moisture and temperature on radon exhalation. *Radiat. Prot. Dosim.*, **7**, 55-58.
- Sultankhodzhaev A. N. (1984). Hydrogeoseismic Precursors to Earthquakes in Earthquake Prediction, UNESCO, Pans 181-191.
- Swakon J., Kozak K., Paszkowski M., Gradzinski R., Loskiewicz J., Mazur J., Janik M., Bogacz J., Horwacik T. and Olko P. (2004). Radon concentration in soil gas around local disjunctive tectonic zones in the Krakow area. *J. Environmental Radioactive*, **78**, 137- 149.
- Tanner A.B. (1980). Radon migration in the ground: A supplementary review. In: Symposium Proc., Natural Radiation Environment III (Gessel T.F. and Lowder W.M., Eds.), Houston, Texas, 23-28 April 1978, *US Dept. of Energy, Washington D.C.*, 5-56.
- Tanner A.B. (1964). Radon migration in the ground: A review. In: Symposium Proc., Natural Radiation Environment (Adams J.A.S. and Lowder W.M., Eds.), *University of Chicago Press, Chicago*, 161-190.
- Thomas D.M. (1988). Geochemical precursors to seismic activity. *Pure and Applied Geophysics*, **126**, 241-266.
- Tiwari R.P. (2002), Status of seismicity in the Northeast India and the earthquake disaster mitigation. *ENVIS Bull.*, **10**, 15-25.

- Tommasino L and Harrison K.G. (1985). Damage track detectors for neutron dosimetry: I. Registration and counting Methods. *Radiat. Prot. Dosim.*, **10**, 207-217.
- Tsvetkova T., Monnin M., Nevinsky I. and Perelygin V. (2001). Research on variation of radon and gamma-background as a prediction of earthquakes in the Caucasus. *Radiation Measurements*, **33**, 1-5.
- Ulomov V.I. and Mahashev B.Z. (1967). A precursor of strong tectonic earthquake. *Dokl. Acad. Sci. USSR, Earth Sci. Sect.*, **176**, 9-11.
- Valković V. (2000). Radioactivity in the environment. *Elsevier*, The Netherlands.
- Varier K.M (2009). Nuclear Radiation Detection, Measurement and Analysis. *Narosa Publishing House*, New Delhi.
- Vaupotič J., Riggio A., Santulin M., Zmazek B. and Kobal I. (2010). A radon anomaly in soil gas at Cazzaso, NE Italy, as a precursor of an $M_L = 5.1$ earthquake. *Nukleonika*, **10**, 507-511.
- Virk H.S. (1993). Radon and earthquake prediction in India: present status. *Nucl. Tracks Radiat. Meas.*, **22**, 483-494.
- Virk H.S. (1996). A critique of empirical scaling relationship between earthquake magnitude, epicentral distance and precursor time for interpretation of radon data. *J. Earthquake Prediction Research*, **5**, 574-583.
- Virk H.S., Sharma A.K. and Sharma N. (2002). Radon and helium monitoring in some thermal springs of North India and Bhutan. *Current Science*, **82**, 1423-1424.

- Virk H.S., Walia V., Sharma A.K., Kumar N. and Kumar R. (2000). Correlation of radon with microseismic events in Kangra and Chamba Valleys of N-W Himalaya. *Geofisica Internacional*, **39**, 221-227.
- Virk H.S., Walia V. and Kumar N. (2001). Helium/radon precursory anomalies of Chamoli earthquake, Garhwal Himalaya, India. *J. Geodynamics*, **31**, 201-210.
- Wakita H., Nakamura Y., Notsu K., Noguchi M. and Asada T. (1980). Radon anomaly: a possible precursor of the 1978 Izu- Oshimakinkai earthquake. *Science*, **207**, 882-883.
- Walia V., Virk H.S., Yang T.F., Mahajan S., Walia M. and Bajwa B.S. (2005a). Earthquake prediction studies using radon as a precursor in NW Himalayas, India: a case study. *Terrestrial, Atmospheric and Oceanic Sciences*, **16**, 775-804.
- Walia V., Su T.C., Fu C.C. and Yang T.F. (2005b). Spatial variations of radon and helium concentrations in soil gas across Shan-Chaio fault, Northern Taiwan. *Radiation Measurements*, **40**, 513-516.
- Walia V., Lin S. J., Hong W. L., Fu C. C., Yanf T. F., Wen K. L. and Chen C. H. (2009). Continuous temporal soil-gas composition variations for earthquake precursory studies along Hsincheng and Hsinhua faults in Taiwan; *Radiat.Meas.*, **44**, 934-939.
- Wattananikorn K., Kanaree M. and Wiboolsake S. (1998). Soil gas radon as an earthquake precursor: some considerations on data improvement. *Radiation Measurements*, **29**, 593-598.

- Whitcomb J.H., Garmany J.D. and Anderson D.L. (1973). Earthquake prediction: Variation of seismic velocities before the San Fernando earthquake. *Science*, **180**, 632-635.
- Zhang G., Patuwo B.E. and Hu M.Y. (1998). Forecasting with artificial neural networks: The state of the art. *International Journal of Forecasting*, **14**, 35-62.
- Zhang Q. and Benveniste A. (1992). Wavelet Network. *IEEE Transactions on Neural Networks*, **3(6)**, 889-898.
- Zmazek B., Todorovski L., Džeroski S., Vaupotič J. and Kobal I. (2003). Application of decision trees to the analysis of soil radon data for earthquake prediction. *Applied Radiation and Isotopes*, **58**, 697-706.
- Zmazek B., Zivcic M., Vaupotic J., Bidovec M., Poljak M. and Kobal I. (2002). Soil radon monitoring in the Krsko Basin, Slovenia. *Applied Radiation and Isotopes*, **56**, 649-657.
- Zoran M., Savastru R. and Savastru D. (2012), Radon levels assessment in relation with seismic events in Vrancea region. *J. Radioanal. Nucl. Chem.*, **293**, 655-663.
- Zurada J.M. (1992). "Introduction to Artificial Neural Systems", West Publishing Company, St. Paul, U.S.A. 683.

List of Research Publications

Publications

During Junior Research Fellow (J.R.F.):

1. **Singh S.**, Jaishi H.P., Tiwari R.P. and Tiwari R.C. (2016), A study of variation in soil gas concentration associated with earthquakes near Indo-Burma subduction zone. *Geoenvironmental Disasters*. 3(22). Doi: 10.1186/s40677-016-0055-8. Published by **Springer**. **ISSN: 2197-8670**
2. **Singh S.**, Jaishi H.P., Tiwari R.P. and Tiwari R.C. (2016), Variations of Radon concentrations in soil with respect to climatic parameters in Mizoram, *Basic and Applied Physics*, Pp 131-138, (Editors: Prof. R C Tiwari, Prof. Zaithanzaauva Pachuau), Narosa Publication (International), New Delhi. **ISBN: 978-81-8487-517-1**
3. Jaishi H.P., **Singh S.**, Tiwari R.P. and Tiwari R.C. (2015), Study of soil-gas thoron concentration associated with seismic activity, *Chiang Mai Journal of Science*, **42(4)**, 972-979 (Taylor & Francis). Published by Faculty of Science Chiang Mai University, Thailand (**ISSN: 0125-2526**), **IF: 0.516**
4. **Singh S.**, Jaishi H.P., Tiwari R.P. and Tiwari R.C., Variation in soil radon concentration along Chite fault in Aizawl district, Mizoram, India. *Radiation protection Dosimetry*, Pp 1-5, doi: 10.1093/rpd/ncu221 (2014). Published by **Oxford Journals (ISSN: 0144-8420)**, **IF: 0.999** (Most read Article, July 2014)

During Field Assistant (F.A.):

1. Jaishi H.P., **Singh S.**, Tiwari R.P. and Tiwari R.C. (2013), Radon and Thoron anomalies along Mat fault in Mizoram, India, *J. Earth System Science*, **122**, 1507-1513, ISSN: 0253-4126 (Print) 0973-774X (electronic), IF: 0.695 (2012), Journal Citation Reports®, Thomson Reuters. Publisher: **Springer** on behalf of the Indian Academy of Sciences.
2. Jaishi H.P., **Singh S.**, Tiwari R.P. and Tiwari R.C. (2014), Temporal variation of soil radon and thoron concentrations in Mizoram (India), associated with earthquakes, *Natural Hazards*, **72**, 443-454, ISSN: 0921-030X (Print) 1573-0840 (Online), DOI: 10.1007/s11069-013-1020-4, IF: 1.639 (2012), Journal Citation Reports®, Thomson Reuters. Publisher: **Springer**.
3. Jaishi H.P., **Singh S.**, Tiwari R.P. and Tiwari R.C. (2014), Correlation of radon anomalies with seismic events along Mat fault in Serchhip District, Mizoram, India, *Applied Radiation and Isotopes*, **86**, 79-84, ISSN: 0969-8043, DOI: 10.1016/j.apradiso.2013.12.040, IF: 1.179 © Thomson Reuters Journal Citation Reports 2013. Publisher: **Elsevier**.
4. Jaishi H.P., **Singh S.**, Tiwari R.P. and Tiwari R.C. (2014), Analysis of soil radon data in earthquake precursory studies, *Annals of Geophysics*, **57**, S0544, ISSN: 2037-416X, DOI: 10.4401/ag-6513, IF: 1.157. Published by INGV, Istituto Nazionale di Geofisica e Vulcanologia (Italy).

Papers Presented

1. A study of Radon and Thoron concentrations in soil as an earthquake precursor in Mizoram. In: 8th National Conference of the Physics Academy of North East, 17th -19th December, 2012, Mizoram University, Aizawl.
2. Temporal variation in thoron concentration as a precursor to earthquakes along Mat Fault in Mizoram, India. In: SSNTDs-18, 18th-20th October, 2013, Aggarwal College Ballabgarh, Haryana, India.
3. Variation of soil Radon concentrations along Chite Fault in Aizawl District, Mizoram, India. In: SEERAS, 26th 30th May, 2014, Nis University, Republic of Serbia.

Conferences and workshops attended

1. National Workshop on Computational Physics, organized by the Dept. of Physics, Mizoram University in Collaboration with University of Hyderabad, held during Feb. 14- 19, 2011 at the Dept. of Physics, Mizoram University.
2. National Workshop on Advances in Electronics, Communication and Information Technology (AECI), held at Mizoram University, during Mar. 23-26, 2011.
3. One day state level seminar on Recent Advances in Radiation Physics, organized by the Dept. of Physics, Mizoram University and UGC-DAE Centre for Scientific Research (CSR), Indore on 15th April, 2011 at Mizoram University.
4. 8th National Conference of the Physics Academy of North East, held in December, 17-19, 2012, organized by the Dept of Physics, Mizoram University under the auspices of the Physics Academy of North East (PANE).

5. National Workshop on Mathematical Analysis, held on 7th and 8th March, 2013 organized by Dept. of Mathematics and Computer Science, Mizoram University.
6. 18th National Symposium on Solid State Nuclear Track Detector and Their Applications (SSNTDs-18) held during Oct. 18-20 2013 at Aggarwal College, Ballabgarh, Faridabad (Haryana), India.
7. National Workshop on Dynamical System held from 26th to 27th Nov. 2013 at the Dept. of Mathematics and Computer Science, Mizoram University.
8. UGC sponsored One Week Workshop on SPSS held from 2nd -7th Dec. 2013 at Mizoram University.
9. Three days workshop on Active Fault Mapping held from 3rd to 5th May 2014, organized by the Dept. of Geology, Mizoram University and sponsored by Ministry of Earth Sciences (MoES), Govt. of India.
10. National Seminar on Geology, Tectonics, Geo-Hazards & Natural Resources of North East India held from 3rd to 4th Nov. 2014, organized by the Dept. of Geology, Pachhunga University College, Aizawl, Mizoram and sponsored by Ministry of Earth Sciences (MoES), Govt. of India.
11. Science Academies' Refresher Course in Experimental Physics held from 7th to 22nd May 2015, organized by NIT, Aizawl, Mizoram and sponsored by The National Academy Of Sciences, India.

Brief Bio-data of the Author

1. **Name** : SANJAY SINGH
2. **Father's Name** : Shri Hari Mohan Singh
3. **Mother's Name** : Smt. Sodina Devi
4. **Address** : Project veng, Kolasib, Mizoram
5. **Designation** : Research Scholar (Mizoram University)
6. **Date of Birth** : 10/10/1986
7. **Educational qualification** :

Degree	Year	University/ Board	Division	Subjects taken
High School/HSLC	2002	M.B.S.E	Second	English, Science, Mathematics, Geography, History, Alternative English
HSSLC	2004	M.B.S.E	Third	Phy., Math., Bio., Chem., English
B.Sc.	2008	Mizoram University	Second	Physics (Honors), Mathematics, Chemistry
M.Sc.	2010	Mizoram University	First	Physics (Advanced Electronics)

8. **Research Experience** : 5 Years (Field Assistant -3 years, JRF &SRF -2 years)
9. **Area of research interest** :Radiation and Environmental Physics
10. **Publication** :Research Papers- 7
11. **Conferences and Workshops attended** :11 nos.

The information provided above is true to the best of my knowledge and belief.

(Signature)

Appendix: Formulae

Statistical treatment of the data has been done in SPSS version 16.0 statistical package. However, the calculations can also be performed manually by using the following formulae.

1. Correlation coefficient (r) between the two set of variables 'x' and 'y' can be obtained by the following relation:

$$r = \frac{\sum((x - \bar{x})(y - \bar{y}))}{\sqrt{(\sum(x - \bar{x})^2 \sum(y - \bar{y})^2)}}$$

Where \bar{x} and \bar{y} are the means of x and y respectively.

2. Standard deviation (SD):

$$SD = \sqrt{\frac{\sum(x - \bar{x})^2}{N - 1}}$$

Where, N is the total number of observations.

3. Standard error of mean (SEM):

$$SEM = \frac{SD}{\sqrt{N}}$$

4. Standard error of estimates (S_e):

$$S_e = SD(y) \times \sqrt{1 - r^2}$$

Where, $SD(y)$ is the standard deviation of y -scores.

5. Degrees of freedom (df) for regression (reg) and residuals (res):

df_{reg} equals the number of variables (dependent + independent) minus 1.

df_{res} equals number of observations minus number of variables.

6. Sum of squares (SS):

$SS_{reg} = \sum (y' - \bar{y})^2$ is the regression sum of squares.

$SS_{res} = \sum (y - y')^2$ is the residual sum of squares.

Here, y' is the predicted value of y .

7. Mean Square (MS):

$$MS_{reg} = \frac{SS_{reg}}{df_{reg}}, \text{ and } MS_{res} = \frac{SS_{res}}{df_{res}}.$$

8. T-test (t): T-value can be obtained by dividing the value of each regression coefficient by its respective standard error. A t-test is used to find out the significance of the predictor variables.

9. F-ratio (F): F-ratio equals the ratio of MS_{reg} to that of MS_{res} . It determines the viability (significance) of the model.

$$F = \frac{MS_{reg}}{MS_{res}}$$

10. Significance (p-value):

The significance of the t-test and F-ratio can be obtained from the t-distribution and F-distribution tables respectively.

Table 1: Data of Radon concentration and meteorological parameters during the period of observation.

Date (MM/DD/YYYY)	Radon Bq/m³	Rainfall (mm)	Temp. (C)	Relative Humidity (%)	Pressure (mbar)
3/1/2013	904.76	0	22.175	51.98	963.05
3/8/2013	1268.71	0	22.2	49.995	964.75
3/15/2013	2255.10	0	23.45	48.71	962.9
3/22/2013	1465.99	3.7	23.6	47.495	961.45
3/29/2013	1911.56	2.2	26.15	47.995	959.9
4/5/2013	1636.05	14.3	26.325	52	958.85
4/12/2013	1612.24	0	27.15	42.85	958.45
4/19/2013	1649.66	40.6	24.35	60.35	958.75
4/26/2013	1350.34	0.8	25.5	55.64	961.1
5/3/2013	1146.26	40.9	26.225	71.85	956.8
5/10/2013	1248.30	311.1	21.3	85.495	958.6
5/17/2013	1397.96	167.9	25.1	79.14	955.95
5/24/2013	1540.82	6.6	27.15	73.425	955.65
5/31/2013	1931.97	49.9	27.1	83.495	954.8
6/7/2013	2595.24	88.5	27.645	77.925	955.885
6/14/2013	3693.88	18.7	28.255	77.21	952.455
6/21/2013	1853.74	21.8	28.02	77.78	952.59
6/28/2013	2816.33	83.9	27.395	85.92	953.16
7/5/2013	2207.48	49.2	27.155	78.875	952.46
7/12/2013	1258.50	23.2	27.385	83.355	954.82
7/19/2013	1615.65	68.7	26.96	82.355	953.055
7/26/2013	1874.15	106.1	27.26	89.135	951.25
8/2/2013	1588.44	101.3	26.415	87.6	940.59
8/9/2013	1343.54	78.6	26.455	82.64	955.87
8/16/2013	908.16	123.8	25.56	88.71	955.84
8/23/2013	1132.65	101	26.36	89.135	953.085
8/30/2013	1258.50	198.9	26.02	85.35	960.37
9/6/2013	272.11	41.5	26.65	79.745	931.915
9/13/2013	1312.93	81	25.755	88.855	959.21
9/20/2013	1374.15	88.4	26.54	88.995	954.915
9/27/2013	578.23	89.1	26.41	86.135	956.4
10/4/2013	193.88	44	24.715	88.685	958.245

10/11/2013	2554.42	49.8	24.48	84.565	960.94
10/18/2013	1646.26	5.6	25.91	84.64	960.685
10/25/2013	2340.14	51.4	23.81	88.925	962.63
11/1/2013	1180.27	26.4	21.675	85.125	963.5
11/8/2013	1795.92	0	20.94	74.995	965.07
11/15/2013	370.75	0	20.9	76.28	961.83
11/22/2013	163.27	0	20.575	74.565	963.625
11/29/2013	632.65	0	20.35	79.785	963.05
12/6/2013	1632.65	0	20.165	82.165	964.165
12/13/2013	1081.63	0	18.985	76.535	961.895
12/20/2013	1000.00	0	15.825	68.71	963.535
12/27/2013	1384.35	0	16.345	80.07	966.545
1/3/2014	727.89	0	16.085	75.785	966.025
1/10/2014	1010.20	0	15.595	82.64	964.74
1/17/2014	1095.24	0	18.43	77.065	966.605
1/24/2014	874.15	0	19.19	76.85	968.135
1/31/2014	642.86	0	18.84	75.355	965.575
2/7/2014	823.13	0	18.5	66.565	961.55
2/14/2014	1187.07	2.6	19.75	64.635	961.3
2/21/2014	996.60	11.5	17.45	72.995	964.8
2/28/2014	1044.22	0	20.35	64.925	965.75
3/7/2014	741.50	0	20.95	60.065	964.4
3/14/2014	901.36	0	21.4	51.495	964.6
3/21/2014	867.35	14.1	24.25	56.425	962.9
3/28/2014	1023.81	11.4	24.6	60.07	961.2
4/4/2014	1030.61	4.2	26.975	50.055	958.4
4/11/2014	972.79	22.9	25.1	66.425	960.8
4/18/2014	894.56	0	27.35	47.14	960.95
4/25/2014	1527.21	0	28.85	47.925	959.85
5/2/2014	1578.23	34.5	27.425	63.65	960.35
5/9/2014	1486.39	209.4	25.3	78.21	959.75
5/16/2014	935.37	161.3	26.15	73.78	957
5/23/2014	1517.01	0	28.75	62.635	957.25
5/30/2014	1377.55	121.1	27.5	78.495	959.1
6/6/2014	2527.21	8.2	27.75	69.83	956
6/13/2014	1425.17	5.9	29.15	72.85	951.6
6/20/2014	2017.01	14.6	27.3	86.21	950.3
6/27/2014	2316.33	132.6	26.05	82.21	955.9
7/4/2014	1680.27	40	27.2	81.14	953.375

7/11/2014	1360.54	45.2	27.95	76.995	956.15
7/18/2014	2037.41	177.2	27.6	87.495	952.5
7/25/2014	1006.80	97.2	27.4	83.425	951.9
8/1/2014	921.77	156.5	27.625	83.955	953.55
8/8/2014	1710.88	41.6	27.4	83.71	951.95
8/15/2014	1547.62	73.3	26.1	85.135	954.9
8/22/2014	1510.20	53	26.25	82.065	956.9
8/29/2014	1615.65	28.1	26.7	84.995	957.5
9/5/2014	1486.39	145.7	26.2	91.075	956.125
9/12/2014	1833.33	111.1	26.35	90.14	957.7
9/19/2014	551.02	98.9	26.9	87.78	955.85
9/26/2014	1598.64	43.3	25.3	83.35	959.2
10/3/2014	1727.89	20.3	25.55	83.4	961.05
10/10/2014	1513.605	12.5	26.7	81.92	959.15
10/17/2014	1139.456	65	25.35	88.625	961.7
10/24/2014	1139.456	0	24.7	82.785	962.25
10/31/2014	816.3265	9.1	22.45	86.425	962.75
11/7/2014	646.2585	0	22.15	81.9	960.05
11/14/2014	394.5578	0.6	23.85	82.3	962.55
11/21/2014	302.7211	0	20.95	79.885	963.25
11/28/2014	323.1293	0	19.6	81.225	962.5
12/5/2014	363.9456	0	18.8	82.84	962.65
12/12/2014	571.4286	0	19.15	85.185	964.05
12/19/2014	442.1769	0	18.6	85.135	965.9
12/26/2014	806.1224	0	17.6	77.79	964.45
1/2/2015	1326.531	0	19.3	83.94	964.2
1/9/2015	880.9524	20.8	18.34	88.92	963.55
1/16/2015	408.1633	0	17.39	75.15	965.2
1/23/2015	721.0884	3	17.955	80.985	965.9
1/30/2015	646.2585	0	17.275	72.37	965.6
2/6/2015	564.6259	0	17.005	60.485	967.05
2/13/2015	336.7347	0	17.29	65.475	964.8
2/20/2015	527.2109	0	17.735	66.335	963.35
2/27/2015	653.0612	20.7	21.34	64.685	961.85
3/6/2015	795.9184	31.6	21.92	65.69	962.05
3/13/2015	629.2517	0	20.6	41.51	963.25
3/20/2015	357.1429	5.2	23.055	46.64	962.65
3/27/2015	431.9728	0	23.87	48.985	961.25
4/3/2015	1241.497	47.5	23.785	66.575	964.4

4/10/2015	921.7687	60.3	24.19	69.735	958.7
4/17/2015	1044.218	0	26.14	63.435	960.8
4/24/2015	1006.803	182.1	23.375	70.76	959.8
5/1/2015	578.2313	66.5	22.8	80.57	960.35
5/8/2015	778.9116	42.3	24.3	72.085	958.55
5/15/2015	1125.85	7.9	25.85	71.97	958.2
5/22/2015	931.9728	89.2	26.2	77.26	955.9
5/29/2015	670.068	80.9	25.755	76.55	955.45

Table 2: Data of Thoron concentration and meteorological parameters during the period of observation

Date (MM/DD/YYYY)	Thoron Bq/m³	Rainfall (mm)	Temp. (C)	Relative Humidity (%)	Pressure (mbar)
4/11/2014	81.81	22.9	25.1	66.425	960.8
4/18/2014	609.20	0	27.35	47.14	960.95
4/25/2014	185.11	0	28.85	47.925	959.85
5/2/2014	431.61	34.5	27.425	63.65	960.35
5/9/2014	362.33	209.4	25.3	78.21	959.75
5/16/2014	66.95	161.3	26.15	73.78	957
5/23/2014	24.35	0	28.75	62.635	957.25
5/30/2014	302.90	121.1	27.5	78.495	959.1
6/6/2014	655.03	8.2	27.75	69.83	956
6/13/2014	480.84	5.9	29.15	72.85	951.6
6/20/2014	1219.84	14.6	27.3	86.21	950.3
6/27/2014	495.70	132.6	26.05	82.21	955.9
7/4/2014	33.66	40	27.2	81.14	953.375
7/11/2014	1526.67	45.2	27.95	76.995	956.15
7/18/2014	1643.04	177.2	27.6	87.495	952.5
7/25/2014	0.72	97.2	27.4	83.425	951.9
8/1/2014	991.77	156.5	27.625	83.955	953.55
8/8/2014	751.52	41.6	27.4	83.71	951.95
8/15/2014	531.33	73.3	26.1	85.135	954.9
8/22/2014	446.29	53	26.25	82.065	956.9
8/29/2014	350.52	28.1	26.7	84.995	957.5
9/5/2014	122.63	145.7	26.2	91.075	956.125
9/12/2014	241.85	111.1	26.35	90.14	957.7
9/19/2014	91.84	98.9	26.9	87.78	955.85
9/26/2014	218.94	43.3	25.3	83.35	959.2
10/3/2014	318.12	20.3	25.55	83.4	961.05
10/10/2014	511.30	12.5	26.7	81.92	959.15
10/17/2014	48.90	65	25.35	88.625	961.7
10/24/2014	131.60	0	24.7	82.785	962.25
10/31/2014	300.75	9.1	22.45	86.425	962.75
11/7/2014	180.45	0	22.15	81.9	960.05

11/14/2014	146.60	0.6	23.85	82.3	962.55
11/21/2014	116.54	0	20.95	79.885	963.25
11/28/2014	233.08	0	19.6	81.225	962.5
12/5/2014	169.17	0	18.8	82.84	962.65
12/12/2014	199.25	0	19.15	85.185	964.05
12/19/2014	281.95	0	18.6	85.135	965.9
12/26/2014	285.71	0	17.6	77.79	964.45
1/2/2015	285.71	0	19.3	83.94	964.2
1/9/2015	236.84	20.8	18.34	88.92	963.55
1/16/2015	7.52	0	17.39	75.15	965.2
1/23/2015	191.70	3	17.955	80.985	965.9
1/30/2015	7.52	0	17.275	72.37	965.6
2/6/2015	334.59	0	17.005	60.485	967.05
2/13/2015	139.10	0	17.29	65.475	964.8
2/20/2015	52.63	0	17.735	66.335	963.35
2/27/2015	78.94	20.7	21.34	64.685	961.85
3/6/2015	210.52	31.6	21.92	65.69	962.05
3/13/2015	48.87	0	20.6	41.51	963.25
3/20/2015	296.99	5.2	23.055	46.64	962.65
3/27/2015	93.98	0	23.87	48.985	961.25
4/3/2015	225.56	47.5	23.785	66.575	964.4
4/10/2015	93.98	60.3	24.19	69.735	958.7
4/17/2015	233.08	0	26.14	63.435	960.8
4/24/2015	195.49	182.1	23.375	70.76	959.8
5/1/2015	360.90	66.5	22.8	80.57	960.35
5/8/2015	447.37	42.3	24.3	72.085	958.55
5/15/2015	150.38	7.9	25.85	71.97	958.2
5/22/2015	270.68	89.2	26.2	77.26	955.9
5/29/2015	827.07	80.9	25.755	76.55	955.45
